An ab initio study of ion solvation in water

Heuft, J.M.

Publication date
2006
Document Version
Final published version

An ab initio study of ion solvation in water

ACADEMISCH PROEFSCHRIFT

ter verkrijging van de graad van doctor
aan de Universiteit van Amsterdam
op gezag van de Rector Magnificus
Prof. mr. P. F. van der Heijden
ten overstaan van een door het college voor promoties ingestelde
commissie, in het openbaar te verdedigen in de Aula der Universiteit

op woensdag 13 december 2006, te 10.00 uur

door

Jasper Martijn Heuft

geboren te Amsterdam

Promotiecommissie:

Promotor:

- prof. dr. ir. B. Smit

Copromotor:

- dr. E. J. Meijer

Overige leden:

- prof. dr. H. J. Bakker
- prof. dr. P. G. Bolhuis
- prof. dr. A. Fasolino
- prof. dr. D. Frenkel
- prof. dr. M. Sprik

Faculteit der Natuurwetenschappen, Wiskunde en Informatica

The research reported in this thesis was carried out at the Van 't Hoff Institute for Molecular Sciences, Faculty of Science, Universiteit van Amsterdam (Nieuwe Achtergracht 166, 1018 WV, Amsterdam, The Netherlands).

Contents

Chapter 1

Introduction

In this chapter we will introduce the most important concepts of this thesis. The first section describes the general background of the subject of aqueous solvation, and the solvation of simple ions in particular. The second part gives a short overview of the computational methods that are used to study these systems. A short introduction of density functional theory (DFT) for electronic structure calculations is followed by a description of the Car-Parrinello scheme of molecular dynamics. In the third section we discuss the more practical aspects of simulations of ionic solvation in water, such as the choice of system size, concentrations, temperature, etc. A short description of the most common and relevant techniques to analyse simulation results concludes this section. Finally, in the fourth and last section of this chapter, we define the scope of this thesis and introduce the primary research goals in a preview of the subjects that are covered in this study.

1.1 Solvation

1.1.1 Water

Water has always received a very large amount of scientific attention. From a purely physical and chemical point of view, water is a special liquid. The relatively high boiling point and unique solvating abilities are largely due to extensive hydrogen bonding between water molecules. The water molecule is dipolar (see figure 1.1) with a dipole moment of 1.86 D[1] in the gas phase and ca. 3 D in the liquid phase.[2] The hydrogen atoms are relatively electron poor while the oxygen atoms are electron rich. To disperse electron density, oxygen atoms can form hydrogen bonds with electron accepting hydrogen atoms of other molecules. The two formal lone electron pairs of the oxygen atom donate part of their electron density to the hydrogen atoms and, as such, form a hydrogen bond. Formation of a hydrogen bond between water molecules yields an energy of 2.6 ± 0.1 kcal/mol.[3] This value, based on very accurate Raman experiments, represents the energy of a single acceptor–donor interaction between water molecules in the liquid phase. Ideally, every water molecule could donate and accept two hydrogen bonds, as depicted schematically in figure 1.2. This is indeed the case for pure ice which has a crystal structure that is built up from tetrahedrally surrounded water molecules.[4] But even in the liquid phase, the water tetrahedrons dominate the structure of the liquid to a smaller or larger extent, depending on structural fluctuations due to the temperature. A snapshot of a typical pure liquid water simulation at ca. 300 K is shown in figure 1.3. One can identify several tetrahedrally surrounded water molecules, along with a large number of water molecules that are members of partial water tetrahedrons.

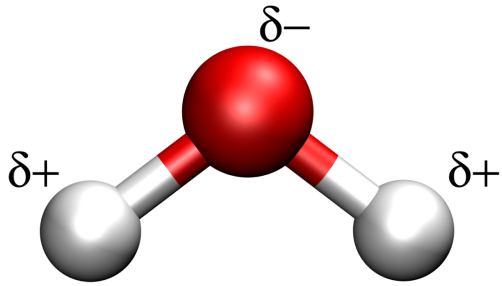

Figure 1.1: The water molecule. The dark grey sphere represents the oxygen atom and the white spheres are the hydrogen atoms. The $\delta+$ and $\delta-$ signs indicate the relative charge distribution in the molecule.

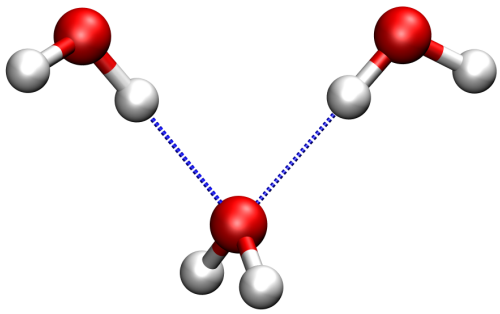

Figure 1.2: Schematic representation of hydrogen bonds (dotted lines) between water molecules. This structure is replicated in all directions when more water molecules are present. The O–H distance in a typical water hydrogen bond is ca. 1.8 Å, with an optimal O–H–O angle of 180°.

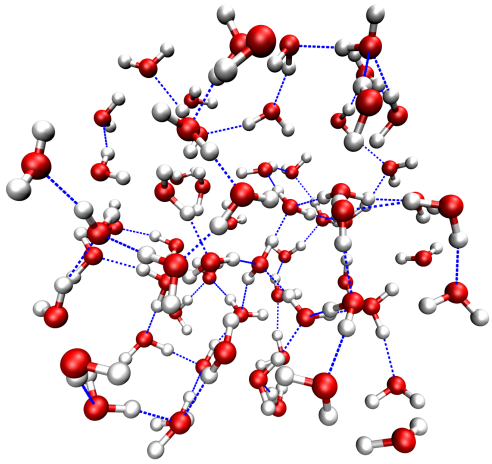

Figure 1.3: Snapshot of a simulation of liquid water at 300 K. The dotted lines represent hydrogen bonds.

The radial distribution function (RDF), that is discussed in more detail in section 1.3.2, allows us to describe the structure of a liquid in a more quantitative way. The RDFs for pure liquid water at 300 K are shown in figure 1.4. The sharp and well-defined peaks in the RDFs reflect the structured nature of the liquid. The first O–H peak at 1.8 Å (the intramolecular O–H peak at 1.0 Å is omitted for clarity) is followed by a very low minimum and represents the hydrogen-bonded O–H pairs. The normalised integral of the peak corresponds to exactly 1 oxygen atom and 2 hydrogen atoms, which nicely supports the idea of an average tetrahedral coordination of every water molecule.

The structure of liquid water is dominated by the hydrogen bond interactions and this, naturally, also affects the dynamical properties of water in many ways. One may expect that diffusion of water molecules is rather slow for a molecule as small as water, due to the hydrogen bond network. Indeed, this is the case but one must always bear in mind that the hydrogen bond network is not at all static. Hydrogen bonds are continuously broken and formed in the liquid phase of water. This fluxional behaviour is very important in the analysis of the behaviour of aqueous solvation shells around ions and phenomena such as proton transfer, as we will see in subsequent chapters.

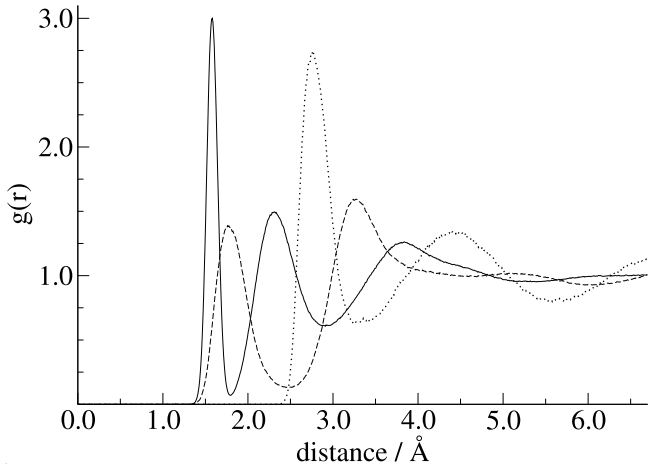

Figure 1.4: Radial distribution functions of pure liquid water, O–H (dashed line), O–O (dotted line) and H–H (solid line). The intramolecular O–H peak at 1.0 Å is omitted for clarity.

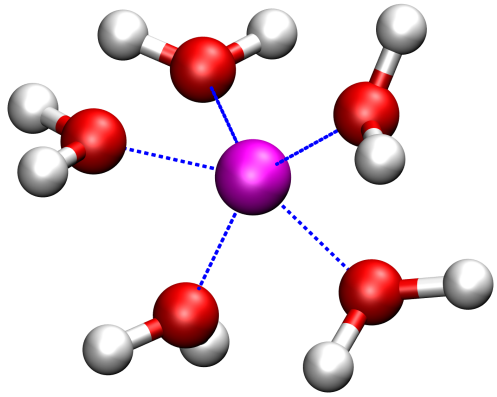

Figure 1.5: Water molecules surrounding a positive ion.

1.1.2 Ions in water

Introducing ions into pure liquid water causes a disruption of the natural hydrogen bond network. The water molecules have to rearrange in order to accommodate the particle. Because of this, hydrogen bonds between water molecules are broken and this is energetically unfavourable. However, because ions themselves can form hydrogen bonds with water, doing so can compensate for the loss of inter-water hydrogen bonds and result in a negative total free energy of solvation. The contribution of this favourable ion-water interaction depends on the strength and the number of the hydrogen bonds that are formed upon solvation of the ion. These two parameters are determined by the charge and the size of the ion. A high charge results in a strong hydrogen bond, while a smaller charge leads to a weaker hydrogen bond. Furthermore, the sign of the charge is of importance for the solvation energy. The solvation of anions is more favourable than that of cations because the layout of the first solvation shell of anions is more compatible with the natural structure of liquid water.[5] Schematic images of the orientation of the water molecules around positive ion and negative ions are shown in figure 1.5 and 1.6, respectively. The effect of the size of the ion is not so straightforward. A large ion disrupts the local water network to a larger extent, which is unfavourable. Also, the charge is more delocalised in larger ions, leading to weakening of the hydrogen bonds with water. On the other hand, a larger ion can have a larger solvation shell and therefore forms hydrogen bonds with more water molecules, which is again favourable. The net effect highly depends on the specific ion and the geometry and size of its solvation shell. The trend, however, is that large ions have a smaller energy of solvation than small ions.

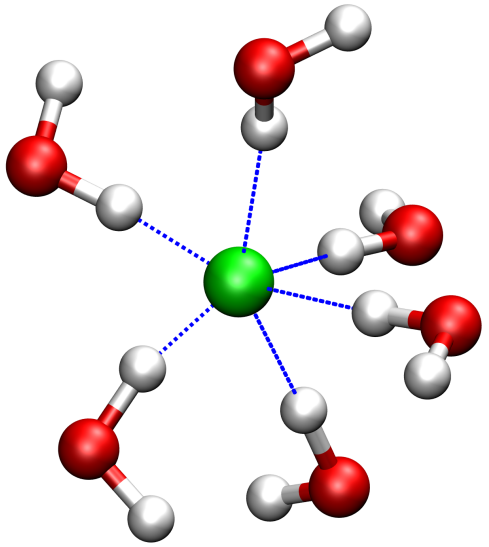

Figure 1.6: The first solvation shell of water around a negative ion.

The common halogen ions, F^-, Cl^-, Br^- and I^-, form a very good series to systematically study these effects on their solvation in water. The charge and outer electron configuration are all identical and the only differences between these ions are their relative sizes and masses. For an idea of the relative strength of the interactions, the $X^-(H_2O)$ (X = F, Cl, Br, I) bond enthalpies are given in table 1.1, accompanied by the radii of the ions.[6] The solvation of halogen ions has been studied extensively, both experimentally and computationally. Most attention is paid to the structural and dynamical properties of the solvation shell of water molecules. The ions are often categorised as being either a 'structure-maker' or a 'structure-breaker'. These terms

ion	ionic radius/Å[a]	ΔH^0/kcal/mol
fluoride	1.33	-26.2 ± 0.8[b]
chloride	1.81	-14.7 ± 0.6[c]
bromide	1.96	-11.7 ± 0.4[c]
iodide	2.20	-10.3 ± 0.3[c]

a. Reference 6
b. Reference 7
c. Reference 8

Table 1.1: Ionic radii of the common halogen ions and hydrogen bond energies for $X^-(H_2O)$.

reflect the overall influence that an ion has on the structure of the bulk of the water. Although the notion is very persistent and, in fact, textbook material, quite some recent studies[5,9] indicate that the structure making or breaking effect doesn't actually extend beyond the first or second solvation shells.

The number of coordinating water molecules and the geometry of the coordination sphere can be probed using X-ray and neutron diffraction experiments. Due to the slow nature of these techniques, however, they cannot yield information on the dynamical features. This is better suited to the field of Fourier Transform Infrared (FT-IR) spectroscopy. Unfortunately, it is very difficult to isolate the response of the coordinating water molecules from that of the bulk water molecules. Recent advances in the field of nonlinear pump-probe spectroscopy offer a very elegant solution to this problem. Summarised, water molecules directly surrounding the ion are excited selectively using a pump laser pulse. Their response is probed, after a variable time interval, by a second, probe laser pulse.[10] The time resolution of pump-probe experiments is currently in the order of femtoseconds, which makes them excellently suited to determine properties such as the residence time and the rotational reorientation time of water molecules in the coordination sphere of an ion. This technique makes a large range of dynamical properties now directly experimentally accessible, although the technique is not universally applicable to every system and some ions still elude direct investigations.

The discussion above on the experimental techniques that are used to study the solvation of ions, forms only a short overview of the possibilities. More detailed discussions on experiments, their advantages, disadvantages and their results are presented in the subsequent chapters, since these depend greatly on the system of interest. Also, this allows us to directly compare experimental results and our data side-by-side.

Parallel to the numerous experimental studies, computational research also has provided much insight in the details of aqueous ion solvation. Using molecular dynamics (MD), one can follow the motion of atoms and distribution of electrons with a temporal resolution of femtoseconds. Hence, they provide a direct way to investigate certain properties that can not, or only indirectly, be studied in experiments. A very relevant example is the computational study of the aqueous solvation of Br^- by Raugei *et al.*,[11] which has led to a direct insight in the geometry and dynamics of the ionic solvation sphere and the importance of electronic effects such as ion polarisability. The choice of computational method and the interaction parameters are crucial for a proper description of the aqueous solutions.[12] This is not trivial. For the description of pure water alone, a multitude of methods has been applied, ranging from simple forcefields[13] to advanced *ab initio* simulations.[14] Introducing an ion to

the system complicates things further. It has been shown that the problem of aqueous ion solvation is sensitive to polarisability of both the water molecules and the ions,[15] geometrical constraints on the water model, many-body effects, and many more subtle effects. If any of these are not implemented correctly this may have consequences for both structural and dynamical features of the system. Although implementing all these effects is, indeed, possible, by either using advanced forcefield models or *ab initio* type techniques, the required computer power grows accordingly. Fortunately, due to the increase of the availability and power of computer clusters and supercomputers, more and more problems lie within reach of computational methods.

Further discussion on the requirements of computational studies is in section 1.3 of this introduction. Details that are relevant for the specific systems in this thesis are presented in the introductions of the respective chapters.

1.1.3 Acids and bases in water

The discussion, so far, has dealt exclusively with isolated ions in water. As such, these systems correspond to solutions where the ions do not directly interact with each other. The second part of this thesis extends the studied systems to acidic and basic solutions at higher concentrations. We focus on acids and bases that, under ambient conditions, dissociate completely in water. First we will discuss here the implications of higher ion concentrations for the system. After that, a short introduction on the structural and dynamical features of acidic and basic solutions follows.

An increase in the concentration directly implies a further disruption of the natural hydrogen bond network of water. In fact, at concentrations of ca. 5 mol/l and higher, almost all water molecules are part of one ionic solvation shell or another. Because of the relative scarcity of water molecules, the interactions between the ions and water molecules and between the ions themselves, become more important. For every ion, it is energetically most favourable to have a complete solvation shell of water molecules. However, when the amount of water molecules is no longer sufficient to completely solvate every separate ion, the ions will compete for the water molecules that are available. The strength of the hydrogen bonds that the ion can form with water molecules is a very important factor in this competition. Upon solvation, an acid or base dissociates in ions with charges of opposite sign. Therefore, depending on the concentration and the charge shielding due to the solvation sphere of water molecules around the ions, a Coulombic attraction is present between ion pairs, while ions of equal sign repel each other. This effect can lead to a wide range of structural features, from isolated, individually solvated ions, to solvent-separated ion pairs and

even direct contact-ion pairs. Formation of large-scale structures, such as long-living water-bridged ion networks, can result from the systems goal to optimise all interactions, delicately balancing the attracting and the repelling forces. Briefly summarised, aqueous solutions of acids and bases offer an almost infinite amount of interesting and sometimes surprising properties. This justifies the large amount of research that they attract.

A very large part of that research has dealt with the nature of the solvated excess protons in acidic solutions. The proton mobility in water is abnormally high with a value almost 5 times higher than one would expect based on structural diffusion of hydrogen nuclei.[4] The key concept of proton transport in water is that structural diffusion, i.e. the physical translation of positive hydrogen ions, is only partly responsible for proton mobility. A more important contribution is the transport of the positive charge that defines the excess proton with respect to all other present hydrogen atoms. Because this is a purely electronic property, its dynamic behaviour is faster than the translation of hydrogen nuclei, and therefore increases the effective mobility of the proton species. Ever since Von Grotthuss first investigated[16] this phenomenon, thousands of papers have discussed the details of proton transfer in water. It is a difficult subject to study experimentally, due to the small time and length scales that are involved. Only with the combination of NMR, (nonlinear) IR, Raman, X-ray, neutron diffraction and many other techniques, the microscopic mechanism of proton transfer, the Grotthuss process, could be understood in detail. Very recently, ultrafast infrared spectroscopy experiments,[17] gave unprecedented real-time insights in the kinetics and intermediate species of this process.

Advanced computational studies have added greatly to the understanding of the details of proton transfer, because of their unparallelled temporal and spatial resolution. Although the last words on the workings of the Grotthuss process have not yet been spoken, and many discussions remain (see e.g. references 18, 19), the following overview describes the mechanism in all the detail that we need for our present studies.[20] An excess proton in water is never isolated but always part of a larger proton–water cluster, smallest of which is the hydronium ion H_3O^+. Two of the most important larger clusters, especially for the discussion on the Grotthuss mechanism, are the Eigen cation $H_9O_4^+$ (fig. 1.7) and the Zundel cation $H_5O_2^+$ (fig. 1.8). The transfer of a proton starts from an $H_9O_4^+$ structure. In the first step, one of the outer water molecules loses a hydrogen bond with an external water molecule. This causes the O–O distance of the central water molecule and that outer water molecule to decrease by ca. 0.15 Å. An $H_5O_2^+$ like structure is formed. The proton can now transfer, without energy barrier, from the first to the second oxygen atom. Hydrogen bonding of the previously central water molecule with an external water molecule leads to an

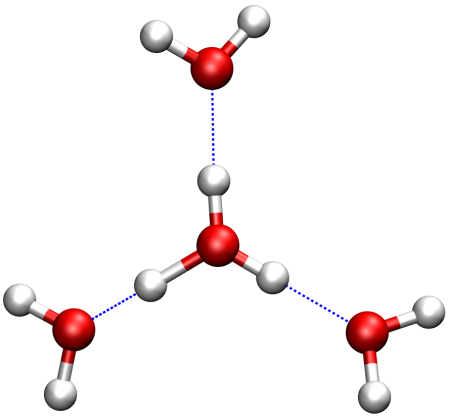

Figure 1.7: The Eigen cation, $H_9O_4^+$.

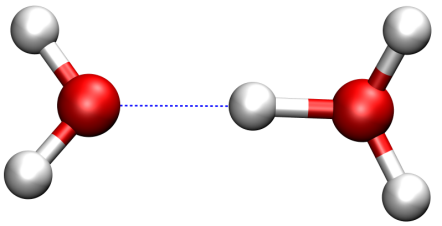

Figure 1.8: The Zundel cation, $H_5O_2^+$.

increase of the O–O distance again, forming a new $H_9O_4^+$ cluster and completing the proton transfer. The rate limiting step in this process is the cleavage of the hydrogen bond in the beginning, which costs 2.6 kcal/mol and takes approximately 1 ps under ambient conditions. Recent *ab initio* MD simulations[21] further elaborate on the details of the complex behaviour of the hydrated proton, stressing the fact that the description of above process is an idealisation of reality. To think of proton transfer in terms of well-defined structures and transition states can be misleading. One should keep in mind that the behaviour of hydrated protons is by nature, very fluxional. In concentrated acid solutions, the situation becomes even more complex. Proton transfer is affected by the presence of counterions and other excess protons, as we will see in chapter 5 on the solvation of hydrochloric acid. Further details, specific to the case of the solution of hydrochloric acid, and the novel insights that our simulations can offer, are discussed in the introduction of that chapter.

Compared to the hydronium ion, there has been a relatively small amount of interest in the hydroxide ion OH^-. Although diffusion of the OH^- ion is slower than that of a proton in water, it still is faster than expected for pure structural diffusion. This implies that, like the Grotthuss mechanism for the proton, there is a comparable process that drives OH^- mobility. However, due to the few studies regarding this phenomenon, much less is known on the details of the transport of hydroxide ions. In an elegant combination of the restrictions that are imposed by the results from NMR, Raman and IR experiments, and including the results from computational studies, the following mechanism,[22] as proposed by Agmon, is a very good starting point. Two of the hydroxide–water clusters that are most important for this mechanism are $H_7O_4^-$ and $H_3O_2^-$, shown in figure 1.9 and 1.10. Note the structural similarities to the cor-

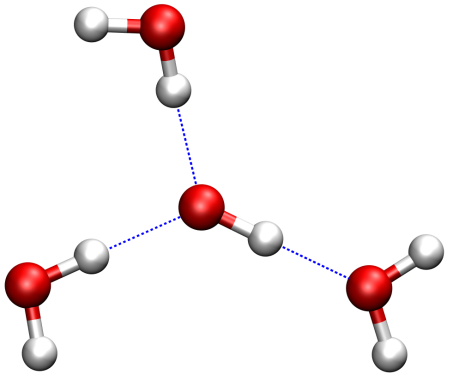

Figure 1.9: The $H_7O_4^-$ anion.

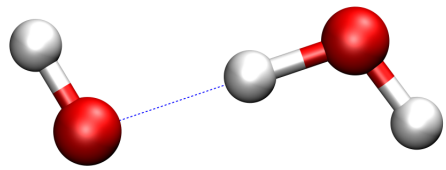

Figure 1.10: The $H_3O_2^-$ anion.

responding proton–water water clusters in figure 1.7 and 1.8. Starting from the local $H_7O_4^-$ cluster, a hydrogen bond with a water molecule in the second solvation shell of OH^- breaks. Upon decreasing of the central O–O distance, the proton can, barrierless again, shuttle between the two oxygen atoms. When the proton transfers to the former OH^- ion and the resulting water molecule now hydrogen bonds to an external water molecule, the O–O distance increases again and the transfer is complete. The mechanism shows many similarities to the previously discussed Grotthuss mechanism. A large difference, however, is the fact that decreasing the O–O distance costs 0.5 kcal/mol in addition to the 2.6 kcal/mol, associated with breaking a hydrogen bond in liquid water. Hence, the total energy cost amounts to 3.1 kcal/mol. This explains the slower rate of OH^- transfer and agrees with experimental and computational results. In a more recent *ab initio* path-integral molecular dynamics study,[23] including nuclear quantum effects, an alternative mechanism is proposed that starts of with the cleavage of a first-shell hydrogen bond. The authors stress that this indicates that OH^- transport is substantially different than proton transport, unlike the mechanism that is discussed above. Evidently, the mechanism of hydroxide transfer is still a point of debate and further research is of great importance to resolve the details of the process. The very recent neutron-diffraction experiments by Imberti *et al.*[24] offer very useful detailed data on the structural features of the solution of KOH, which are very helpful for our work and future studies on this subject. Similar to the description of the Grotthuss mechanism, one must remember that the ideal scenarios described here are very much affected by the presence of other ions in the solution. We will discuss these influences in chapter 6 on the solvation of lithium hydroxide. Because of the many similarities between acids and bases, and the mobility of excess protons and OH^- ions in particular, concentrations and other simulation parameters have been kept the

same in the simulations in this thesis, in order to be able to consistently compare both systems.

1.2 Theory

After a global introduction of the aqueous solvation of ions, acids and bases in the previous section, we will now motivate the theoretical methods that are necessary to properly study these systems. It is clear that aqueous solvation is a complex topic. A sound computational study should properly address the following, non-exhaustive list of issues:

- many-body interactions,
- formation and cleavage of covalent bonds,
- hydrogen bonding,
- polarisability of water molecules and ions,
- fast (fs) structural rearrangements.

There are many classical force-fields that aim to incorporate most, if not all of these issues, but this is a very challenging task. It has been shown that simulations with these force-fields can offer very accurate results, but usually their application is limited as they are optimised for specific systems or properties. *Ab initio* methods, that explicitly include the electrons into the calculations, offer a more natural way of dealing with the issues that are mentioned above. In fact, many of the issues are a direct result of the distribution and flow of the electrons in a molecular system. Of course, quantum mechanics is not the holy grail of computational chemistry. Approximations to the quantum description are necessary for all but the most simple practical applications. Countless studies, however, show the advantages of *ab initio* over classical methods, especially where the above-mentioned issues are important. One of the major practical disadvantages is the computational cost of *ab initio* based simulations. In terms of computation power, speed and storage, they do require more resources, i.e. are more expensive. Indeed a study, such as described in this thesis, would have been unfeasible 10 years ago. The fact that it is possible now is not only a result of the enormous increase of computation power, but also, for a large part, due to the elegant combination of density functional theory and molecular dynamics in the Car-Parrinello approach,[25] as developed by Car and Parrinello in 1985. This approach will be discussed in this section, following the introduction of electronic structure calculations.

1.2.1 Electronic structure

In theory, all static properties of any system can be determined by solving the time-independent Schrödinger equation:

$$\widehat{\mathcal{H}}\Psi = \mathsf{E}\Psi. \tag{1.1}$$

Here, $\widehat{\mathcal{H}}$ is the Hamiltonian operator, with Ψ a eigenfunction representing the state of the system and the eigenvalue E the associated energy. For systems more complicated than the hydrogen atom, there is no exact analytical solution. Therefore, in order to use equation 1.1 for chemically or physically interesting calculations, a number of approximations is needed. In the Born-Oppenheimer approximation we neglect the influence of electronic excited states and assume the electrons to respond instantaneously to translations of the nuclei, due to the relatively small mass of the electron. By decoupling the ionic and electronic subsystems we can treat the nuclei as classical particles and restrict the quantum mechanical treatment to the electrons alone. The influence of the ions on the electronic structure can be incorporated as an external potential. Within this approximation, the electronic Hamiltonian $\widehat{\mathcal{H}}_e$ becomes:

$$\widehat{\mathcal{H}}_e = \widehat{\mathcal{T}}_e + \widehat{\mathcal{U}}_e + \widehat{\mathcal{V}}_n, \tag{1.2}$$

where $\widehat{\mathcal{T}}_e$ and $\widehat{\mathcal{U}}_e$ denote the electronic kinetic and interaction contributions, respectively, and $\widehat{\mathcal{V}}_n$ represents the external potential as function of the positions of the ions. Even with these approximations, calculation of the electronic multi-dimensional wavefunction Ψ_e is still computationally challenging for complex and/or large systems. Density functional theory (DFT) is based on the Hohenberg-Kohn theorem which states that for a given external potential there is a one-to-one relation between the ground-state electronic wavefunction Ψ_0 and total electronic density distribution ρ_0:

$$\Psi_0 \leftrightarrow \rho_0. \tag{1.3}$$

For the rest of the discussion the system is assumed to be in the ground state. Relation 1.3 implies that instead of solving the Schrödinger equation for the many-electron wavefunction, knowledge of the ground-state electron density is sufficient to determine all properties of the system. Combining 1.1 and 1.3 gives the general form for the functional $\mathcal{F}_{HK}$ that relates the electron density and energy E_e in the Hohenberg-Kohn framework:[26]

$$\mathsf{E}_e(\rho) = \langle\Psi|\widehat{\mathcal{H}}_e|\Psi\rangle = \mathcal{F}_{HK}(\rho) + \mathcal{V}_n(\rho), \tag{1.4}$$

with:

$$\mathcal{F}_{HK}(\rho) = \mathcal{T}_e(\rho) + \mathcal{U}_e(\rho). \tag{1.5}$$

Here, $\mathcal{T}_e(\rho)$ is the electronic kinetic energy functional and $\mathcal{U}_e(\rho)$ is the electronic interaction energy functional. Kohn and Sham (KS) approached the expression of these terms by first introducing one-electron orthonormal Kohn-Sham orbitals, such that:

$$\rho(r) = \sum_{i=1}^{N} \phi_i^*(r)\phi_i(r). \tag{1.6}$$

This equation defines the electronic density at point r as the sum over the square of all N Kohn-Sham orbitals ϕ_i. The total energy in Kohn-Sham theory is given as:

$$\mathcal{E}_e^{KS}(\rho) = \mathcal{T}_e^{KS}(\rho) + \mathcal{U}_e^{KS}(\rho) + \mathcal{V}_{ext}(\rho). \tag{1.7}$$

These terms are all expressed here in atomic units ($\hbar = m = 1$). The first term, the kinetic energy functional, is:

$$\mathcal{T}_e^{KS}(\rho) = -\frac{1}{2}\sum_{i=1}^{N} \langle \phi_i | \nabla^2 | \phi_i \rangle. \tag{1.8}$$

The electronic interaction energy functional consists of a Hartree contribution due to classical Coulombic interaction and a non-classical exchange-correlation (XC) contribution:

$$\mathcal{U}_e^{KS}(\rho) = \frac{1}{2}\int \frac{\rho(r)\rho(r')}{|r - r'|} dr dr' + E_{XC}(\rho). \tag{1.9}$$

Finally, with the expression for the electron-nuclei interaction energy:

$$\mathcal{V}_{ext}(\rho) = \int \rho(r) v_{ext}(r) dr, \tag{1.10}$$

where $v_{ext}(r)$ is the potential due to the nuclei, we now have a complete set of equations that can be solved self-consistently to yield the ground-state energy. The only unspecified part of the expression is the exchange-correlation energy E_{XC}. Over the years, a large number of approximations for E_{XC} has been developed. The local density approximation (LDA) that is based on the electron density of a homogeneous electron gas provided good results for various properties in solid state physics. However, it has insufficient accuracy to be applied quantitatively in most chemical systems. Only with the development of generalised gradient-corrected approximations (GGA), accurate prediction of chemical properties became feasible. These approximations include a dependence on the gradient of the density and, as such, are much more flexible to suit real-world applications. Still, there is no exact expression and an educated choice for the type of exchange-correlation functional is necessary for each new problem. The functional that is used throughout this thesis is the BLYP functional, developed by Becke, Lee, Yang and Par.[27,28] It is very popular for simulations of liquid water[29] and solvated species, due to the excellent results that are obtained.

1.2.2 Car-Parrinello molecular dynamics

With DFT we have an efficient method available for the calculation of the energy and forces, optimisation of the geometry, the distribution of the electronic density, etc. However, the real power of computational chemistry lies in the extension of calculating static properties to the simulation of dynamical behaviour. Molecular dynamics is a very appropriate technique for this task. Integration of the forces on the nuclei results in their velocities and using, for instance, the velocity Verlet algorithm,[30] the positions of the nuclei are updated. With the new nuclear positions, the electronic density changes, which leads to new forces on the nuclei, and so forth. This scheme represents Born-Oppenheimer molecular dynamics and includes an optimisation of the electronic density for every timestep. As such, this method is quite expensive and nowadays only feasible for small simulation, either in size or time. In 1985, Car and Parrinello presented a revolutionary molecular dynamics scheme that circumvents costly direct electron density optimisation.[25] By assigning a fictitious mass to the electronic degrees of freedom, both the nuclei and the electron density can be propagated in time, hereby eliminating the need to solve the Kohn-Sham equations every MD timestep. The following Lagrangian describes this technique:

$$\mathcal{L}_{cp}(r, \dot{r}, \phi, \dot{\phi}) = \sum_I \frac{1}{2} M_I \dot{r}_I^2 + \sum_i \frac{1}{2} \mu_i \langle \dot{\phi}_i | \dot{\phi}_i \rangle - E_e(r_I, \rho) + \sum_{i,j} \Lambda_{ij} (\langle \phi_i | \phi_j \rangle - \delta_{ij}). \tag{1.11}$$

Here, M_I are the masses of the nuclei and μ_i are the fictitious masses associated with the electronic degrees of freedom, r_I are the position vectors of the nuclei. The last term represents orthonormality requirements for the wavefunction for which the Lagrange multipliers Λ_{ij} are introduced.

To keep the sum of E_e and the nuclear kinetic energy constant, it must be ensured that the dynamics of the electron density and the nuclei are decoupled. Only in the adiabatic limit, where both the electronic kinetic energy and the energy of the nuclear subsystem are constant, the Car-Parrinello approach yields an accurate nuclear trajectory. Proper adiabaticity is determined by the choice of the fictitious electron mass μ. A small value requires a small timestep to integrate the equations of motion, which is more expensive. But a too large value increases coupling of the ionic and electronic subsystem, causing the electrons to deviate from the Born-Oppenheimer surface, and resulting in an inaccurate nuclear trajectory. As both options are undesirable, one must use an optimal value that avoids both extremes. For our simulations, this choice is motivated in the discussion of the Car-Parrinello parameters in section 1.3.1.

The equations of motion that correspond to the Car-Parrinello Lagrangian are, for the ionic subsystem:

$$M_I \ddot{r}_I(t) = -\frac{\partial E_e(r,\rho)}{\partial r_I}, \tag{1.12}$$

and for the electronic subsystem:

$$\mu_i \ddot{\phi}_i(t) = -\frac{\delta E_e(r,\rho)}{\delta \phi_i^*} + \sum_j \Lambda_{ij}\phi_j. \tag{1.13}$$

The DFT Kohn-Sham orbitals are usually expanded in plane waves:

$$\phi_i(r) = \frac{1}{\sqrt{\Omega}} \sum_G^{G_{max}} \phi_i(G) e^{iGr}, \tag{1.14}$$

where G is a vector in reciprocal space that satisfies the periodic boundary conditions and G_{max} is the maximum length of the G vectors, determining the basis set size. Ω is the volume of the simulation cell, $\phi_i(r)$ is related to $\phi_i(G)$ by a three-dimensional Fourier transform. Because of their simple form, these functions are very efficient to manipulate. One disadvantage however, that is directly related to their simple form, is that for rapidly oscillating wavefunctions, a large number of plane waves are needed to properly express the total wavefunction. These situations usually occur very close to the nucleus. Fortunately, this is often also the region where the electron density is not directly chemically relevant. Therefore, effective core potentials, or pseudopotentials, can be used to replace the wavefunction near the core by a smooth function that reproduces the all-electron wavefunction beyond a certain cutoff. Real plane waves are then only used for the valence electrons beyond this cutoff. This technique saves a lot of computational effort, but one must always test the cutoff of the pseudopotential for proper energy convergence. For the type of simulations that are present in this thesis, these tests consist of comparing geometries and bonding energies for small ion–water clusters with all-electron calculations.

1.3 Simulation details

1.3.1 System setup

In this section we will discuss a number of practical issues that one must pay attention to when performing Car-Parrinello simulations of aqueous solutions of halogen ions, acids and bases.

System size
The solvated anions that are studied here, F^-, Cl^- and I^- induce a structural effect on their surrounding water molecules. Radial distribution functions show that this effect extends to the second water solvation shell of the ion. For all aqueous solutions studied in this thesis we employ periodic boundary conditions[30] to eliminate surface effects and mimic the real solution as best as possible. The size of the periodically replicated simulation box should be chosen such, that it can contain at least two solvation shells of water molecules around the ion, without overlapping with a periodic image. At ambient conditions, this requires approximately 64 water molecules. In the simulations of HCl and LiOH, the system size was chosen approximately twice as large. This allows easier identification of local and larger-scale structures, such as proton-water clusters and water-bridged ion networks.

Concentration
The concentration of the single isolated halogen ions is chosen such that the ions do not significantly influence their periodic images. This allows us to investigate their solvation shells without further interference. The concentration of the HCl and LiOH solutions is purposely higher, because the direct interaction between the ions is actually what we want to investigate. Concentration plays an important role in these systems and significantly influences the structural and dynamical features of the system. Both solutions are studied at a high and a low concentration. By comparing the results for these two concentrations we can identify the concentration effects and study the competition for solvation of the present ions.

Temperature control
In the simulations of the solvated halogen ions we use a Nosé-Hoover thermostat to control the temperature. The use of a thermostat has the practical advantage that the temperature as a simulation parameter is constant and well-defined. We do not expect that the thermostat will influence the dynamical properties of the ionic solvation shell, as our chosen thermostat period is two orders of magnitude shorter than the typical timescale of rearrangements in the solvation shells. The simulations of the solvation

of HCl and LiOH involve the dynamics of protons and hydroxide ions. Since these dynamics occur on a much shorter timescale, a thermostat might influence their behaviour to a larger extent. Therefore, in these simulations, the temperature of the nuclei is not controlled by a thermostat to eliminate unphysical effects.

Car-Parrinello parameters

For the halide ions simulations we chose a value of 900 a.u. for the fictitious electron mass. This choice was based on the good results obtained by Silvestrelli *et al*. for pure liquid water.[29] Recent studies[31,32] have indicated that for values of μ beyond a certain threshold the calculated structure and dynamics is influenced by a coupling between the ionic motion and fictitious electronic degrees-of-freedom, yielding, for water, a less structured radial distribution functions and faster dynamics. For deuterated water the threshold for μ is circa 700 a.u., implying that the results of our calculations with $\mu = 900$ a.u. (*viz*. the isolated ion solvations) are affected. However, for $\mu = 900$ a.u. the structure and dynamics of water compare well with experimental data for bulk water.[32] This should be considered fortuitous, but suggests that the dynamics and structure of water around an ionic solute is also reasonably well described when performing simulations with $\mu = 900$ a.u. The simulations of the solvation of HCl and LiOH were performed with $\mu = 700$ a.u. to eliminate possible unphysical effects.

All hydrogen atoms are assigned the mass of deuterium in order to improve decoupling of the dynamics of the ionic and electronic subsystem over a longer period of time, and allowing for a larger timestep in the numerical integration of the equations of motion. Although increasing the mass of the water molecules will influence the dynamics of water, the effects on dynamics due to the interactions with the ions will be much stronger. The net effect, therefore, is assumed negligible.

1.3.2 Analysis techniques

The main output of our molecular dynamics simulations is the trajectory of all the nuclei in time. For structural analysis the first and most important tool is the radial distribution function:

$$g(r) = \frac{V}{N^2}\langle \sum_i \sum_{j \neq i} \delta(r - r_{ij}) \rangle, \tag{1.15}$$

where V/N^2 is the normalisation relative to an ideal gas, and $\delta(r - r_{ij})$ is a Dirac delta function with r_{ij} the interatomic separation. Plots of this function give quantitative time-averaged information on the surrounding structure of selected species. The geometry of the solvation shell around an ion can be visualised by plotting the distri-

bution of H_2O–ion–H_2O angles. Combination of coordination numbers from RDFs and the angle distribution gives a structurally complete picture of the solvation sphere of an ion. The quantitative analysis of dynamical properties is intrinsically more difficult. We mainly use correlation functions to gain insight in the dynamical behaviour of species that are present in the solutions. These functions give us residence times of water molecules in solvation shells, and allow us to compare lifetimes of hydronium ions at different concentrations. But eventually it is inevitable to simply watch the trajectory as a movie. This analysis technique offers the most direct insight in the behaviour of the system of interest. Using his or her chemical and physical intuition and knowledge, the observer can identify interesting events, isolate important structures, and connect seemingly unrelated properties. These observations often form the basis for further, more quantitative analysis of specific events or structural features.

1.4 Scope of this thesis

This thesis concerns the solvation of simple ions in water. The first half deals with a structured, in-depth study of the solvation of the halogen ions chloride, fluoride and iodide. We aim to give a consistent picture of the solvation shell of these ions in water. Although, at first sight, one could assume that these systems are all quite alike, we observe some very distinct but also some subtle differences. We start with a study of the solvation of the chloride ion. This project lays down the foundation for further studies here. Using CPMD we obtain a detailed description of the direct solvation shell of water molecules around the ion. This includes both structural and dynamical features. The next chapter, concerning the fluoride ion, builds upon this knowledge and facilitates a comparison between the two ions. Although many properties are indeed alike, there are some major differences. For instance, due to its smaller size and the more localised charge, the fluoride ion has a much more rigid solvation shell. This allows us to accurately describe the conformation of the coordinated sphere of water molecules. Additionally we can properly follow and describe dynamical events that take place in the direct vicinity of the fluoride ion. The study of the iodide concludes our walk down the periodic table. The iodide ion is large and its negative charge is quite diffuse. This has very clear consequences for its solvation. The solvation shell surrounding the ion is very disordered, compared to both other halogen ions.

In the second part of this thesis we extend our systems quite dramatically. Not only are the simulated systems much larger, they no longer concern isolated ions. First we study a hydrochloric acid solution at two concentrations. This research extends the current state of these simulations simply due to the increased size of the simulated

systems. By including multiple chloride and hydronium ions, we are able to observe large-scale structures, such as the formation of a water-chloride ion network. Also, we can analyse the interactions between the positive hydronium ions and the negative chloride ions in their competition for complete solvation shells. The transport of the excess protons is of course very much affected by the presence of the chloride ions, and this system allows us to observe the dynamics in detail. This leads to interesting new insights on a molecular level of this very important and widely used chemical substance. Finally, we focus at the solvation of a basic solution. Using the exact same framework as our hydrochloric acid simulation, we study the aqueous solution of lithium hydroxide. Not only is this a much anticipated answer to the almost complete knowledge vacuum that exists regarding lithium hydroxide, it also allows us to directly and consistently compare a basic and an acidic solution.

Chapter 2

Density functional theory based molecular-dynamics study of aqueous chloride solvation[†]

Abstract

The aqueous solvation shell of chloride is studied using DFT-based molecular dynamics simulations. This method enables us to obtain a detailed understanding of the structural, dynamic and electronic properties of the system. Special attention is paid to the dynamic properties of the first solvation shell. The results obtained here are in good agreement both with experiments and other simulations. Our results suggest that the surrounding shell of water molecules is quite rigid. We observe no influence of the chloride ion on the electronic and structural properties of the coordinating water molecules.

[†]This chapter is based on J.M. Heuft and E.J. Meijer *J. Chem. Phys.* **2003**, *119*, 11788.

2.1 Introduction

Aqueous solvation shells around ions play an important role in many chemical and biological reactions. Due to electrostatic interactions between the ion and the polarised water molecules a well-defined shell of water molecules forms around the ion. Knowledge of the structural, dynamic and electronic properties of these solvation shells is essential for a detailed understanding of the behaviour of ions in solution.

To gain more insight in these properties, water solvated ions have been the subject of a large number of experiments[33–37] and computer simulations.[11,38–51] Both methods, however, prove to have their difficulties and/or limitations. Most experimental techniques are limited by the fact that information on the solvation shell water molecules is clouded by the response of the bulk water molecules. Only recently it has become possible, using nonlinear spectroscopic techniques, to obtain a detailed picture of the microscopic behaviour of the solvated ion and surrounding water molecules on a femtosecond timescale. Dynamic properties such as the residence time of water molecules in the solvation shell around ions are now experimentally accessible.[35] Molecular simulations employing empirical force fields that ignore the polarisability of the water molecules have difficulties in describing both the structural[15,52] and the dynamic[38] properties of the system. Improving the force fields by including more interaction sites and polarisability is essential for a proper description of ion solvation.[53,54] The aforementioned problems of molecular simulations employing empirical force fields essentially disappear with the Car-Parrinello[25] approach to *ab initio* molecular dynamics (CPMD). It explicitly takes into account the electronic structure using density functional theory (DFT) and includes inter- and intra-molecular interactions, including those arising from the polarisability, in an implicit way. This makes CPMD an excellent technique for the simulation of aqueous ion solutions.

Here we examine the solvation of the chloride ion in water on molecular length and time scales, paying special attention to the properties of the first solvation shell. We investigate the structural properties, as well as dynamic and electronic properties.

2.2 Computational Details

Electronic structure calculations are performed using the Kohn-Sham formulation[26] of DFT.[55] A gradient correction for the exchange and correlation energy is applied by the BLYP functional.[27,28] This functional is known for its good description of aqueous systems.[56,57] We compared the energy optimised geometries of $Cl^-(H_2O)_n$

method	$Cl^-(H_2O)$	$Cl^-(H_2O)_2$ [a]	$Cl^-(H_2O)_2$ [b]	$Cl^-(H_2O)_3$ [a]	$Cl^-(H_2O)_3$ [b]	$Cl^-(H_2O)_4$
CPMD ΔE_{bond}	-14.2	-13.0	-12.9	-12.7	-12.6	-12.5
ADF ΔE_{bond}	-13.8	-12.8	-13.0	-12.1	-12.2	-12.4
CPMD ΔE_{seq}	-14.2	-11.5	-11.7	-12.1	-12.2	-12.0
ADF ΔE_{seq}	-13.8	-11.9	-12.1	-10.6	-10.7	-12.8

a. planar conformation
b. non-planar conformation

Table 2.1: Comparison of bonding energies per ion–water hydrogen bond and sequential energies of solvation for a number of small chloride water clusters. All values are in kcal/mol.

clusters ($n = 1, \ldots, 4$), obtained with CPMD* and a state-of-the-art atomic orbital based package (ADF†) to determine the validity of parameters in the CPMD calculations, in particular the plane wave cutoff and the parameters of the pseudopotentials. In CPMD the KS orbitals are expanded in plane waves with an energy cutoff of 70 Ry. For the static cluster calculations the interactions between the periodic images were eliminated by a screening technique similar to that of reference 60. Only valence electrons are explicitly considered. The interaction between the core and valence electrons is taken into account using the semi-local norm-conserving Martins-Troullier pseudopotential. The pseudopotential cutoff radius is 0.50, 1.10 and 1.34 a.u. for H, O and Cl, respectively. Differences among ADF and CPMD are within 0.05 Å for bond lengths and 1.5 kcal/mol for the energies (see table 2.1) and thus we concluded that this combination of pseudopotential and cutoffs is suitable for this system.

To determine a proper system size for the *ab initio* molecular dynamics simulation, a number of chloride-water systems, varying in the number of water molecules, were simulated with empirical force-field based molecular dynamics. The classical simulations were performed with the DL_POLY‡ package. We used the extended simple point charge (SPC/E) model[52] for the water molecule, in combination with the chloride-water potential from Smith *et al.*[44] Systems consisting of one chloride ion and 32, 64 and 256 water molecules were simulated in an NPT ensemble at 300 K under atmospheric pressure. The radial distribution functions (RDFs) of these simulations

*CPMD 3.4.3, J. Hutter, A. Alavi, T. Deutsch, M. Bernasconi, St. Goedecker, D. Marx, M. Tuckerman, M. Parrinello, MPI für Festkörperforschung and IBM Zürich Research Laboratory 1995-1999

†ADF 2000.02,,[58,59] SCM, Theoretical Chemistry, Vrije Universiteit, Amsterdam, The Netherlands, http://www.scm.com . Molecular orbitals are expanded in an even-tempered quadruple ζ Slater-type basis set augmented with 2p and 3d polarisation functions for H and 3d and 4f polarisation functions for O. For Cl an even-tempered Slater-type basis set including 6 2p functions augmented with 3d and 4f polarisation functions was used.

‡DL_POLY is a package of molecular simulation routines written by W. Smith and T.R. Forester, copyright The Council for the Central Laboratory of the Research Councils, Daresbury Laboratory at Daresbury, Nr. Warrington (1996).

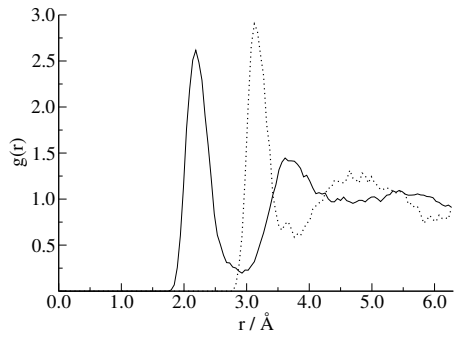

Figure 2.1: Radial distribution functions for Cl–H (solid line) and Cl–O (dotted line).

showed that the structural influence of the ion extends till the second solvation shell around the chloride ion. A system containing 64 water molecules is sufficient to accommodate two solvation shells and was therefore taken as system size in the present CPMD simulation. The final configuration from the 64-water force-field simulation was used as the initial configuration for the CPMD simulation.

In the CPMD simulation the edge of the periodically replicated cubic simulation box was fixed at 12.59 Å corresponding to the experimental density. The temperature was fixed at 300 K by a Nosé-Hoover thermostat[61] with a frequency of 66.7 fs (500 cm^{-1}). The fictitious electron mass was set to 900 a.u. We replaced all the hydrogen atoms by deuterium. The simulation timestep was 6 a.u. (0.145 fs). There was a proper decoupling of the dynamical ionic and electronic subsystem: we observed no drift in the electronic kinetic energy during the total simulation time of 17 ps. The total charge of a cubic cell is -1 e due to the presence of the chloride ion. The negative charge is counteracted by discarding the $k = 0$ term in the Ewald summation, essentially shielding the negative charge by a uniformly distributed positive background charge.

2.3 Results and Discussion

Structure

The radial distribution functions for the Cl–H and Cl–O distances are shown in figure 2.1. The pronounced first peak and low first minimum indicate a highly structured first solvation shell. A water molecule is defined to be inside the first solvation shell if the distance between the chloride ion and a hydrogen or oxygen atom falls within the first peak of the corresponding RDF. Integration of the first peak of the RDF plots

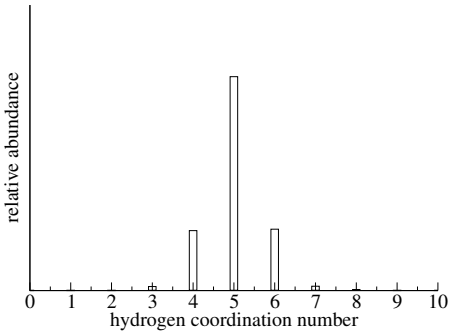

Figure 2.2: Histogram of the coordination number based on the Cl–H distance.

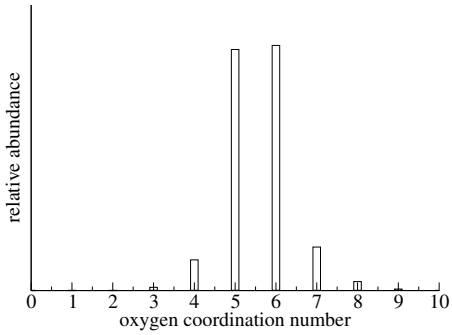

Figure 2.3: Histogram of the coordination number based on the Cl–O distance.

yields a coordination number of 5.2 and 5.8, based on the g_{ClH} (integrated up to 2.93 Å) and g_{ClO} (integrated up to 3.76 Å) functions, respectively. The distribution of the coordination numbers based on the Cl–H and Cl–O distances is shown in figure 2.2 and figure 2.3, respectively. The average value for the coordination number is 5.0 based on the Cl–H distance and 5.6 based on the Cl–O distance. This last value is also calculated by Tongraar *et al.*[62] and close to the experimental value of 6.[37] The distribution of H-Cl–H and O-Cl–O angles in the first solvation shell are shown in figure 2.4. The graph shows a maximum around 80° suggesting that the surrounding geometry is close to octahedral. This is consistent with the calculated coordination number.

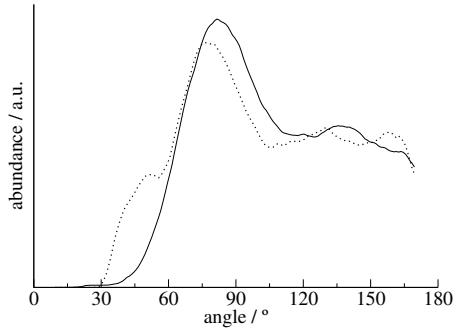

Figure 2.4: Distribution of the H–Cl–H angle (solid line) and O–Cl–O angle (dotted line) within the first solvation shell.

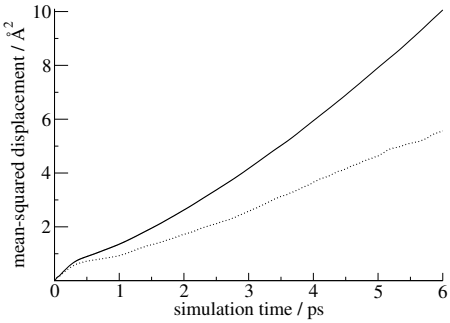

Figure 2.5: Mean-squared displacement of the water molecules inside (dotted line) and outside the first solvation shell (solid line).

Dynamics

In order to study the dynamic properties, we looked at the diffusion coefficient and residence time of water molecules. The mean-squared displacement, depicted in figure 2.5, shows that the diffusion coefficient of the water molecules is highly dependent on the presence of the chloride ion. The diffusion coefficient of the water molecules in the solvation shell around the chloride ion is approximately 2 times smaller than the diffusion coefficient outside this shell. The ratio of the two diffusion coefficients is computed from the slope of the mean-squared displacement of the water molecules inside and outside the first solvation shell in the $2-6$ ps time interval. The residence time of a water molecule in the first solvation shell is the average time that a water molecule spends in this shell. Here we used Impey's definition for the residence time:[38,45]

$$n_{Cl}(t) = \frac{1}{N_t} \sum_{n=1}^{N_t} [\theta(r,t) \times \theta(r,0)], \tag{2.1}$$

where $\theta(r,t)$ is the Heaviside unit step function, which is 1 when a water molecule is within the first solvation shell of the ion and 0 otherwise. N_t is the average number of water molecules in this shell. A plot of the time average of this function ($n_{Cl}(t)$) is shown in figure 2.6. The residence time is defined as the decay time of the mono-exponential fit of this function, for which we find a value of 12 ps. We estimate the margin of error at approximately 3 ps. Experimentally, the residence time can be probed indirectly by pump-probe spectroscopy. Using this technique Kropman *et al.* determined a value of 12 ± 4 ps by fitting the measured transient spectrum to a number of Brownian oscillators.[35] The time constant τ_c of the Brownian oscillator that represents the O-H$\cdots$Cl$^-$ component is assumed to be a measure for the residence time of a water molecule in the coordination shell. A more direct comparison could

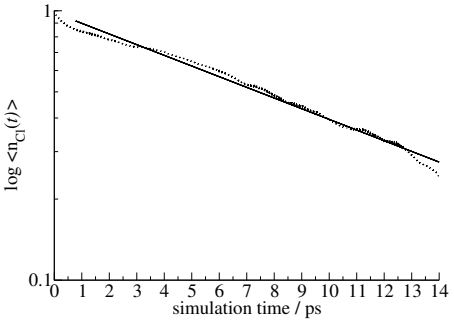

Figure 2.6: Logarithmic plot of the time averaged residence time correlation function as defined by Impey *et al.*[38,45] (dotted line) and the mono-exponential fit (solid line) of this function with a characteristic time constant of 12 ps.

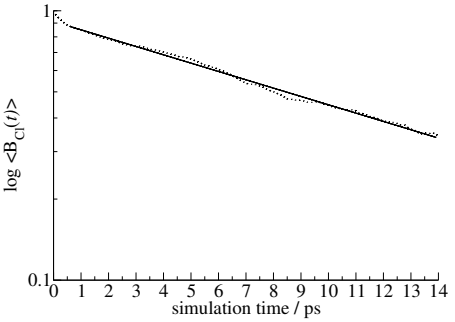

Figure 2.7: Logarithmic plot of the time averaged bond length correlation function for the Cl–H hydrogen bond length in the first solvation shell (dotted line). The solid line is a fit of a mono-exponential function with a time constant of 14 ps (see text).

be obtained by relating τ_c to the calculated decay time of the H–Cl^- bond length time correlation function, defined as:

$$B_{Cl}(t) = \frac{1}{N_t} \sum_{n=1}^{N_t} [l(r,t) \times l(r,0)], \tag{2.2}$$

where $l(r,t)$ is the distance between the chloride ion and the nearest hydrogen atom of a water molecule in the first coordination shell at a particular time. The time average of this function is shown in figure 2.7, accompanied by the mono-exponential fit. The characteristic time constant of the fit is 14 ps, with an estimated error margin of approximately 3 ps. This value agrees, within the margin of error, with the experimental result of 12 ± 4 ps. Not only does this result prove that the method used is well adapted for this system, also the assumption that the correlation time constant is an indication for the residence time seems to be valid.

The frequency spectrum of the velocity autocorrelation function of all water atoms is shown in figure 2.8. A red shift of the O–H stretch vibration (around 2300 cm^{-1}) of ca. 100 cm^{-1} is observed, when going from the bulk water molecules to the solvation shell molecules. This should be attributed to the strong hydrogen bonding of the solvated water molecules to the chloride ion. There was no observable change in the geometry of the solvated water molecules when compared to the bulk water molecules.

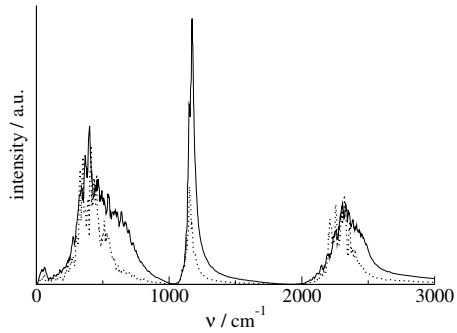

Figure 2.8: Comparison of the frequency spectra of deuterated water molecules in the first solvation shell (dotted line) and outside this shell (solid line).

Electronic properties

The molecular charge distribution was studied using the method of maximally localised Wannier functions. It provides an unambiguous route to assign dipole moments to individual molecules in a condensed phase by assuming that the electronic charge is distributed as point charges located on the Wannier Function Centres (WFCs). We find no direct influence of the chloride ion on the dipole moment of the water molecule. The calculated dipole moment of the water molecules inside and outside the first solvation shell are equal, 3.14 ± 0.57 and 3.15 ± 0.65 D, respectively, and similar to the value of 3 D obtained by CPMD-BLYP for pure bulk water.[2] Figure 2.9 shows the distribution of the dipole moment of water molecules inside and outside the first solvation shell of chloride. The fact that there is no difference in the dipole

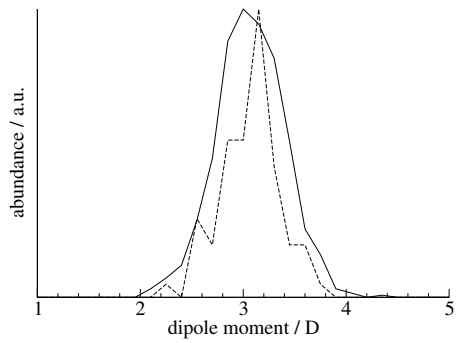

Figure 2.9: Distribution of the dipole moment of water molecules in the first solvation shell (dashed line) and bulk water molecules (solid line).

moment has also been observed in a CPMD calculation of the aqueous solvation of the bromide ion.[11] Based on the positions of the chloride ion and the surrounding WFCs we computed the dipole moment for the ion. In most of the 13 sampled conformations the dipole moment is around 1 D, in accordance with the results of Tobias *et al*.[50] However, in two cases the dipole moment is as large as 4 and 5 D. A more extensive sampling of the positions of the WFCs is necessary for a better defined dipole moment of the chloride ion.

2.4 Conclusions

We report the results of a DFT-based molecular dynamics simulation of the aqueous solvation of one chloride ion. The observed solvation structure agrees with results from previous simulations and experiments. The results on the dynamic behaviour of the system support the idea that the first coordination shell around the chloride ion is relatively rigid. The diffusion coefficient of water molecules in the first solvation shell is decreased by a factor of ca. 2, compared to bulk water molecules. We calculated a value of 12 ps for the first solvation shell residence time, which is in good agreement with recent pump-probe spectroscopic measurements. In order to arrive at a more direct comparison between the spectroscopic results and our results, we defined a bond length time correlation function. The decay time of this function is also in good agreement with the experimental value. Furthermore, our results show that there is only a very small influence of the chloride ion on the charge distribution of the coordinating shell of water molecules. The dipole moment of coordination shell water and bulk water molecules is identical. Also the geometry of the water molecules remains unchanged. However, the frequency spectrum of the water molecule does show a small influence of the chloride ion. The O–H stretch vibration of solvation shell molecules is red-shifted by ca. 100 cm^{-1}. This effect is attributed to the formation of strong hydrogen bonds between the chloride ion and the water molecule.

Chapter 3

Density functional theory based molecular-dynamics study of aqueous fluoride solvation[†]

Abstract

We use density functional theory based molecular-dynamics simulations to study the aqueous solvation of the fluoride anion. Our studies are focused on the first solvation shell and have resulted in detailed information on its structural and dynamical properties. The fluoride ion leads to the formation of a rigid solvation shell, qualitatively consistent with simulation and experimental studies, classifying fluoride as a 'structure making' particle. However, quantitatively we find the solvation shell to be less structured and more mobile than predicted from empirical force field simulations. The influence on the intramolecular electronical and structural properties of water are minimal, as observed for other halogens. We propose two distinct mechanisms for the exchange of bulk and first solvation shell water molecules.

[†]This chapter is based on J.M. Heuft and E.J. Meijer *J. Chem. Phys.* **2005**, *122*, 094501.

3.1 Introduction

Aqueous solvation of ions plays an important role in a wide range of chemical and biological systems. The aqueous solvation of simple atomic ions has been the subject of numerous experimental and theoretical studies, focusing on small ion-water clusters,[63–69] bulk solvation[7,8,35,38,62,70–77] and biological applications.[78–80] The interactions between the charged ion and the neighbouring water molecules may have a distinct effect on the structure and dynamics of the water surrounding the ion. It is well known that water forms a highly structured network of hydrogen bonds in the liquid phase. Introducing an impurity such as an ion into the network can severely influence the local water structure. Depending on a number of factors such as Van der Waals radii, charge and polarisability, the solvation of the ion may range from a strongly bonded, well defined ion-water complex that enhances the bulk water network structure, to a situation where the ion binds weakly to the water molecule and strongly disrupts the bulk water network structure locally. These types of ions are commonly referred to as structure makers and breakers, respectively. In the present chapter we will consider the aqueous solvation of the fluoride anion. Experimental data on the microscopic properties of aqueous fluoride solvation is rather limited, whereas the computer simulation studies appear to yield conflicting results for various properties. X-ray diffraction[81] of a dilute fluoride solution yields a coordination number of 4.5, with the position of the first peak of the fluoride-oxygen radial distribution function at 2.62 Å. Recent computer simulations employing empirical force fields[45,76,82] yield a coordination number of ca. 6, with a sharply peaked radial distribution of the water molecules around the fluoride. In contrast, Monte Carlo simulations based on hybrid quantum mechanical/empirical force fields (QM/MM) suggest a lower coordination of 4-5,[62,70,83] and a broader first peak of the fluoride-water radial distribution functions. Experimental studies of dynamics of the fluoride hydration have provided data for the anion self-diffusion and the rotational correlation time of the solvating water molecules.[77] Molecular dynamics (MD) simulations[38,45,82] yield self-diffusion values quantitatively similar to the experimental value. These simulations also provide estimates for the residence time of the first shell water molecules in the range of $20 - 29$ ps. Other aspects of the dynamics of fluoride hydration, such as the water-exchange mechanism between the first and second solvation shell have not yet been properly addressed.

In this chapter we will study the aqueous solvation of the fluoride anion using *ab initio* molecular dynamics. We will use density functional theory (DFT) to describe the interatomic interaction and use the Car-Parrinello approach to perform the MD simulations. These simulations will provide us with detailed structural, dynamical

and electronic properties. The viability of this approach has been demonstrated in a number of studies of the hydration of other ions.[11,48,72,73,84–89]

Important advantages of DFT-MD over force-field MD are that it intrinsically incorporates the many-body interactions including polarisation and that it accounts for the intra-molecular motion and therefore allows for a direct comparison with spectroscopy of intra-molecular vibrations. Additionally, it yields detailed information on the electronic properties, such as the energy levels of electronic states and the charge distribution. These advantages also partly apply to QM/MM based simulations of fluoride hydration.[62,70,83] However, the QM/MM method still relies partly on empirical force fields and may yield spurious effects due to coupling of the quantum and classical regions. Moreover, these QM/MM studies employed the Monte Carlo method, and consequently did not yield dynamical properties.

3.2 Computational Details

For the present study of aqueous fluoride solvation we followed a similar setup as for our earlier study of the chloride ion.[72] This allows us to compare the results of the two ions in a consistent way. Electronic structure calculations are performed using the Kohn-Sham formulation[26] of DFT,[55] where we employed the gradient-corrected BLYP functional.[27,28] This functional provides a good description of aqueous systems.[56] Molecular dynamics simulations are performed using the Car-Parrinello approach,[25] as implemented in the CPMD software package[†]. The Kohn-Sham orbitals are expanded in plane waves with an energy cutoff of 70 Ry. Only valence electrons are considered explicitly, with a semi-local norm-conserving Martins-Troullier pseudopotential taking into account the interactions between the core and valence electrons. The cutoff radius for the pseudopotentials is 0.50, 1.10 and 1.00 a.u. for H, O and F, respectively. The system consists of one fluoride ion and 64 water molecules in a periodic cubic cell of 12.5^3 Å^3, yielding the experimental density. A cell of this size contains two solvation shells. The temperature of the system during the simulation is set to 300 K and controlled by a Nosé-Hoover thermostat[61] with a period of 66.7 fs (500 cm^{-1}). It is not expected that the thermostat will influence the dynamical properties of the fluoride solvation shell, as the thermostat period is two orders of magnitude shorter than the typical timescale of the rearrangement of the fluoride solvation shell. Overall charge neutrality is achieved by adding a uniform positive background charge to compensate for the negative charge of the fluoride ion. All hy-

[†]CPMD 3.7.1, Copyright IBM Corp 1990-2004, Copyright MPI für Festkörperforschung Stuttgart 1997-2001.

method	$F^-(H_2O)$	$F^-(H_2O)_2$[a]	$F^-(H_2O)_2$[b]	$F^-(H_2O)_3$[a]	$F^-(H_2O)_3$[b]	$F^-(H_2O)_4$
CPMD ΔE_{bond}	-26.8	-23.3	-23.6	-21.1	-20.9	-18.9
ADF ΔE_{bond}	-31.0	-25.8	-25.8	-22.6	-22.5	-20.1
Gaussian[c] ΔE_{bond}	-26.7	-23.4	-23.5	-21.1	-21.0	-19.0
CPMD ΔE_{seq}	-26.8	-19.9	-20.4	-16.6	-15.6	-12.8
ADF ΔE_{seq}	-31.0	-20.5	-20.6	-16.3	-15.8	-13.1
Gaussian[c] ΔE_{seq}	-26.7	-20.0	-20.2	-16.5	-16.3	-12.8
Experimental ΔH_{seq}[d]	-26.2±0.8	-19.2±0.5		-15.3±0.4		-13.9±0.4

a. planar conformation
b. non-planar conformation
c. Reference 66
d. References 7 and 8

Table 3.1: Comparison of bonding energies per bond and sequential energies of solvation for a number of small fluoride water clusters. All values are in kcal/mol.

drogen atoms are assigned the mass of deuterium in order to improve decoupling of the dynamics of the ionic and electronic subsystem over a longer period of time, and allowing for a larger timestep in the numerical integration of the equations of motion. The fictitious mass μ associated with the plane-wave coefficients is set at 900 a.u. allowing for a timestep of 6.0 a.u. (0.145 fs) in the numerical integration of the equations of motion. We observe no drift in the electronic kinetic energy during the total simulation time of 20.3 ps, including 2 ps for equilibration. We compared energy-optimised geometries of small fluoride–water clusters ($F^-(H_2O)_{1-4}$), obtained from CPMD, literature[66] and ADF[†] to validate the parameters in the CPMD simulations, in particular the plane wave cutoff and the parameters of the pseudopotentials. Table 3.1 lists the results. The sequential energies of solvation and total binding energies of the fluoride–water clusters are within 0.6% of the values that were calculated by Baik *et al.*[66] using a BLYP/6-311++G** basis set. The differences in energies with ADF are somewhat larger, 1 - 3% for the larger water clusters ($n > 1$). Bond lengths and angles are identical within 2% when compared to ADF and within 3% when compared to Baik *et al.*

[†]ADF 2002.02, SCM, Theoretical Chemistry, Vrije Universiteit Amsterdam, The Netherlands, http://www.scm.com. Molecular orbitals are expanded in a quadruple ζ Slater-type basis set augmented with 2p and 3d polarisation functions for H and 3d and 4f polarisation functions for O and F.

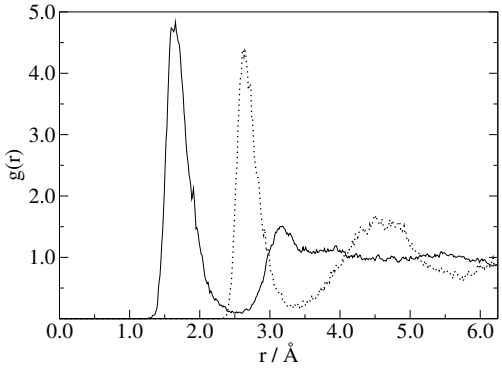

Figure 3.1: Radial distribution functions for F–H (solid line) and F–O (dotted line).

ion	R_{H_1}/Å (n_R)	R_{H_2}/Å	R_{O_1}/Å (n_R)	R_{O_2}/Å
F^-	1.66 (5.0)	3.16	2.66 (5.1)	4.53
Cl^-	2.19 (5.2)	3.69	3.13 (5.8)	4.84

Table 3.2: Positions and normalised integrals of peaks in the radial distribution functions of fluoride and chloride.[72]

3.3 Results and Discussion

In this section we will compare our present results for fluoride to our previous DFT-MD study of the aqueous solvation of chloride.[72]

Structure The radial distribution functions (RDFs) for F–H and F–O are shown in figure 3.1. Table 3.2 contains a summary of quantitative data from the RDFs, including data for the chloride anion for comparison. Both for the F–O and F–H RDF the first peak is pronounced and followed by a deep minimum. This suggests a well-defined first solvation shell with an almost complete depletion of water molecules between the first and second solvation shell. The RDFs also give information on the effect the ion has on the water structure on a larger length scale. After the first two peaks of the hydrogen RDF, encompassing both hydrogen atoms of the first shell water molecules, the RDF appears structureless. Although the differences are small, it seems that chloride yields a slightly more structured second solvation shell. This must be attributed entirely to the larger size of the chloride ion. The difference between the RDF peak positions for Cl–H and F–H is a consequence of the difference of the Van der Waals radii of the ions. This explanation also holds for the Cl–O and F–O RDFs.

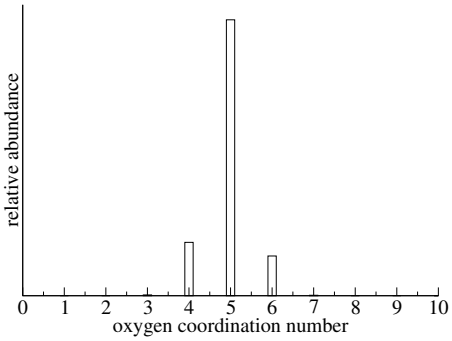

Figure 3.2: Histogram of the coordination number based on the F–O distance.

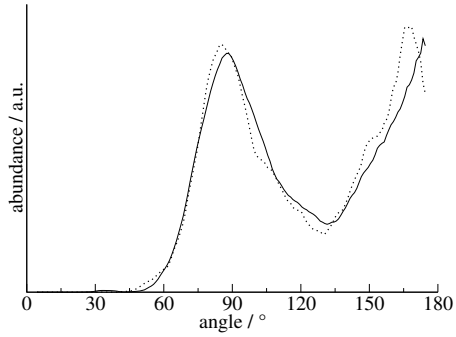

Figure 3.3: Distribution of the H–F–H angle (solid line) and O–F–O angle (dotted line) of water molecules in the first solvation shell.

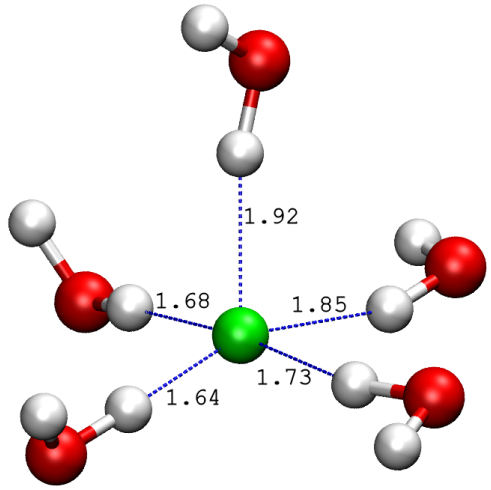

Figure 3.4: Square pyramidal coordination sphere of fluoride. The numbers accompanying the H-bonds (dotted lines) are the interatomic distances in Å.

We define a water molecule to be in the first solvation shell if it is within the minimum beyond the first peak of a RDF. For the F–O and F–H RDFs this distance is 3.41 Å and 2.60 Å, respectively. The average coordination number obtained by integrating the first peak of the RDF up to this minimum yields a value of 5 for both the F–O and F–H RDF. The distribution of coordination numbers based on the F–O distance is plotted in figure 3.2 and is sharply peaked at 5. The F–H distance based coordination distribution (not plotted) is virtually the same. These structural data are quantitatively similar to those obtained with a Monte Carlo simulation using a newly developed *ab initio* based water-fluoride potential.[83] Compared to two recent QM/MM simulation studies[62,70] that yielded a coordination of 4.5 and a F–O RDF first peak height of ca. 3, our data show a slightly more structured coordination, with a peak height of ca. 5. In contrast, when compared to most simulations based on empirical potentials yielding coordinations of approximately 6 with F–O RDF first peak heights of around 8, our simulation shows a significantly less structured coordination.

Figure 3.3 provides a picture of the angular distribution of the water molecules in the first solvation shell. Plotted are the distributions of the H–F–H and O–F–O angles, showing maxima at 90° and 180° and a minimum near 120°. This distribution suggests that a square pyramidal structure is dominant over the trigonal bi-pyramid arrangement. A typical square pyramidal configuration is shown in figure 3.4. These observations are consistent with the findings of QM/MM simulations.[62,70]

Inspection of the hydrogen bonding of the first solvation shell water molecules shows that they participate rather naturally in the bulk water hydrogen bond network. The average total number of hydrogen bonds of water molecules in the first coordination sphere is only slightly smaller than in pure bulk water,[90] 3.1 versus 3.4, with 50 % of the hydrogen bonds located within the first shell and 50 % involving water molecules from the second solvation shell. Apparently, the ion and its first coordination shell do not form an isolated sphere but it is integrated quite naturally in the surrounding highly structured hydrogen bond network, consistent with the common notion that fluoride is a structure maker.

Dynamics

An important characteristic of the solvation dynamics is the vibrational spectrum of the coordinating water molecules. In figure 3.5 we plot the frequency spectrum of the velocity autocorrelation function of the first solvation shell water molecules and that of the bulk water molecules to study the influence of the ion on the vibrational motion. The O–H stretch vibration shows a red-shift of 100 cm^{-1}. This shift is similar to that observed for chloride, and can be attributed to the relatively strong hydrogen bond with the fluoride ion.

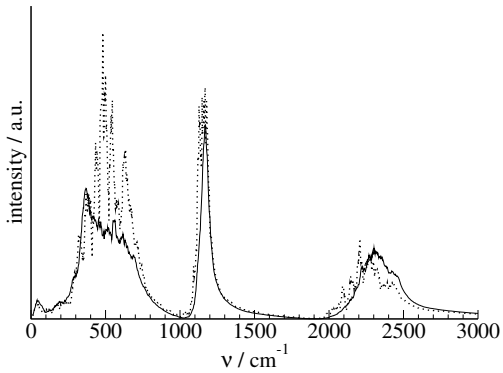

Figure 3.5: Comparison of the calculated frequency spectra of deuterated water molecules in the first solvation shell (dotted line) and outside this shell (solid line).

A second important characteristic of the solvation dynamics is the average residence time of water molecules in the first solvation shell, and the related exchange mechanism of these water molecules with the surrounding. To quantify the residence time we employed the time correlation function defined by Impey,[38] as shown in figure 3.6, accompanied by its mono-exponential fit. The decay time of this function yields a residence time of 16 ps, with an estimated error margin of approximately 3 ps. Alternatively, we considered the F–H bond length time correlation function:

$$B_F(t) = \frac{1}{N_t} \sum_{n=1}^{N_t} [l_n(t) \times l_n(0)], \tag{3.1}$$

where N_t is the average number of water molecules in the first solvation shell and $l_n(t)$ is the distance between the fluoride ion and the nearest hydrogen atom of a water molecule n in the first coordination shell at a particular time t. The characteristic decay time of the exponential fit of this function, shown in figure 3.7, is 16.8 ps. The error margin is estimated at circa 3 ps.

If we compare these values for the residence time to the first solvation shell residence time observed in our DFT-MD simulation of the solvation of the chloride anion, 12 ps and 14 ps, respectively, the slower dynamics of the fluoride shell is evident. This conclusion is supported by comparing the slope of the mean squared displacement function, shown in figure 3.8. While the chloride anion showed a two-fold difference between the mobility of water molecules in the shell and bulk water molecules, this factor is 3 in the case of the fluoride ion. Our results for the residence time indicate somewhat faster dynamics than those obtained with empirical force field simulations,

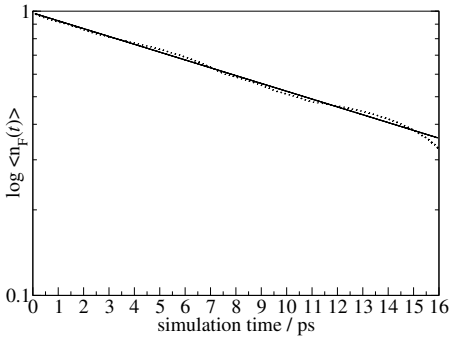

Figure 3.6: Logarithmic plot of the time averaged residence time correlation function as defined by Impey *et al.* (dotted line) and the mono-exponential fit (solid line) of this function with a decay time of 16 ps.

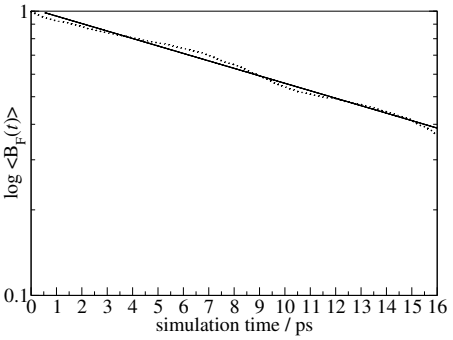

Figure 3.7: Logarithmic plot of the time averaged bond-length correlation function for the F–H hydrogen-bond length in the first solvation shell (dotted line). The solid line is a mono-exponential fit with a characteristic time constant of 16.8 ps.

that yield residence times in the range of $20-29$ ps.[38,45,82] This discrepancy between DFT-MD and force field simulations is consistent with the more structured solvation shell observed in the force field simulations, as mentioned above. No experimental data for the residence time for fluoride solvation shell are available. However, the good agreement between DFT-MD[72] and experiment[35] for the residence time for chloride (12 ps) suggests DFT-MD provides a more accurate value for the residence time than empirical force field simulations.

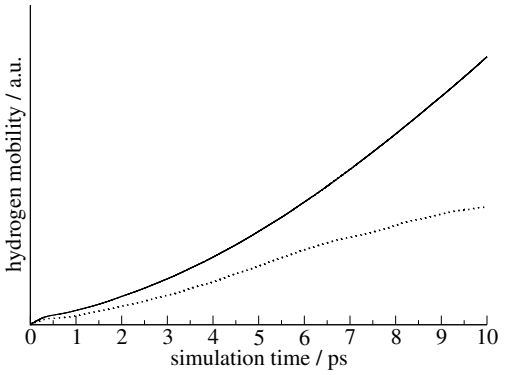

Figure 3.8: Comparison of the mobility of the water molecules inside (dotted line) and outside (solid line) the first solvation shell.

The structural analysis indicated that the arrangement of the water in first solvation shell around the fluoride was predominantly a square pyramid (see figure 3.4). Closer inspection revealed that in this arrangement one of the water molecule is usually somewhat more mobile than the other four. Both the F–H distance and the F–H–O angle of this molecule fluctuate more than for the other coordinating water molecules. For this molecule the F–H distance is on average circa 1.8 Å, but occasionally increases for short periods to values of up to 3.0 Å. Apparently its hydrogen bond with fluoride is weaker than that of the other water molecules. It turns out that this also plays a role in the water-exchange exchange mechanism between the first and second solvation shell. In the 20 ps trajectory we observed in total 6 water exchanges. Note that, given an average coordination of 5, this is consistent with calculated residence time of 16 ps. Analysis of the 6 exchange processes revealed two distinct mechanisms. Illustrative snapshots of the first mechanism are shown in figure 3.9, showing the initiating state (a), two intermediate states (b and c) and final situation (d). This mechanism is a sequential process: first the most mobile first shell water molecule moves away from the fluoride up to a F–H distance of approximately 3 Å (figs. 3.9(a) and 3.9(b)), yielding a 4-fold coordinated fluoride ion. Subsequently, a second shell water molecule, initially hydrogen bonded to a first solvation shell water molecule, rotates such that this hydrogen bond is broken and one with the fluoride ion is formed (figs. 3.9(c) and 3.9(d)). During the exchange the other 4 solvation shell water molecules rearrange, sometimes forming a tetrahedral-like structure.

The second mechanism proceeds in a more concerted manner and shows different relative positions of the entering and leaving water molecule. In the sequential mechanism the exchange involves two water molecules next to each other, making an angle of ca. 90°. In contrast, in the concerted mechanism a water molecule approaches the base of the pyramidal structure and pushes a water molecule at the opposite side of the fluoride ion out. Snapshots illustrating this mechanism are depicted in figure 3.10. Figure 3.10(a) shows the predominant five-fold coordination sphere with one elongated water-fluoride hydrogen bond (topmost water molecule). A second solvation shell water molecules rotates, approaches from below, and forms a hydrogen bond with fluoride. At the same time the opposite water molecule leaves the fluoride. This exchange involves a short lived intermediate six-fold coordinated structure (fig. 3.10(b)). The final configuration is again a 5-fold coordinated square pyramid (fig. 3.10(c)). Of the 6 observed exchanges, the sequential mechanism seems prevalent (4×) over the concerted process (2×). A single exchange process occurred in 0.3–1.0 ps.

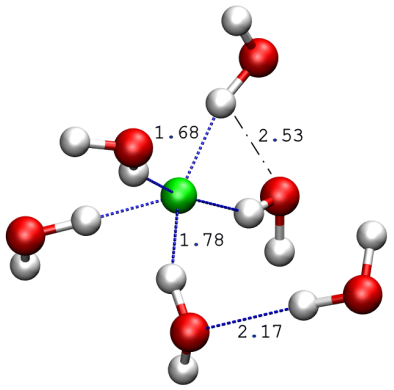

(a) (0.0 ps) The situation just before the event, a slightly distorted pyramidal coordination of 5 water molecules.

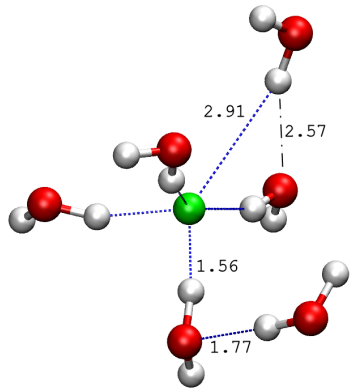

(b) (0.2 ps) Situation during the event. One hydrogen–fluoride hydrogen bond is elongated (top-right) while room is created for the bottom-right water molecule to approach.

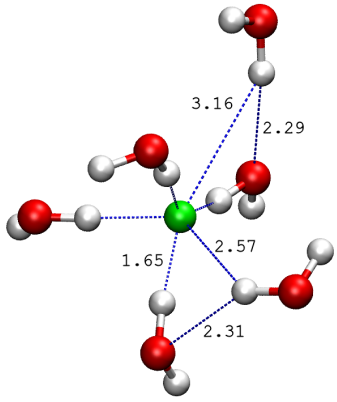

(c) (0.3 ps) The water molecule at the bottom-right, currently in the second solvation shell, is rotating. It forms a hydrogen bond with fluoride while the water molecule at the top-right is rotating away from the fluoride ion.

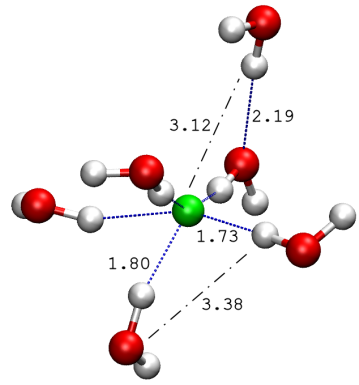

(d) (0.4 ps) Final situation. The water molecule in the bottom-right has rotated completely and forms a full hydrogen bond with fluoride. The water molecule at the top-right has entered the second solvation shell and now forms a hydrogen bond with a first solvation shell water molecule.

Figure 3.9: Process I of water exchange in the first solvation shell. Numbers indicate the length in Å of H-bonds (dotted lines) and some interatomic distances (dash-dotted lines).

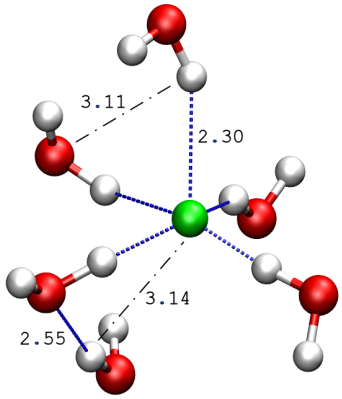

(a) (0.0 ps) Before the exchange process the F–H bond of the topmost coordinating water molecule elongates.

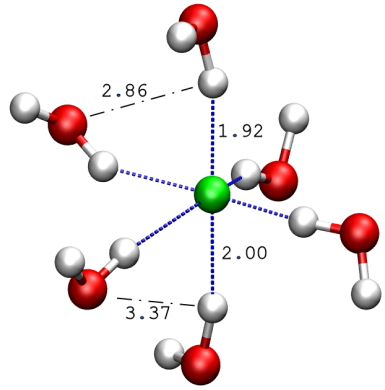

(b) (0.4 ps) Situation during the exchange. The lower-middle water molecule rotates to form a hydrogen bond with fluoride. This results in a temporary six-fold coordination sphere.

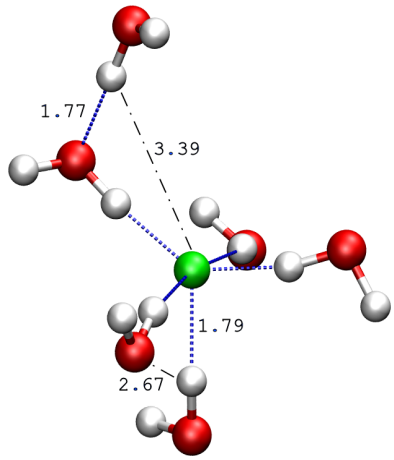

(c) (0.8 ps) Final situation. The six-fold coordination is unstable. The topmost water rotates and moves away from the fluoride to enter the second solvation shell. A distorted pyramidal structure remains.

Figure 3.10: Process II of water exchange in the first solvation shell. Numbers indicate the length in Å of H-bonds (dotted lines) and some interatomic distances (dash-dotted lines).

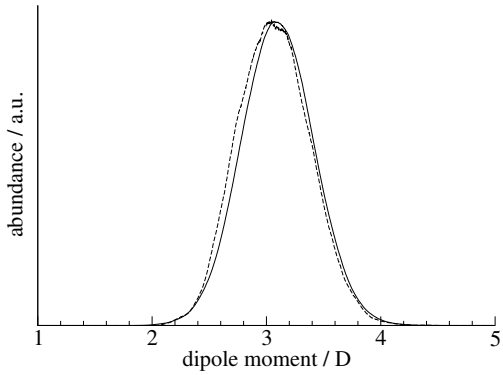

Figure 3.11: Distribution of the dipole moment of water molecules in the first solvation shell (dashed line) and bulk water molecules (solid line).

Electronic properties

We quantified the molecular charge distribution using the method of maximally localised Wannier functions.[91,92] We found that in spite of the presence of a fluoride ion, the first solvation shell water molecules have a dipole moment similar to that of the other water molecules: 3.07 D and 3.10 D, respectively, both with a standard deviation of 0.3 D. Also, the distribution of dipole moments of the first solvation shell and other water molecules is very similar, as shown in figure 3.11. The average water dipole moment is equal to the value found in a DFT-MD simulation of bulk water[2] (3 D). Earlier studies of the bromide[11] and chloride anion also found that the ion has no significant influence on the average dipole moment of water molecules in its vicinity. Based on the positions of the ion and its Wannier Function Centres the dipole moment of the fluoride anion ranges from 0.06 to 0.72 D with an average of 0.39 D. For comparison, we calculated an average value of 1 D for chloride. Either the polarisability of the fluoride ion is smaller due to its smaller size or the coordination of water is on average more symmetric, or possibly a combination of both.

3.4 Conclusions

DFT-based molecular dynamics simulations of the aqueous solvation of the fluoride anion has provided us with detailed information on the influence of the ion on the solvent. The localised negative charge on the ion leads to the formation of a well-defined first solvation shell. Water molecules form strong hydrogen bonds with a well-defined distribution of bond-lengths, and remain bonded for a relatively long period of time,

typically 16-17 ps. The fluoride solvation shell appears to integrate well in the normal water structure, with all first shell water molecules having almost the same number of donating and accepting hydrogen bonds as bulk water molecules. This supports the common notion that of the halogen anions, fluoride is the strongest structure maker. Analysis of the mechanism by which water exchange between the first solvation shell and its surrounding takes place, shows two distinct processes. One pathway proceeds via a four-fold coordinated intermediate, whereas the other pathway goes via a six-fold coordinated intermediate, with both mechanisms occurring within 1 ps. As also found in DFT-MD studies of chloride[72] and bromide[11] solvation, the presence of fluoride does not give rise to first solvation shell molecules with a geometry or charge distribution different from bulk water molecules. The only distinction appears for the asymmetrical O–H stretch vibration of first solvation shell molecules. It is red-shifted by about 100 cm^{-1} when compared to bulk water molecules, a feature also observed in chloride solvation.

When compared to recent force fields simulations[45,76,82] our DFT-MD simulations show a less structured coordination and shorter first shell residence times. This supports the conclusions from earlier Monte Carlo simulations employing *ab initio* fluoride-water force fields,[62,70,83] that empirical force fields tend to give rise to a too rigid fluoride solvation shell. Our results may be considered valuable data for further improvement of empirical force fields for aqueous fluoride solvation.

Acknowledgements

We thank Michael L. Klein and Bernd Ensing for inspiring discussions.

Chapter 4

Density functional theory based molecular-dynamics study of aqueous iodide solvation[†]

Abstract

We study the solvation of iodide in water using density functional theory based molecular-dynamics simulations. Detailed analysis of the structural and dynamical properties of the first solvation shell is presented, showing a disruptive influence of the ion on the local water structure. Iodide–water hydrogen bonding is weak, compared to water–water hydrogen bonds. This effective repulsive ion–water interaction leads to the formation of a quite unstructured solvation shell. The dynamics of water molecules surrounding the iodide is relatively fast. The intramolecular structural and electronical properties of water molecules around the ion are not affected.

[†]This chapter is based on J.M. Heuft and E.J. Meijer *J. Chem. Phys.* **2005**, *123*, 094506.

4.1 Introduction

The aqueous solvation of halide ions has been the subject of many experimental and theoretical studies. The properties of solvated ions and surrounding water molecules are important in a large variety of chemical reactions and in biochemical processes. Examples are thyroid afflictions[93–95] and oxidation reactions by peroxidases.[96]

The presence of an ion in an aqueous solution may significantly influence the local water structure. Liquid water under ambient conditions is known to have a highly structured network of hydrogen bonds. An ion interferes with this structure and may influence the behaviour of water molecules locally. Here, properties such as the ionic radius and the strength of the ion–water interaction play an important role.

Acknowledging the importance of this subject, systematic studies of halogens are required to obtain a full understanding of halide ions. In the present chapter we focus on a study of the solvation of the iodide ion, employing *ab initio* molecular dynamics simulations. Among the halides, iodide has the largest ionic radius and the weakest ion–water interaction.

X-ray diffraction studies yield coordination numbers that are significantly scattered, ranging from 6 to 9.[97–99] The first peak of the I–O radial distribution function (RDF) is measured to be in the range $3.60-3.76$ Å. Recent X-ray Absorption Near Edge Structure (XANES) experiments[100] have provided more detailed information on the local structure of the solvated ion. It is shown that the I–H–O angle is slightly nonlinear and that the spectra can be satisfactorily described by taking into account the first hydration shell only. Analysis[101,102] of the O–H stretching vibration in small iodide–water clusters confirms that iodide forms rather weak hydrogen bonds with only a small charge-transfer character. Recent advances in femtosecond mid-infrared nonlinear spectroscopy opened up the possibility to isolate the response of coordinating water molecules from the bulk and probe their dynamical behaviour. Studies employing this technique showed a relatively long correlation time of the I–H–O stretch vibration (18 ± 5 ps).[35] This is associated with a long persistence time of water molecules in the first solvation shell of iodide, longer than in that of chloride (12 ± 4 ps).[72] Surprisingly, measurements of the orientational dynamics in the iodide solvation shell show faster rotational dynamics of the water molecules than in the case of chloride and fluoride ions.[103] Although these observations are not mutually exclusive, they do indicate interesting behaviour of water molecules in the vicinity of iodide, and warrant further investigation.

A large number of studies aimed at the structures of small water–iodide clusters has

been reported. Of special interest is whether interior or surface solvation is preferred. Numerous experiments (e.g. refs. 8, 104, 105) suggest that iodide prefers surface solvation in small water clusters. Theoretical studies confirm the surface solvation of iodide in clusters up to 64 water molecules, due to its weak interaction with water.[106–108] On a larger scale, interesting effects on the microscopic solvation structure and ion concentration near the air/water interface are observed both theoretically[109] and experimentally.[110]

Various force-field based computational studies, either employing Monte Carlo (MC) or molecular dynamics (MD) techniques, of the bulk solvation of the iodide ion have been reported.[40,45,65,82,83,111–113] Structural data obtained from these simulations include an I–O RDF first peak in the range $3.55 - 3.78$ Å and an I–H first peak in the range $2.55 - 2.93$ Å. The first and second RDF peaks show incomplete separation, which suggests a diffuse solvation shell. The calculated coordination number varies from 7.3 to 9.7 based on coordinating oxygen and from 6 to 6.6 based on coordinating hydrogen. The large range of the coordination numbers shows the difficulty of defining a solvation shell due to its diffuse character. The dynamical behaviour of the solvation has been directly probed in studies of the residence time of water molecules in the first solvation shell, that yield values in the range from 7.7 ps to 13.8 ps, depending on parameters of the force-field.

The relatively large spread in measured and calculated structural properties such as the coordination number, and lack of a uniform picture of the dynamics of the solvation shell asks for a detailed high-level theoretical approach to resolve the inconsistencies regarding the solvation of the iodide ion. Here, we study the aqueous iodide solvation using the Car-Parrinello approach to *ab initio* molecular dynamics. Density functional theory (DFT) is used to describe the interatomic forces and thus intrinsically includes all electronic and many-body interactions. This approach has been applied to the aqueous solvation of other halide ions,[11,72,114] where it has provided new insights in the microscopic behaviour of the solvation of halogen ions. For example, by elucidating the mechanism for the shell–bulk water exchange process in the fluoride solvation shell. We employ DFT-MD to investigate the structural, dynamical and electronical properties of the solvation of the iodide ion in water.

4.2 Computational Details

For the present study of aqueous iodide solvation we followed a similar setup as for our earlier study of the chloride[72] and fluoride ion.[114] This allows us to com-

pare the results of all ions in a consistent way. Electronic structure calculations are performed using the Kohn-Sham formulation[26] of DFT,[55] where we employed the gradient-corrected BLYP-functional.[27,28] This functional provides a good description of aqueous systems.[56] Molecular dynamics simulations are performed using the Car-Parrinello approach,[25] as implemented in the CPMD software package[†]. The Kohn-Sham orbitals are expanded in plane waves up to an energy of 70 Ry. Only valence electrons are considered explicitly, with a semi-local norm-conserving Martins-Troullier pseudopotential taking into account the interactions between the core and valence electrons. The cutoff radius for the pseudopotentials is 0.50, 1.10 and 2.10 a.u. for H, O and I, respectively. The system consists of one iodide ion and 64 water molecules in a periodic cubic cell of 12.7^3 Å^3, yielding the experimental density. A cell of this size contains two solvation shells. The temperature of the system during the simulation is set to 300 K and controlled by a Nosé-Hoover thermostat[61] with a period of 66.7 fs (500 cm^{-1}). Overall charge neutrality is achieved by adding a uniform positive background charge to compensate for the negative charge of the iodide ion. All hydrogen atoms are assigned the mass of deuterium in order to improve decoupling of the dynamics of the ionic and electronic subsystem over a longer period of time, and allowing for a larger timestep in the numerical integration of the equations of motion. The fictitious mass associated with the plane-wave coefficients is set at 900 a.u. allowing for a timestep of 6.0 a.u. (0.145 fs). We observe no drift in the electronic kinetic energy during the total simulation time of 20.4 ps, including 2 ps for equilibration.

To validate our computational approach, in particular the plane-wave cutoff and pseudopotential parameters, we compared energy-optimised structures obtained from our CPMD simulations, literature[8,115] and ADF[‡]. Table 4.1 lists the results. The sequential energies of solvation and total binding energies of the iodide–water clusters ($n < 4$) are within 13% of the values that were calculated by Kim *et al.*[115] using an MP2/6-311++G** basis set. The differences in energies with ADF are similar, but decrease with increasing cluster size. Bond length and angles are identical within 5% when compared to ADF and within 4% when compared to Kim *et al*. A comparison with experimental sequential solvation enthalpies[8] shows very good agreement for the smaller ($n < 4$) iodide–water clusters.

[†]CPMD 3.7.1, Copyright IBM Corp 1990-2004, Copyright MPI für Festkörperforschung Stuttgart 1997-2001.

[‡]ADF 2002.02, SCM, Theoretical Chemistry, Vrije Universiteit Amsterdam, The Netherlands, http://www.scm.com. Molecular orbitals are expanded in a triple ζ Slater-type basis set augmented with 2p and 3d polarisation functions for H and 3d and 4f polarisation functions for O. A ZORA basis set augmented with 5d and 4f polarisation functions was used for I.

method	$I^-(H_2O)$	$I^-(H_2O)_2$[a]	$I^-(H_2O)_2$[b]	$I^-(H_2O)_3$[a]	$I^-(H_2O)_3$[b]	$I^-(H_2O)_4$
CPMD ΔE_{bond}	-9.94	-9.13	-9.64	-9.08	-9.14	– 9.98
ADF ΔE_{bond}	-11.1	-10.6	-10.8	-9.82	-9.98	– 10.5
Gaussian[c] ΔE_{bond}	-10.6		-10.7		-9.67	-9.23
CPMD ΔE_{seq}	-9.94	-8.32	-9.34	-8.97	-8.14	– 12.5
ADF ΔE_{seq}	-11.1	-10.0	-10.4	-8.30	-8.44	– 12.0
Gaussian[c] ΔE_{seq}	-10.6		-10.8		-8.90	-7.90
Experimental ΔH_{seq}[d]	-10.3±0.3		-9.5±0.2		-9.2±0.2	-9.2±0.4

a. planar conformation
b. non-planar conformation
c. Reference 115
d. Reference 8

Table 4.1: Comparison of bonding energies per bond and sequential energies of solvation for a number of small iodide–water clusters. All values are in kcal/mol.

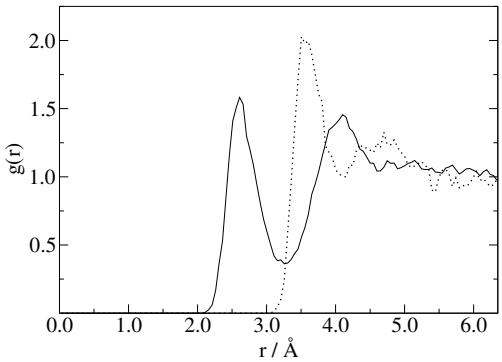

Figure 4.1: Radial distribution functions for I–H (solid line) and I–O (dotted line).

source	R_{H_1}/Å (n_R)	R_{H_2}/Å	R_O/Å (n_R)
present work	2.61 (5.1)	4.10	3.55 (6.6)
MCDHO MC[a]	2.71 (6)	-	3.64 (8.3)
TIP4P MD[b]	2.77	-	3.71 (9.7)
SPC/E MD[c]	2.70	-	3.60 (7.3)

a. Reference 83
b. Reference 113
c. Reference 40

Table 4.2: Positions and normalised integrals of peaks in the radial distribution functions of iodide.

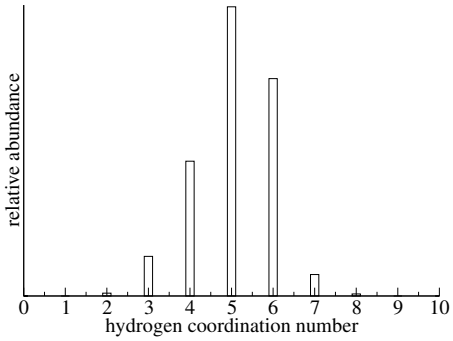

Figure 4.2: Histogram of the coordination number based on the I–H distance.

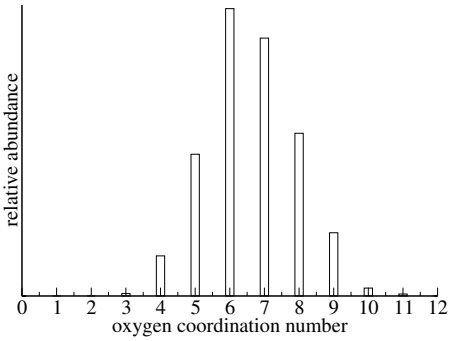

Figure 4.3: Histogram of the coordination number based on the I–O distance.

4.3 Results and Discussion

Structure

Figure 4.1 shows the radial distribution functions for I–H and I–O. Quantitative data from the RDFs is summarised in table 4.2, accompanied by literature data. The positions of the RDF peaks agrees well with other simulations. The low intensity first peak is followed by a high minimum, especially in the I–O RDF. A second peak is appearing in the I–H RDF but hardly present in the I–O RDF. The incomplete separation of the peaks, in combination with the fact that they are relatively broad and low, leads to the conclusion that the solvation shell of iodide is rather unstructured and diffuse. Based on the RDFs, a first solvation water molecule is characterised by an I–H distance less than 3.26 Å or an I–O distance less than 4.15 Å. Integration of the RDF first peaks leads to a coordination number of 5.1 and 6.6, based on the RDFs of I–H and I–O, respectively. Most force field simulations tend to predict higher coordination numbers ranging from 7.7 - 9.7.[45,82,112,113] Figures 4.2 and 4.3 show the histograms of the distribution of the coordination numbers, based on the I–H and I–O distance criterium, respectively. Both distributions are very broad, providing more evidence for a unstructured solvation shell. Consistent with the conclusion of an unstructured coordination sphere are the H–I–H and O–I–O angle distributions of water molecules in the first solvation shell, shown in figure 4.4. The clearest feature is a peak around 80°, for both angle distributions. Smaller peaks are visible at ca. 130°and 150°, for the H–I–H and O–I–O angle, respectively. None of the features, however, are very distinct and visual inspection of the solvation shell does not lead to the identification of well-defined characteristic conformations of water molecules around the iodide ion.

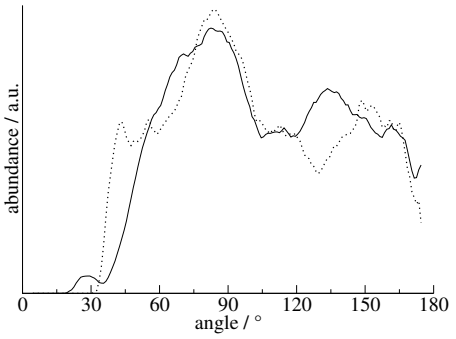

Figure 4.4: Distribution of the H–I–H angle (solid line) and O–I–O angle (dotted line) of water molecules in the first solvation shell.

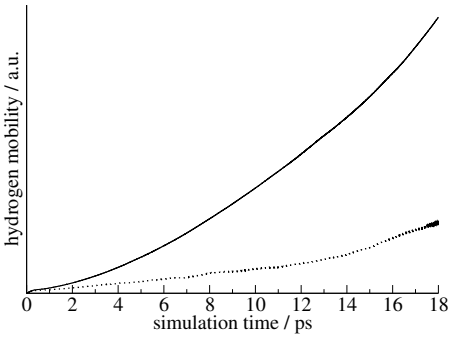

Figure 4.5: The mobility of water molecules within (dotted line) and outside (solid line) the first solvation shell.

The last structural property we investigate is the local hydrogen-bond network around the iodide ion. Analysis of the hydrogen bonding of first solvation shell water molecules shows that 63% of all hydrogen bonds are formed within this shell, while only 37% extend into the bulk water. Previously we found that the coordination sphere of fluoride integrates naturally into the water hydrogen-bond structure with a 1:1 ratio of intra- and extra-shell hydrogen bonds. Iodide forms more of an isolated sphere of surrounding water molecules that participate less in the local water structure. The total number of hydrogen-bonds of solvation shell water molecules is lower too, 2.5 per water molecule on average. For comparison, solvation shell water molecules around fluoride have on average 3.1 hydrogen bonds, pure bulk water molecules have 3.4.[90]

Dynamics

The unstructured layout of the solvation shell is reflected in its dynamical behaviour. During the total simulation time of 20.4 ps there are 15 shell-bulk water exchange processes. Figure 4.5 shows the relative mean-squared displacement of inner- and outer-shell hydrogen atoms. The ratio of the slopes in the linear regime is 1.9, slightly lower than 2 for chloride,[72] indicating faster dynamics. The shell persistence time correlation function[38] is shown in figure 4.6. The residence time that we calculate from this function is 7.3 ps and is in good agreement with 7.7 ps from forcefield MD simulations[45] using the SPC/E model for water. The O–H bond-length correlation function[114] is shown in fig. 4.7. The mono-exponential fit of this function has a characteristic time constant of 9.9 ps. Both our values are consistent with each other within the estimated margin of error of ca. 3 ps. However, Koneshan *et al.*, using the SPC/E model, calculates a value of 13.8 ps.[82] Also, the experimental value of 18 ± 5 ps,[35] obtained using femtosecond mid-infrared nonlinear spectroscopy, disagrees with our

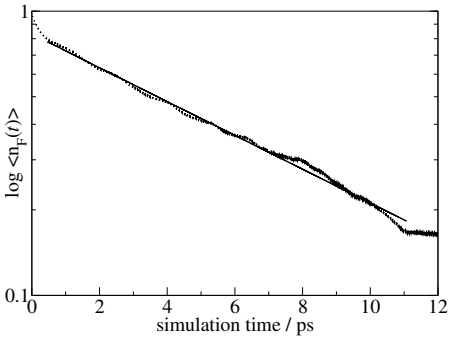

Figure 4.6: Logarithmic plot of the time averaged residence time correlation function (dotted line) and its mono-exponential fit (solid line) with a decay time of 7.3 ps.

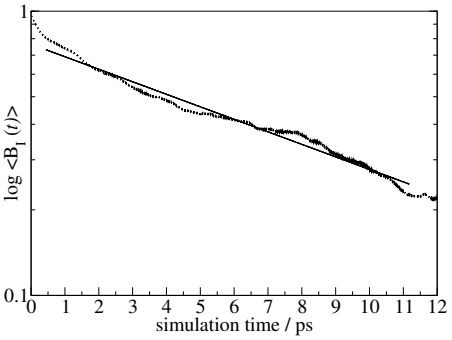

Figure 4.7: Logarithmic plot of the time averaged bond length correlation function (dotted line) and its mono-exponential fit (solid line) with a decay time of 9.9 ps.

results. To understand the discrepancy with this latter value, we calculated the vibration correlation time of the I$\cdots$H–O intramolecular O–H bond, which can be compared more directly to the experimental result. The time constant of this correlation function is 9.7 ps, consistent with our calculated residence time. The faster dynamics of our simulated system might be caused by the difference in concentration. Kropman *et al.* show that the I$\cdots$H–O vibration correlation time is concentration dependent, ranging from 18 to 25 ps for concentrations of 1 to 6 M.

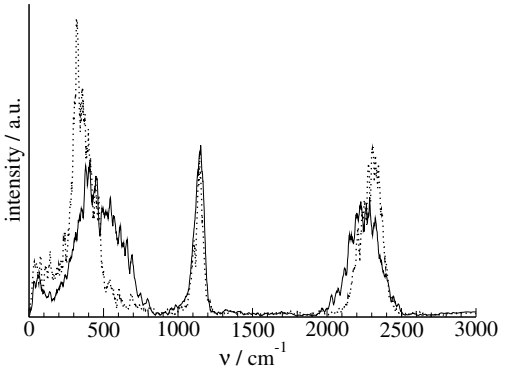

Figure 4.8: Comparison of the frequency spectra of deuterated water molecules within (dotted line) and outside (solid line) the first solvation shell of iodide.

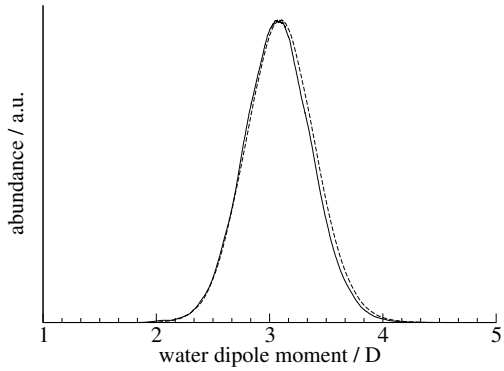

Figure 4.9: Distribution of the dipole moment of water molecules in the first solvation shell (dashed line) and bulk water molecules (solid line).

The asymmetrical O–H stretch vibration of water molecules from the first solvation shell is blue-shifted by approximately 70 cm^{-1}, compared to the stretch vibration of water molecules outside the shell (fig. 4.8). The excellent agreement with the experimentally measured shift (65 cm^{-1}), from double difference infrared spectroscopy,[37] should be considered coincidental, however, since the absolute values of the vibrational frequencies do not agree. Iodide follows the trend that for increasing ion radius $F^- < Cl^- < Br^- < I^-$, the O–H stretching frequency increases due to weakening of the hydrogen bond with the ion. Chloride– and fluoride–water hydrogen-bonds are stronger than inter-water hydrogen bonds, resulting in a red-shifted O–H vibration. The blue-shift in the case of iodide indicates that hydrogen bonding with the ion is weaker than the normal inter-water hydrogen bonding. This effective repulsive interaction is possibly the most important reason behind the diffuse character and fast dynamics of the solvation shell. The diffusion constant of the iodide ion that we calculate from the mean squared displacement is $2.8 \cdot 10^{-5}$ $cm^2 \cdot s^{-1}$. This agrees with the value of $2.2 \cdot 10^{-5}$ $cm^2 \cdot s^{-1}$ that we obtain by interpolation of the experimental results[116] to a temperature of 300 K. We have been unable to discover a well-defined mechanism for the bulk-shell water exchange process.

Electronic properties

Dipole moments are calculated using the method of maximally localised Wannier functions. The dipole moment of the iodide ion is 1.3 ± 1.1 D, with the origin of the reference frame chosen at the position of the ion. This value nicely fits the trend of increasing dipole moment with increasing ion radius. Chloride and fluoride have a dipole moment of ca. 1 D and 0.4 D, respectively. As is the case for all other halogens that have been studied, iodide does not affect the dipole moment of surrounding

water molecules. Both inside and outside the coordination sphere these have a dipole moment of 3 ± 0.6 D. A plot of the dipole moment distribution of water molecules inside and outside the first solvation solvation shell of iodide is shown in figure 4.9.

4.4 Conclusions

We present the results of a DFT-based molecular dynamics simulation of the solvation of the iodide ion in water. Iodide is the largest of the common halogens and has a relatively weak interaction with water. The combination of these factors results in a relatively unstructured solvation shell. The ion has a disruptive influence on the local water structure. Water molecules in the first solvation shell have only 2.5 hydrogen bonds on average, significantly less than in pure bulk water (3.4). Also, these hydrogen bonds are predominantly located within the first shell of water molecules. The solvated ion does not integrate well in the natural water structure.

The diffuse character of the solvation shell of iodide is apparent when we look at the dynamical behaviour of water molecules in the shell. They are bonded to the ion for a relatively short period of time (8-10 ps), compared to other halogen ions. This indicates that the iodide–water interaction is indeed weak, further proof of which we can find in the analysis of the vibrational spectrum of shell water molecules. The asymmetrical O–H stretch vibration shows a blue-shift in the shell water molecules, compared to the stretch vibration of water molecules in the bulk. The iodide–water hydrogen bond is weaker than the water–water hydrogen bond. This is essentially the explanation for the unstructured, diffuse and highly dynamical character of the solvation shell of iodide. Due to the unstructured nature of the iodide solvation we have been unable to identify and describe a well-defined mechanism for the shell–bulk water exchange process.

The presence of the iodide ion does not induce a geometry or charge distribution in shell water molecules different from that of bulk water molecules. This is consistent with the results for the other halogens.[11,72]

Chapter 5

A density functional theory based study of the microscopic structure and dynamics of aqueous HCl solutions[†]

Abstract

The aqueous solvation of hydrochloric acid is studied using density functional theory based molecular dynamics simulations at two concentrations. The large simulation boxes that we use allow us to investigate larger-scale structures such as the water-bridged chloride ion network. We find a strong concentration dependence for almost all structural and dynamical properties. Excess protons are mostly present both as Eigen and Zundel structures, either as a direct hydronium-chloride contact-ion pair or a solvent-separated ion pair. Increasing the concentration has a detrimental effect on the natural hydrogen bonded network of water molecules. This effect is visible in our studies as a decrease of the persistence time of the solvation shells around the chloride ions. Also the number of proton hops, determined by a new and well-defined identification procedure, suffers from the breakdown of the natural hydrogen bond network.

[†]This chapter is based on J.M. Heuft and E.J. Meijer *Phys. Chem. Chem. Phys.* **2006**, *8*, 3116.

5.1 Introduction

Aqueous solvation of ions and simple halogenic acids[34,37,38,82,117–121] is an important issue. In recent years, advances in the field of nonlinear spectroscopy[122] and *ab initio* simulations[46,123,124] have improved our knowledge greatly. However, there still is a number of incompletely resolved issues that require further research.

Liquid water forms an intricate network of hydrogen bonds. Amongst other interesting features, this network facilitates abnormal proton mobility when a source of excess protons is added. The transfer of excess protons in water has been studied experimentally using a variety of techniques. Macroscopic values for the abnormal proton mobility are accessible from NMR experiments[125] by comparing proton and oxygen diffusion. These studies, however, provide little information on the mechanism of the process or structural features of intermediate species. The transport of protons is of course highly dependent on the microscopic structure of the liquid. This structure can be probed by neutron and X-ray diffraction experiments,[117,121] although many properties are not directly accessible and can only be studied indirectly. Theoretical models need to be fitted to experimentally measured parameters, so results from these studies are influenced by the choice of the model.[118] Also, diffraction experiments are relatively slow, and can not resolve fast dynamical processes. In this regime, ultrafast infrared and UV spectroscopy is aptly suited. It provides high temporal resolution of the dynamical features of intermediates species in acid-base reactions[17,126] but the technique is limited to the use of very specific photoacids.

Computational studies have proven to be invaluable in elucidating many properties of aqueous acid solutions and the proton transfer mechanism in particular. On a molecular level, the structural and dynamical properties of this so-called Grotthuss process[18,20,21,127–132] have been thoroughly investigated, although discussions remain. The issue whether the Zundel ($H_5O_2^+$) or Eigen (H_3O^+) cation is the predominant form in which the excess proton is present, continues to receive much attention.[19,120,133,134] Their role and relative importance in the process of proton transfer are still debated.[17,20,128,135,136] In this chapter we will address these issues but also include the influence of chloride ions, in an *ab initio* based study of the aqueous hydrochloric acid solution.

Most computational studies focus on the behaviour of the excess protons and the water molecules. But the source of excess protons, in reality, is usually an acid, which implies the presence of counterions. The role of these counterions can be interesting for properties of the system as a whole. Relatively few detailed studies[46,123,137,138]

include the counterions explicitly, due to the increase of complexity that they imply.

There is a number of issues that require special attention when setting up a computational study of these systems. A system consisting of polarisable water molecules and halogen ions, where hydrogen bonds and covalent bonds are continuously broken and formed, requires a method that intrinsically includes these features. Previous studies have shown[11,56,123,139] that density functional theory (DFT) based CPMD simulations are an excellent tool for proper description of these dynamical features. A second consideration should be the size of the simulation box. The Grotthuss mechanism by itself involves two solvation shells around a single excess proton, that are both important for the process of proton transfer. The spatial distribution of the chloride counterions with respect to each other and the excess protons is also of interest, and should be accessible from the simulation. Therefore we have chosen a rather large simulation box, including 119-113 water molecules to solvate 6-12 HCl molecules. The amount of water, relative to the number of HCl molecules, determines the structural and dynamical details of the solvation. The diversity of present species, water molecules, chloride ions and excess protons, leads to multiple different interactions. The relative importance of these can be studied by comparing simulations at different acid concentrations. This approach has been applied by Sillanpää *et al*. in their first principles study of highly concentrated hydrochloric acid solutions.[123] Indeed, they find a distinct concentration effect on the intermolecular structure of water and the structure of the coordination shells around the charged species, as well as on the dynamical properties, such as hydrogen bond dynamics.

In this chapter we study the aqueous solvation of hydrochloric acid using *ab initio* based DFT molecular dynamics simulations. Our previous studies of water in the presence of halogen ions[72,114,140] form the basis of this investigation. Since the concentration is very important for all properties, we compare a dilute and a concentrated system. We examine structural features such as the formation of local protonic water clusters, contact-ion pairs and larger networks of water-bridged chloride ions. The dynamical analysis focuses on the lifetimes of transitional species that are present in the solution and the mobility of the solvated excess protons.

5.2 Computational Details

Electronic structure calculations are performed using the Kohn-Sham formulation[26] of DFT,[55] where we employed the gradient-corrected BLYP-functional.[27,28] This function is known for a good description of aqueous systems.[56,57] Molecular dynam-

ics simulations are performed using the Car Parrinello approach,[25] as implemented in the CPMD software package[†]. The Kohn-Sham orbitals are expanded in plane waves with an energy cutoff of 70 Ry. Only valence electrons are considered explicitly, with a semi-local norm-conserving Martins-Troullier pseudopotential taking into account the interactions between the core and valence electrons. The cutoff radius for the pseudopotentials is 0.50, 1.05 and 1.34 a.u. for H, O and Cl, respectively. The concentrated solution contains 12 chloride ions, 12 protons and 113 water molecules (1:9.4, 5.3 mol·l^{-1}) in a body centred cubic (BCC) simulation box with a lattice constant of 19.54 Å. The dilute system consists of 6 chloride ions, 6 protons and 119 water molecules (1:19.8, ca. 2.7 mol·l^{-1}). The BCC simulation box has a lattice constant of 19.56 Å. At the start of the simulations, the systems are equilibrated at 350 K by simple velocity scaling of the ions. After equilibration the temperature is no longer controlled, to avoid non-physical effects of a thermostat on the dynamics of the simulation. The temperatures of the concentrated and dilute solutions are 333 ± 26 K and 332 ± 33 K, respectively. For comparison reasons, we performed simulations of pure water and the solution of a single proton under comparable conditions and input parameters. The pure water simulation contains 64 water molecules in a BCC simulation box with a lattice constant of 15.66 Å. A proton was added to this system for the separate solvated proton simulation. Both systems where equilibrated according to the above mentioned procedure. During the production run, the temperature of the pure water system is 329 ± 31 K, the solution of the proton in water is 323 ± 31 K. All hydrogen atoms are assigned the mass of deuterium in order to improve decoupling of the dynamics of the ionic and electronic subsystem over a longer period of time, and allowing for a larger timestep in the numerical integration of the equations of motion. The fictitious mass associated with the plane-wave coefficients is set at 700 a.u. allowing for a timestep of 6.0 a.u. (0.145 fs) in the numerical integration of the equations of motion. All simulation were run for at least 20 ps after equilibration to gather data.

5.3 Results and Discussion

A number of definitions is needed to enable a consistent analysis of the structural and dynamical properties of our simulations of the hydrochloric acid solvation. First of all, for purposes such as the radial distribution functions (RDFs), the position of a hydronium ion is defined as the position of the oxygen atom of H_3O^+. This oxygen atom will be indicated as OH_3^+. For identification of the hydronium ion the following

[†]CPMD 3.7.1, Copyright IBM Corp 1990-2004, Copyright MPI für Festkörperforschung Stuttgart 1997-2001.

criterium is used. A hydrogen atom is associated with a specific oxygen atom if its distance to this oxygen atom is less than a specific value. The oxygen atoms that have three hydrogen atoms around them, are labelled as hydronium. For all hydrochloric acid solutions, this distance cutoff was set at 1.226 Å. With this distance cutoff the number of hydronium ions in a simulation is, on average, equal to the number of present chloride ions. The same cutoff was used for the identification of hydronium ions in our reference solvated proton solution. However, this identification procedure is inappropriate for tracking of the excess protons to quantify the hopping rate, as it would lead to inconsistent results. The number of hydronium ions can fluctuate from one timestep to another. This makes consistent correlation functions and other analyses that depend on the history of hydronium ions impossible. To deal with this problem we used a more deterministic algorithm of labelling the hydronium ions. Every timestep, the n oxygen atoms with the smallest total distance to the closest three hydrogen atoms, are labelled as hydronium. Here, n is the number of chloride ions in the hydrochloric acid solutions, $n = 1$ in the case of the solvated proton solution. This procedure is more strict and facilitates identification of proton transfer events. For all but one of the following analyses we used the first method of hydronium identification. Only the analysis of the hopping rate, at the end of the dynamics section, employs the second identification method.

Structure

Radial distribution functions provide information on the time-averaged features of the structure of the hydrochloric acid solutions. The structure of the solvent is affected by the presence of the hydrochloric acid molecules. The O–O RDFs, figure 5.1, shows

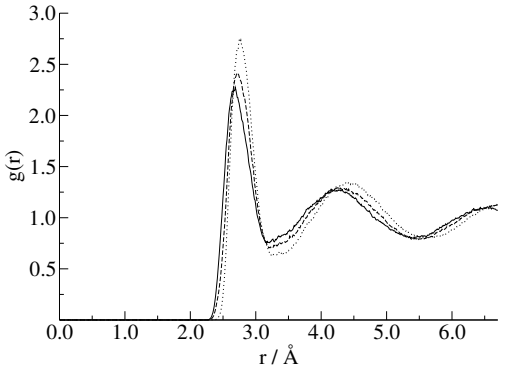

Figure 5.1: O–O radial distribution functions for the dilute (dashed line) and concentrated (solid line) solution. The dotted line represents the O–O radial distribution function of the reference system of pure water.

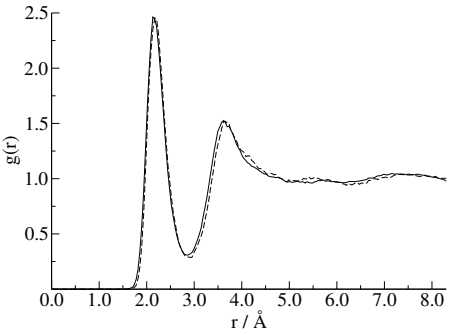

Figure 5.2: Cl–H radial distribution functions for the dilute (dashed line) and concentrated (solid line) solution.

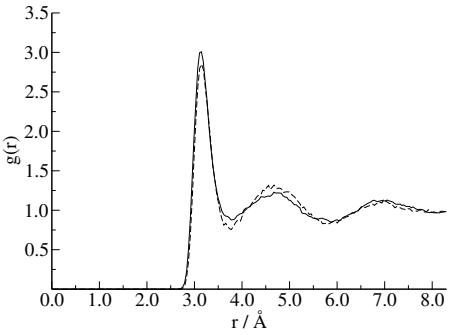

Figure 5.3: Cl–O radial distribution functions for the dilute (dashed line) and concentrated (solid line) solution.

this effect clearly. The height of the peaks decreases and their separation becomes less clear upon increasing the HCl concentration. This indicates that an increase of the HCl concentration has a destructive effect on the natural hydrogen bonded network of water molecules. The chloride ions induce a characteristic structure on the directly surrounding water molecules, very much comparable to the isolated chloride solvation.[72] For both concentrations the Cl–H and Cl–O RDFs, shown in figures 5.2 and 5.3, are very similar.

The Cl–Cl RDF (figure 5.4) shows a clear structure. The two peaks, at 5 and 7.5 Å, correspond to structures where the chloride ions are bridged by one and two water molecules, respectively. Representative snapshots of these structures are shown

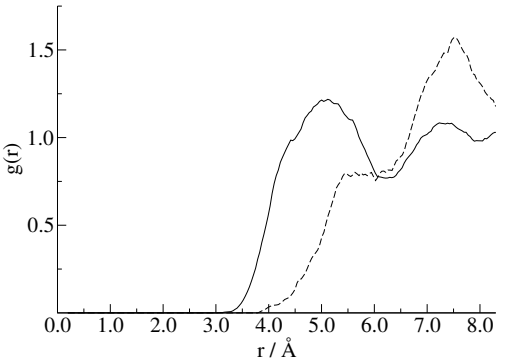

Figure 5.4: Cl–Cl radial distribution functions for the dilute (dashed line) and concentrated (solid line) solution.

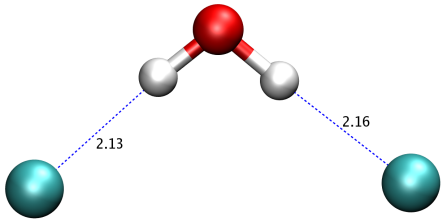

Figure 5.5: Representative snapshot of a single-water bridged Cl–Cl structure. The numbers show the lengths of the hydrogen bonds in Å, the Cl–Cl distance is 4.83 Å.

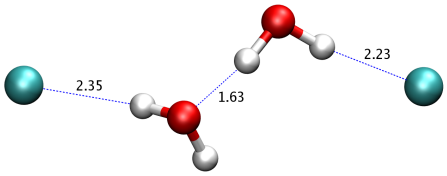

Figure 5.6: Representative snapshot of a double-water bridged Cl–Cl structure. The numbers show the lengths of the hydrogen bonds in Å, the Cl–Cl distance is 7.71 Å.

in figures 5.5 and 5.6. The concentration effect is pronounced. The dilute solution favours the double water-bridged structure, while the concentrated solution contains a larger amount of the single water-bridged structure. The reason for this effect is of course the relatively smaller amount of water that is present to solvate the chloride ions, forcing the ions closer together and to share water molecules in their solvation shells.

The same effect is present between the chloride and hydronium ions, as can be clearly seen in the Cl–OH_3^+ RDF in figure 5.7. At low concentration the peak at 3.0 Å, corresponding to the contact-ion pair (figure 5.8), is very small. This peak is much larger in the more concentrated solution. Apparently, due to the relatively smaller amount of

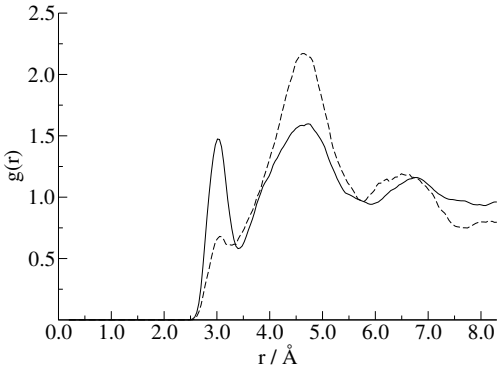

Figure 5.7: Cl–OH_3^+ radial distribution functions for the dilute (dashed line) and concentrated (solid line) solution.

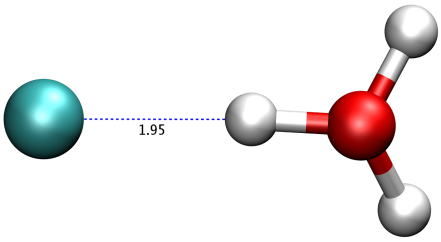

Figure 5.8: Conformation of a contact-ion pair with numbers showing the typical lengths of the hydrogen bonds in Å. The Cl–OH_3^+ distance is 2.97 Å.

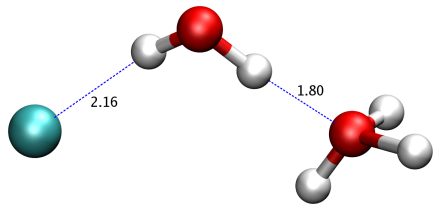

Figure 5.9: Conformation of a solvent-separated ion pair with numbers showing the typical lengths of the hydrogen bonds in Å. The Cl–OH_3^+ distance is 4.47 Å.

water, at higher concentration it is not always possible to independently solvate both the protons and the chloride ions, though this would be energetically favourable. The Coulombic interactions between both ions now result in the formation of a contact-ion pair. The second peak in the RDF, at 4.6 Å, shows the exact opposite behaviour. This peak corresponds to the solvent-separated ion pair, of which a representative snapshot is shown in figure 5.9.

Furthermore, from the relatively larger size of the second peak, we can infer that the solvent-separated ion pair is dominant over the direct contact-ion pair, which has its influence on the dynamical properties of the system, as we will see later in the dynamics section. Finally, the OH_3^+–OH_3^+ RDF, figure 5.10, shows a rather uniform

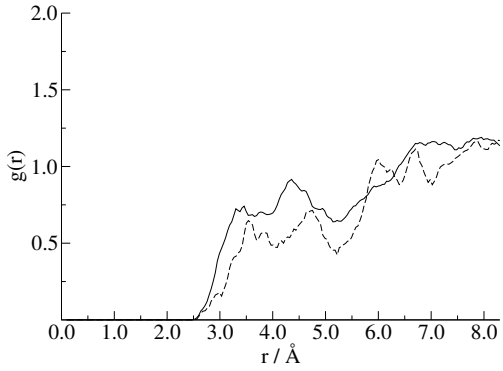

Figure 5.10: OH_3^+–OH_3^+ radial distribution functions for the dilute (dashed line) and concentrated (solid line) solution.

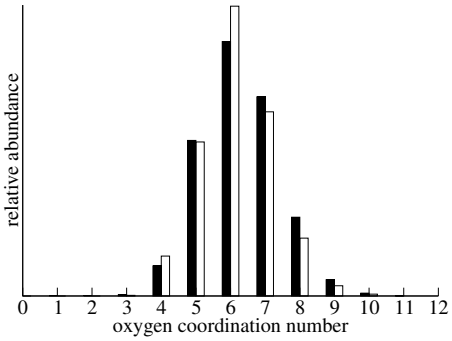

Figure 5.11: Histograms of the coordination number based on the Cl–O distance for the dilute (open bars) and concentrated (filled bars) solution.

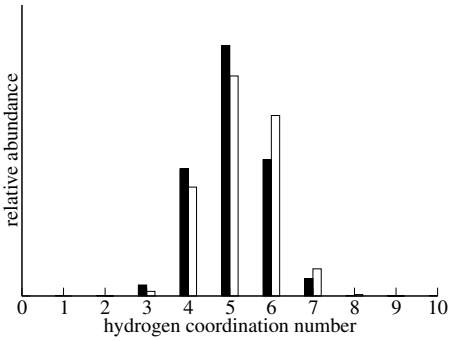

Figure 5.12: Histograms of the coordination number based on the Cl–H distance for the dilute (open bars) and concentrated (filled bars) solution.

distribution of hydronium ions beyond 3.5 Å, with an indication of a small minimum around 5.3 Å. However, we were unable to identify uniquely characteristic structures corresponding to maxima in the RDF due to the fluxional character of the hydronium species.

Integration of the RDFs yields the average number of coordinating water molecules around a chloride ion. There is a small dependence on the concentration. Chloride ions in the concentrated solution are surrounded by 5.0 ± 0.2 water molecules. In the dilute solution, the average coordination number is slightly higher, 5.2 ± 0.2. For this quantitative analysis, the coordination sphere is defined as the first peak in the corresponding Cl–H RDF, up to the first minimum. We chose the Cl–H RDF because this minimum is more unambiguous than that of the Cl–O RDF. Histograms of the coordination numbers, based both on the Cl–O and Cl–H distance criterium are shown in figures 5.11 and 5.12. The histograms both are quite symmetrical, with a slightly higher peak value for the Cl–O histogram. Although the absolute values for the coordination number do not differ, within the error-margin, from each other or the reference solution of a single chloride ion,[72] a trend is definitely present. Chloride in the concentrated solution is solvated, on average, by less water molecules than in the dilute solution. This confirms our overall observation that, on average, both the hydronium and the chloride ions are better solvated separately in the dilute solution. The inter-ionic distances are larger and their solvation shells contain more water molecules. When we compare our results to those from recent Empirical Potential Structure Refinement (EPSR) Monte Carlo (MC) simulations that are constrained to data from neutron diffraction experiments[120] by Botti *et al.*, a number of discrepancies are apparent. The concentration in their studies is identical to that of our concentrated

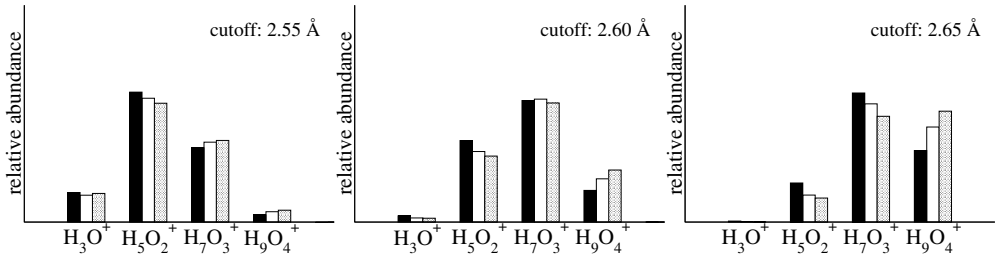

Figure 5.13: Histograms of the local cluster in which the excess protons are present. The concentrated and dilute HCl solutions are represented by the filled and open bars, respectively. For comparison, the dot-filled bars show the data from our reference solvated proton simulation.

system. While the Cl–H and Cl–O RDFs are very similar, peak positions in the Cl–Cl RDF are shifted ca. 1 Å to larger interatomic distances in our results. Peak positions for the OH_3^+–OH_3^+ are rather similar, however, the structure is much more pronounced for the EPSR MC simulations. A discrepancy appears for the Cl–OH_3^+ RDF, with our simulations showing no undissociated HCl molecules, yielding a lower chloride-water coordination number of 4.4. A factor in this could be the fact that in the analysis of the neutron diffraction experiments, the proton is modelled as H_3O^+ ions which limits the possible proton-solvation structures.

For a more detailed picture of the local structure around the excess protons we need more elaborate analysis methods than RDFs and simple visual inspection. Mostly, we are interested in the type of structure in which the excess proton is present. To quantify this we use a simple procedure: a hydronium ion is identified according to the aforementioned first identification scheme. Next, the number of water molecules surrounding this hydronium within a certain cutoff distance of the OH_3^+–O RDF is counted. The cutoff distance was taken to be 2.60 Å. This value was guided by the observation from earlier simulations of aqueous protons[21, 130, 134, 141] that typically ap-

system	H_3O^+	$H_5O_2^+$	$H_7O_3^+$	$H_9O_4^+$	$H_{11}O_5^+$
concentrated	2.57	33.83	50.44	13.14	0.02
dilute	1.71	29.28	51.02	17.95	0.03
reference	1.59	27.38	49.42	21.60	0.00

Table 5.1: Distribution in % of the local structures in which the excess protons are present in the solutions. The reference system contains a single excess proton and 64 water molecules.

pear in configurations interchanging between 1) solvated by three water molecules with equal O–O distances of $\approx$ 2.60 Å (Eigen structure) and 2) solvated by three water molecules with one O–O distances of $\approx$ 2.4 Å and two O–O distances of $\approx$ 2.6 Å (Zundel structure). This strictly defined procedure results in the relative abundances of local protonic structures, characterised by the number of participating water molecules, that are present in the solution. These relative abundances for both concentrations and the reference system are summarised in table 5.1 and are plotted in figure 5.13. As there is some arbitrariness in the choice of the cutoff, the figure also shows the results for cutoff distances of 2.55 Å and 2.65 Å. The table and figure show that, for a cutoff of 2.60 Å, there is significant presence of $H_5O_2^+$, $H_7O_3^+$ and $H_9O_4^+$ ions, with the smaller clusters dominating. Differences between the diluted hydrochloric acid solution and the reference system are small. One systematic trend seems to be present: upon increase of the HCl concentration, the presence of the smaller $H_5O_2^+$ cation has grown, at the cost of the $H_9O_4^+$ ion. This reflects the earlier observation that the amount of present water is insufficient to ideally solvate both ions independently. The results for different cutoff distances show some variation, reflecting to a certain extent the intrinsic difficulty to quantify precisely the relative occurrence of Eigen and Zundel structures. As we will see in the dynamics section, the protonic structures are very fluxional due to fast proton dynamics. Hence, we argue that the structural identification would be better described by a strongly coupled hydrogen bond network, as suggested by Sillanpää *et al*.[123] Note, that the trend of a decreasing cluster size with an increasing HCl concentration is present for all cutoff distances. Also note that the fact that our results for the reference system show significant presence of both Eigen, Zundel and mixed structures is consistent with results of earlier simulations.[21,130,134,141]

Summarising the structural properties yields the following picture. Both ions present compete for a full solvation shell of water. However, because the amount of water is insufficient to accommodate isolated solvation of both species, water molecules are shared between ions. Of course, this effect is strongest in the concentrated solution. The intermolecular water structure is greatly affected by the presence of the intruding ions.

Dynamics

The presence of the chloride ions is expected to have a distinct effect on the dynamical processes that occur in the hydrochloric acid solution. First we focus on the dynamical interaction between the chloride ions and the excess proton structures. Their behaviour is best visualised by the time evolution of distances between the two ions. Representative plots are shown in figure 5.14 for both concentrations. For the dilute solution, we first observe the formation of a short-lived contact-ion pair (fig. 5.8),

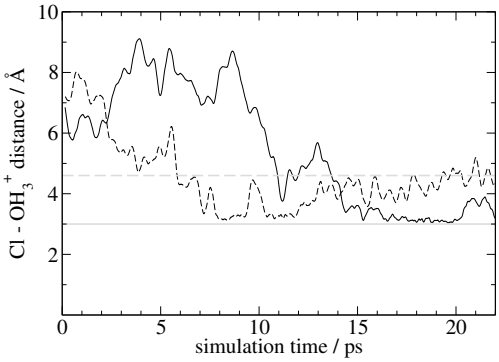

Figure 5.14: This graph shows the time evolution of the Cl–OH_3^+ distance of a selected ion pair during the simulation. The solid line represents an ion pair from the concentrated solution and the dashed line one from the dilute solution. The solid grey line at 3.0 Å shows the position of the RDF peak that corresponds to the contact-ion pair. The dashed grey line at 4.6 Å corresponds to the distance in a solvent-separated ion pair.

around 8-9 ps and 10-12 ps. These structures are not stable and slowly diffuse into a longer-lived solvent-separated ion pair (fig. 5.9), starting around 15 ps. The concentrated solution displays rather different behaviour, the solvent-separated ion pair structure has almost no lifetime at all, but directly diffuses into the contact-ion pair, stable from 14 ps onwards. The larger fluctuations in the Cl–OH_3^+ distance for the solvent-separated ion pair indicate the large flexibility of this structure, while the contact-ion pair is much more rigid. Next, we look at the chloride-water network. In the Cl–Cl RDF and by visual inspection of the trajectory of the simulations we observe the formation of a water-bridged network of the chloride ions. These water bridges are rather stable, based on visual inspection we estimate the lifetime in the order of picoseconds, up to 10 ps. Because the chloride ions are relatively heavy (almost twice as heavy as a water molecule) they move more slowly than water molecules. Due to the formation of the network, involving water molecules, we expect this effect to slow down the water molecules themselves, on average, too.

Experimental NMR studies[125] show that, indeed, the mobility of water decreases with increasing concentration of hydrochloric acid. Using nonlinear spectroscopy, Omta *et al*. show that this effect can be fully explained from the rigid nature of the solvation spheres around the ions. By increasing the concentration of hydrochloric acid, a larger amount of the water molecules is part of a chloride ion solvation sphere, and thus the average mobility would decrease. For the two concentrations that are studied here, we expect a relative decrease in water mobility of approximately 15%, based on the NMR

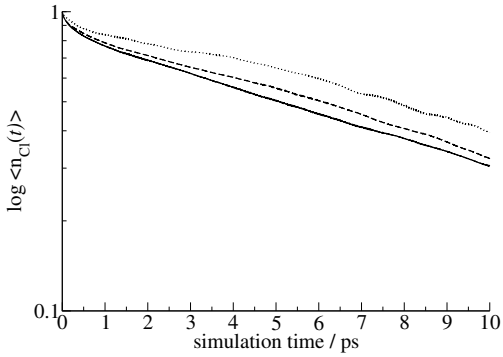

Figure 5.15: Shell persistence correlation functions[38] of water molecules in the first solvation shell of chloride in the dilute (dashed line) and concentrated (solid line) solution of hydrochloric acid. The dotted line represents the reference solution of a single chloride ion in water.

results. Analysis of the mean-squared displacement (MSD) in our simulations shows no differences for the dilute, concentrated or pure water simulations. The estimated margin of error of ca. 30% is too large to allow such a distinction. The concentration of hydrochloric acid does influence the shell persistence correlation function n_{Cl}, as defined in ref. 38, plotted in figure 5.15. Compared to the reference system, a single chloride ion in water, this function decays faster for both hydrochloric acid solutions. The ideal solvation shell around the chloride ion is distorted due to the presence of the excess protons and the other chloride ions. This causes the solvation shells to have a more fluxional character and, hence, a faster decay of their correlation functions. Furthermore, the function decays fastest for the concentrated solution. Evidently, the solvation shell around the chloride ions in the concentrated solution is more fluxional than in the dilute solution.

We define a proton hop as the transfer of a proton from an identified hydronium ion to a water molecule that is identified as a hydronium ion in the next MD timestep. Additionally, the water molecule that receives the excess proton is required to be in the first solvation shell of the originating hydronium ion. This definition as it is, is very much dependent on the choice of the definition of a hydronium ion. The behaviour of protons in an aqueous solution is very fluxional, and an unambiguous identification of hydronium that is consistent in time, is very difficult to achieve. By naively interpreting oscillatory motion of protons as consecutive proton hops that constructively contribute to proton transfer, a very large number of proton hops is observed. This is more a result of the identification algorithm than a feature of reality. To isolate the real proton transfers from one water molecule to another we require the resulting

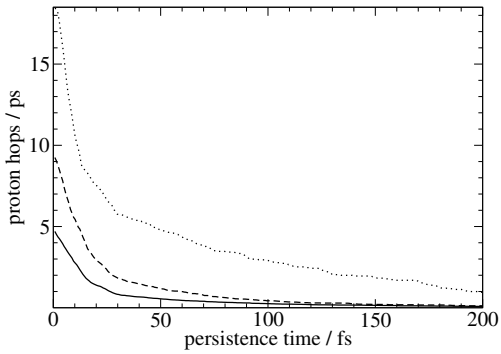

Figure 5.16: Number of observed proton hops per ps per excess proton as function of the persistent lifetime of the resulting hydronium ion for the concentrated (solid line) and diluted (dashed line) HCl solution. For comparison we also plotted the same quantity for the solution of a single excess proton in water (dotted line).

hydronium ion to be detected as such for a specified amount of time. The number of observed proton hops as a function of the amount of time that the resulting hydronium ion is required to exist, is shown in figure 5.16. First of all we notice that in all three graphs, there are two clear kinks, see table 5.2. For all concentrations, these kinks coincide, there is one at ca. 15 fs and one at 30 fs.

This leads us to the observation that, using our detection method, there are three types of proton transfer processes, each with its own characteristic time constant. Our proton hop detection method is susceptible to fast, oscillatory movement of protons, marking these incorrectly as proton hops that constructively contribute to proton transport. The function in figure 5.16, however, is the tool that we need to filter these out. By requiring a hydronium, that is the result of a proton transfer, to live at least 30 fs (the time at which the third, slowest, proton transfer mechanism dominates), we eliminate overcounting the number of proton hops. The slowest process results

system	kink 1 / fs	kink 2 / fs	proton hops / ps
concentrated	15.8	30.7	0.80
dilute	16.0	29.4	1.85
reference	13.2	30.3	5.75

Table 5.2: Positions of the kinks in figure 5.16 for the various systems, accompanied by the number of proton hops per ps.

in a longer living hydronium, so this corresponds to a hydronium ion that passes the proton on in a constructive way. The number of proton hops we observe, using this method, is also tabulated in table 5.2, corrected for the total amount of excess protons present. The value of 5.75 ps^{-1} for our reference solution of a single excess proton is in rather good agreement with the previous result of 5 ps^{-1} by Tuckerman *et al.*[128] The number of proton hops in the hydrochloric acid solutions (dilute: 1.85 ps^{-1}, concentrated: 0.80 ps^{-1}) is much smaller than in the single excess proton simulation. Proton transfer is optimal in a pure water solution. The undistorted natural hydrogen bond network structure facilitates fast proton transport. Introducing contaminants, such as chloride ions and more excess protons, disrupts the hydrogen bonded structure to a larger extent, and leads to a decline in the number of proton hops. Another factor at work here, are the slow chloride ions. As we saw from the RDFs, the solvent-separated ion pair is the dominant form in which the excess proton is present. If we assume that the Grotthuss mechanism of proton transfer still applies in hydrochloric acid solutions, the chloride ions introduce another source of transfer-impediment. The relatively small diffusion constant of the heavy ions, combined with the strong hydrogen bonding between the chloride ion and water molecules, leads to slow dynamics of the solvation shell of the hydronium ion, due to its proximity to chloride. A more distorted and slowed down solvation shell around the hydronium ion diminishes the rate of proton transfer severely.

The last influence on the dynamics of proton transfer we investigate is the average lifetime of hydronium ions. We define the hydronium persistence correlation function:

$$T_{H_3O^+}(t) = \langle h(t) \times h(0) \rangle. \tag{5.1}$$

Here, $h(t) = 1$ if a selected oxygen atom is part of a hydronium ion at time t and 0 otherwise. The function is averaged over the number of hydronium molecules and time origins that are spaced 35 timesteps (5 fs) from each other. This function is plotted for both concentrations and the reference excess proton simulation in figure 5.17. We observe that the trend in the hydronium persistence time is identical to that of the chloride water shell persistence time. It confirms the increase of relatively fast dynamics on increasing the concentration of hydrochloric acid. Note that equation 5.1 only takes the persistence of a hydronium into account. This explains the seemingly inconsistent observation that for the concentrated solution, the average hydronium lifetime is shortest while the number of proton hops is smallest, compared to the dilute and reference solution. The persistence plot does not include conditions on where the excess proton is going and therefore only gives information on the dynamic properties of a hydronium itself. Finally we investigated the vibrational spectrum of the water molecules. The vibrational spectrum of water is independent of the concentration. Headrick *et al.*[19] found distinct characteristic vibrations due to the hydronium

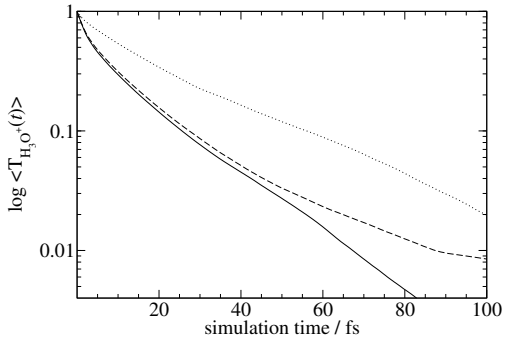

Figure 5.17: Logarithmic plot of the time averaged hydronium persistence correlation function. The dashed line and solid line represent the diluted and concentrated HCl solution, respectively. The dotted line shows the correlation function for the reference solution of one excess proton in water.

species. The statistical error in the results from our simulations is too large to make this contribution visible over the spectrum of the bulk water molecules.

5.4 Conclusions

DFT-based molecular dynamics simulations of the aqueous solution of hydrochloric acid at high and low concentration in a large simulation box have provided us with a wealth of information on the structural and dynamical properties of the system and especially the influence of the concentration. The proton appears as Eigen and Zundel structures in both concentrations. At low concentration the hydronium ion forms mostly solvent-separated ion pairs with the chloride ions, while the direct contact-ion pair increases in abundance if we increase the concentration of hydrochloric acid. We observe the formation of a semi-static water-bridged network of chloride ions. The number of water molecules that bridges two chloride ions is strongly concentration dependent, increasing from 1 to 2 upon decreasing the concentration with a factor of 2. The dynamical behaviour of the solvation shell of water molecules around the chloride ions is relatively fast when compared to the coordination shell of an isolated chloride ion in water. This effect increases with concentration and shows the detrimental influence that the increasing amount of charged species has on the natural hydrogen bond network of water. It is also largely responsible for the dramatic decline of the number of proton hops that we observe by increasing the concentration of hydrochloric acid.

Chapter 6

A density functional theory based study of the microscopic structure and dynamics of aqueous lithium hydroxide solutions

Abstract

We study the aqueous solvation of lithium hydroxide using density functional theory (DFT) based molecular dynamics simulations at high and low concentrations. Large simulation box sizes allow us to identify larger-scale structures, such as water bridged lithium and hydroxide ions. The concentration has an effect on almost all structural properties. Upon increasing the concentration we observe a destructive effect on the natural hydrogen-bonded water structure. Furthermore, the coordination number of water molecules around the ions, as well as the number of bridging water molecules between ions, and the interionic distances, decreases on an increase of the LiOH concentration. We observe a very short lifetime of the hydroxide ion, indicating a very much delocalised negative charge in hydroxide–water clusters. The short lifetime of identifiable hydroxide species severely limits our analysis of the dynamical properties of proton transfer in solvated hydroxide solutions. Throughout this chapter we compare results for the aqueous LiOH solvation with those for the HCl solvation in the previous chapter.

6.1 Introduction

Aqueous basic solutions are of great importance in many chemical reactions. Consequently there has been a large amount of research concerning the solvation of the hydroxide ion in water. Proton transfer constitutes an important process in these solutions. By combining results from experimental techniques such as NMR, X-ray diffraction and computational studies, Agmon proposed a mechanism for the proton transfer[22] in aqueous hydroxide solvations. In that work, the existing idea of hydroxide proton transfer that closely resembles hydronium-like proton transfer is backed by a large number of experimental and computational results to give a consistent and complete picture of the solvation dynamics of the hydroxide ion. It is shown that structural and dynamical features are intimately connected. The outlined mechanism, however, contains some unconfirmed details and inconsistencies with some data. Therefore, a few years later, Tuckerman *et al*.[23] undertook a rigorous computational study, using state-of-the-art simulation techniques to re-examine the structural and dynamical properties of the solvation of OH^- in water. They showed that the process of proton transfer proceeds rather differently for hydroxide solvations than for hydronium solvations. First, a hydrogen bond between the oxygen atom of the hydroxide ion and a first solvation shell water molecule is broken. Then, a weak hydrogen bond is formed between the hydrogen atom of the hydroxide ion and another water molecule. Finally, a proton is transferred from a solvation shell water molecule to the hydroxide, completing the proton transfer process. Especially the beginning of the process, that starts with a rearrangement in the first solvation shell around the ion, constitutes a large difference with the previously proposed, hydronium-like mechanism. Since the introduction of this revised mechanism, it has been embraced by the community[142] and lead to a renewed interest in hydroxide solvation.[24,71,143–145] The paper by Chen *et al*. describes a very interesting and relevant study on the solvation of NaOH and KOH in water, over a range of concentrations. Throughout this chapter we will compare and discuss their and our results.

In studies of the properties of aqueous bases, the hydroxide ion itself, naturally, has received most attention. Relatively few studies[71,143–146] include a cation for a complete description of the system. Those studies that include counterions usually concern the widely used NaOH and KOH. The aqueous solvation of other bases, such as lithium hydroxide, has attracted much less attention. From an experimental point of view this can be explained by the practical difficulties of the substance due to its high reactivity and low vapour pressure. In computational studies, the focus is mostly on the behaviour of one of the ions in an aqueous environment, either the cation Li^+ or the hydroxide ion OH^-. The lithium cation receives much attention because of its appli-

cations in battery technology (the widely used Li-ion batteries). The small and light ion provides a very high energy density, compared to other electric energy storage technologies. The lithium ion also has some important medical applications. Lithium influences neurotransmitter chemistry in nerve cells and increases the production of white blood cells.[147] Both in the technological and medical applications, the Li^+ ion is the active form of the metal, which makes studies on the properties of this ion very relevant. The properties of the aqueous solvation of the lithium cation have been studied using a variety of techniques. Experimentally, neutron diffraction[148,149] and NMR[150] offer insight in the structural features of water directly surrounding the ion. Neutron diffraction yields one of the most important structural quantities: the coordination number, which ranges from 3.3 ± 0.5 to 5.5 ± 0.5, depending on the concentration of the solution. The average residence time of a water molecule in the first solvation shell of Li^+ is approximately 30 ps, as measured in NMR experiments.[77] Further experimental studies are limited and do not provide microscopic details on the solvation of the lithium ion.

Computational studies can provide a more detailed description of the properties of the lithium ion and the effects on the water molecules that surround the ion. Lithium, however, is a rather difficult ion to incorporate in simulations that are based on force fields. Its small size and, consequently, high local charge density lead to a strong polarising influence on coordinating water molecules. The hydrogen bonds that Li^+ forms with water are very strong. For a proper description it is very important to accurately describe these electronic effects. Some recent purely classical computational studies[151–153] reproduce the experimental data very well. Additionally, they provide insight in the structure of the solvation sphere and the dynamics of water exchange mechanisms. Parametrisation of the forcefields remains a difficult subject, therefore a relatively large number of studies[70,154–156] employs QM/MM simulations to evade this problem. Lyubartsev *et al.* studied the Li^+ ion in water using CPMD in a complete *ab initio* approach. All simulations roughly agree with respect to the structural features of the first solvation shell of the lithium ion. At ambient conditions the coordination number is 4, with a tetrahedral water layout around the ion. The Li–H_2O distance is 2.0 Å and the Li–O RDFs show a deep minimum just after the first peak, indicating an almost complete depletion of water molecules between the first and second solvation shell. The dynamical properties of the solvation shell are more problematic to elucidate. Since the Li–H_2O hydrogen bond is so strong, the solvation shell is very rigid. Usually, feasible simulation lengths are insufficient to yield an accurate value for the residence time of water molecules in the solvation shell. Most results, however, indicate that this value lies in the range 20-60 ps. As mentioned above, most studies focus on only one ion and disregard the role of the counterion. An exception is the study of the structure and energetics of small LiOH–H_2O clusters.[147,157] The

very recent study by Veerman *et al.*,[147] using DFT-BLYP and MP2 level calculations, determines the number of water molecules (7) that is needed to completely dissociate a LiOH molecule.

In the present study we investigate the aqueous solvation of LiOH using DFT based molecular dynamics simulations. We study the LiOH solvation at two concentrations in order to be able to identify concentration effects. In both concentrations, water molecules are almost always member of a first or second solvation shell of a lithium ion. The strong hydrogen bonds are therefore expected to have a significant effect on the dynamical properties of the present water. The concentrations are such that complete isolated solvation of both ionic species is not possible due to the scarcity of water molecules. This means that the ions must compete for water molecules to fill their solvation shells. Again, we expect a strong concentration effect on the structural features of the solvation of the ions. A large range of conformational possibilities exists, from direct contact-ion pairs and solvent-separated ion pairs to water-bridged ion networks. Especially interesting is the comparison with the solvation of hydrochloric acid, as presented in chapter 5. The concentrations of the systems in terms of solute/solvent ratio are identical to facilitate a direct and consistent comparison.

6.2 Computational Details

Electronic structure calculations are performed using the Kohn-Sham formulation[26] of DFT,[55] where we employed the gradient-corrected BLYP-functional.[27,28] Molecular dynamics simulations are performed using the Car Parrinello approach,[25] as implemented in the CPMD software package[†]. The Kohn-Sham orbitals are expanded in plane waves with an energy cutoff of 100 Ry. Only valence electrons are considered explicitly, with a semi-local norm-conserving Martins-Troullier pseudopotential taking into account the interactions between the core and valence electrons. The cutoff radius for the pseudopotentials is 0.50, 1.05 and 0.70 a.u. for H, O and Li (all electron), respectively. The concentrated solution contains 12 lithium ions, 12 hydroxide ions and 113 water molecules (1:9.4, ca. 5.7 mol·l^{-1}) in a body centred cubic (BCC) simulation box with a lattice constant of 19.1 Å. The dilute system consists of 6 lithium ions, 6 hydroxide ions and 119 water molecules (1:19.8, ca. 2.8 mol·l^{-1}). The BCC simulation box has a lattice constant of 19.2 Å. At the start of the simulations, the systems are equilibrated at 350 K by simple velocity scaling of the ions. After equilibration the temperature is no longer controlled, to avoid non-physical effects of

[†]CPMD 3.7.1, Copyright IBM Corp 1990-2004, Copyright MPI für Festkörperforschung Stuttgart 1997-2001.

a thermostat on the dynamics of the simulation. The temperatures of the concentrated and dilute solutions are 364 ± 24 K and 356 ± 24 K, respectively. For comparison reasons, we performed simulations of pure water, the solution of a single hydroxide ion, and the solution of a single lithium cation under comparable conditions and input parameters. The pure water simulation contains 64 water molecules in a BCC simulation box with a lattice constant of 15.66 Å. A hydroxide ion was added to this system for the separate solvated hydroxide simulation. Both systems where equilibrated according to the above mentioned procedure. During the production run, the temperature of the pure water system is 329 ± 31 K, the solution of the hydroxide ion in water is 352 ± 32 K. The simulation of the solvation of a single lithium ion contains 1 lithium ion and 64 water molecules in a cubic simulation box with a lattice constant of 12.5 Å to yield the experimental density at ambient conditions. The temperature is controlled by a Nosé-Hoover thermostat[61] at 350 K with a frequency of 500 cm^{-1}. The thermostat is not expected to influence the dynamical properties of the system because the timescales of the thermostat and the important dynamical processes in the simulation differ by an order of two. Overall charge neutrality is achieved by adding a uniform background charge to compensate for the positive charge of the lithium ion. All hydrogen atoms are assigned the mass of deuterium in order to improve decoupling of the dynamics of the ionic and electronic subsystem over a longer period of time, and allowing for a larger timestep in the numerical integration of the equations of motion. The fictitious mass associated with the plane-wave coefficients is set at 700 a.u. allowing for a timestep of 5.0 a.u. (0.121 fs) in the numerical integration of the equations of motion. We observe no drift in the electronic kinetic energy during all simulations. All simulations were run for at least 5 ps. after equilibration to gather data.

6.3 Results and Discussion

Structure

The position of a hydroxide ion is defined as the position of the oxygen atom. For identification of the hydroxide ion the following criterium is used. A hydrogen atom is associated with a specific oxygen atom if its distance to this oxygen atom is less than a certain value. The oxygen atoms that have one hydrogen atom around them, are labelled as hydroxide. For all lithium hydroxide solutions, the O–H distance cutoff was set at 1.228 Å. With this distance cutoff the number of hydroxide ions in a simulation is, on average, equal to the number of present lithium ions. The same cutoff was used for the identification of hydroxide ions in our reference solvated hydroxide solution. In the following discussion, references to an 'O' atom include oxygen atoms

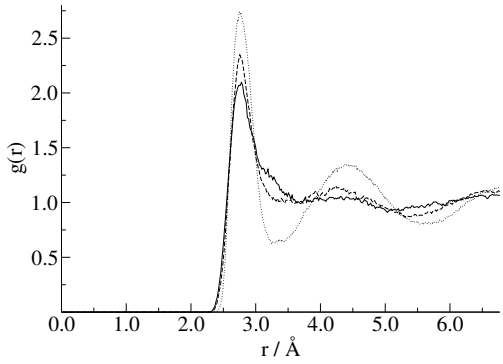

Figure 6.1: O–O radial distribution functions for the concentrated (solid line) and dilute (dashed line) LiOH solution. The dotted line represents the O–O RDF for a reference system of pure water.

both from water molecules and hydroxide ions. Oxygen atoms from hydroxide ions are explicitly referred to as 'OH^-'.

The structural analysis of the LiOH solutions starts with a discussion on the radial distribution functions (RDFs). The O–O RDFs (figure 6.1) show that higher LiOH concentrations have an increasing destructive effect on the natural water network, as expected from the work of Chen *et al.*[144] In comparison to the O–O RDF of a pure water simulation, also shown in figure 6.1, the effect of the added ions is very clear. The first peak lowers significantly on increasing the concentration and the normal water structure beyond the first peak is all but gone for the concentrated solution. The influence on the structure of water is more pronounced here, for LiOH, than it is in the solutions of HCl. Especially the lithium ions disrupt the natural water network in their direct environment to a larger extent than the chloride ions. Again, this is due to the very strongly hydrogen bonded first solvation shell of water molecules around lithium. At the studied concentrations, almost all water molecules have one or more Li^+ ions in their second solvation shell. Additionally, 20-40% (dilute-concentrated) of all water molecules are part of a first solvation shell of lithium. Hence, the influence of the lithium ions extends throughout the solution and distorts the entire water network, most notably visible beyond the first peak in the O–O RDF. Note that this discussion is unrelated to the structure maker/structure breaker issue. The influence on the entire water structure is an effect of the concentration alone, and does not correspond to long-ranged influences of the Li^+ ion. It has been shown[48,153] that the lithium ion has no influence on the water structure beyond its first solvation shell.

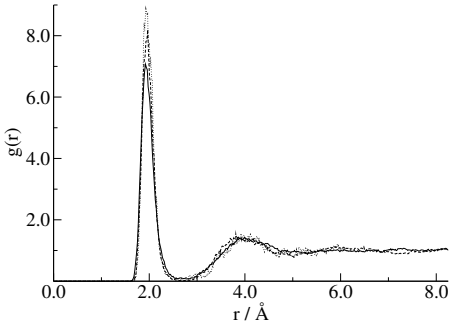

Figure 6.2: Li–O radial distribution functions for the dilute (dashed line) and concentrated (solid line) solution. The dotted line represents the Li–O RDF for the reference system of a single lithium ion in water.

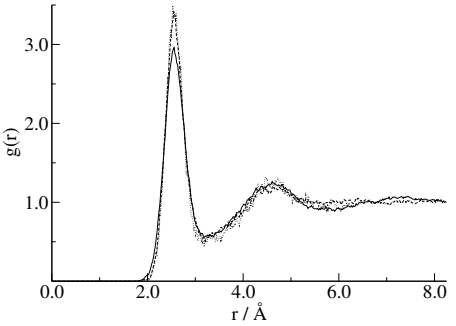

Figure 6.3: Li–H radial distribution functions for the dilute (dashed line) and concentrated (solid line) solution. The dotted line represents the Li–H RDF for the reference system of a single lithium ion in water.

The Li–O and Li–H RDFs of both LiOH solutions and the reference solution of a single lithium ion in water, are shown in figure 6.2 and 6.3, respectively. The structure of the first solvation shell is very clear. Due to the strong hydrogen bonds between the lithium ion and the oxygen atoms of water molecules, we see sharp peaks at a Li–O distance of 2.0 Å. The very low minima directly after these peaks indicate an almost complete depletion of oxygen atoms between 2.5 and 3.0 Å, suggesting a very rigid solvation shell. This is consistent with results from all previous studies[48,149,154–156] of the solvation shell of lithium.

The Li–H RDFs are less structured, as is expected because the hydrogen atoms point away from the lithium ion. In the structure of the Li–O radial distribution functions we see a small influence of the concentration on the height of the first peaks. The most dilute reference system has a first RDF peak value of 9, while the most concentrated solution has its first peak maximum at 7. The concentration has an effect on the average number of water molecules in the first solvation sphere around lithium. To quantify this influence we have calculated the normalised integrals of the first RDF peak for all concentrations. These values are tabulated in table 6.1, columns 1 and 2. From the Li–O values, that are most relevant here, we calculate a coordination number around 4, in agreement with the majority of all simulation and experimental data.[48,77,154–156] For the rest of the discussion a water molecule is defined to be inside the first solvation shell of lithium if the Li–O distance is smaller than the first minimum in the Li–O RDF. Furthermore, we see that increasing the concentration causes the amount of first solvation shell water molecules to decrease slightly from 4.02 to

system	Li–O (2.7)	Li–H (3.2)	Li–OH^- (2.4)	Li–Li	O–OH^- (3.2)	H–OH^- (2.5)
concentrated	3.93	9.84	0.44	0.46 (4.1)	4.26	3.57
dilute	4.00	10.26	0.25	0.23 (4.4)	4.54	3.84
reference	4.02	9.54	-	-	4.31	3.93

Table 6.1: Coordination numbers (normalised integrals of the first RDF peak) for the most important atom and ion pairs. The numbers in brackets denote the integration limit in Å. The reference system is a single lithium ion in 64 water molecules for the Li–O and Li–H coordination number. For the O–OH^- and H–OH^- integrals, the reference system is a single OH^- ion in 64 water molecules.

3.93. In comparison with our studies on the solvation of HCl, in chapter 5, we observe the same behaviour. The relatively smaller amount of water that is available per ion in the high concentration solution results in a smaller average coordination number. Another observation is, however, that the differences in the coordination numbers between the concentrations is smaller than in the case of the HCl solvation. The reason for this is that the lithium ion forms much stronger hydrogen bonds with water than the chloride ion. The energy gain of filling the complete solvation sphere of lithium is therefore much greater. Consequently, the effect of concentration is smaller: the solvation shells of lithium are filled first, and the remaining water molecules are available for the solvation of the hydroxide ions and the formation of a hydrogen-bonded water network. The histograms of the coordination numbers for the concentrated, diluted and reference solution are shown in figure 6.4, based on the Li–O distance criterium. As the minimum in the Li–O RDF is most well-defined, the histogram based on this quantity is most important. We observe, for all concentrations, a very narrow distri-

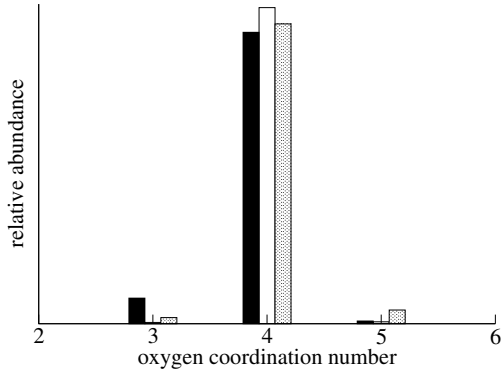

Figure 6.4: Histograms of the coordination number based on the Li–O distance for the concentrated (filled bars), dilute (open bars) and reference solution (dot-filled bars).

bution around 4, indicative of a very rigid and well-defined solvation shell. A small concentration effect is visible. In the most dilute solution, the reference solvation of a single Li^+ ion in water, there is a small amount of five-coordinated lithium present in the solution. This contribution disappears in the dilute LiOH solution. Here, the coordination is almost exclusively, 4. At the highest concentration, we observe a small yet significant amount of three-coordinated lithium. These observations are consistent with the notion that the amount of water that is available to solvate a single Li^+ ion steadily decreases with the increase of the LiOH concentration.

The Li–OH^- RDFs are shown in figure 6.5. The form of the RDFs is qualitatively identical to the Li–O RDFs, but the minima after the first peak are more pronounced, as well as the overall structure of the complete RDFs. The concentration effect is mostly present as a difference in the relative amount of direct contact-ion and solvent-separated Li–OH^- pairs in the solution. From the normalised integrals of the first peak (table 6.1, column 3), we observe that almost twice as many contact-ion pairs are present in the concentrated solutions than in the dilute solution. In agreement with our observations of the HCl solvation, a higher concentration forces the formation of more contact-ion pairs. Again, isolated and complete solvation of each charged species is energetically most favourable. In both solutions, there is an insufficient amount of water for complete solvation of all charged species in the solution. The formation of the very strong Li–OH^- hydrogen bond becomes increasingly more favourable upon increase of the concentration.

The lithium ions in the solution form a water-bridged network, comparable to that of the chloride ions in the HCl solutions. The Li–Li RDF (figure 6.6) in combination

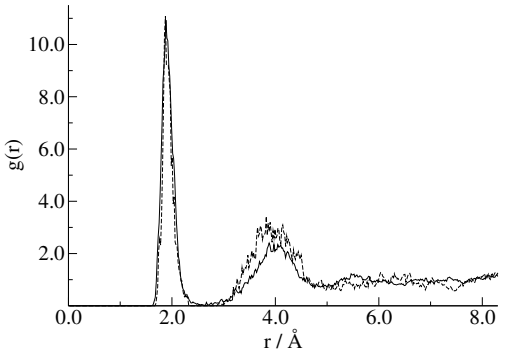

Figure 6.5: Li-OH^- radial distribution functions for the dilute (dashed line) and concentrated (solid line) solution.

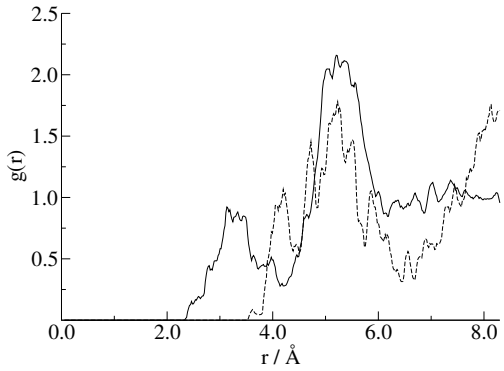

Figure 6.6: Li-Li radial distribution functions for the dilute (dashed line) and concentrated (solid line) solution.

with visual inspection of the trajectories of the simulations, allows us to identify the most important species that are formed. In the concentrated LiOH solution RDF we observe a broad peak in the range 2.2-4.2 Å, that is completely absent in the RDF of the dilute solution. Analysis of the trajectories indicate that the structure that corresponds to this peak is the water- or hydroxide-bridged Li–Li pair. Representative snapshots of these structures are shown in figure 6.7 and 6.8. The fact that the RDF peak is relatively broad is caused by the presence of both structures in the solution. The hydroxide–lithium hydrogen bond is stronger than the water–lithium hydrogen bond. Effectively, due to the smaller Li–O distances in the hydroxide-bridged lithium pair, the lithium ions are drawn closer together by approximately 0.3 Å, on average.

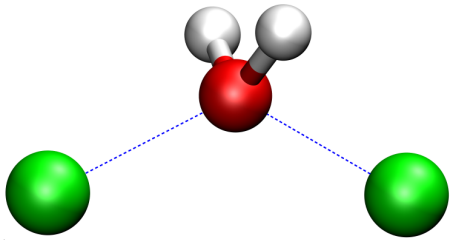

Figure 6.7: Snapshot of the water-bridged Li–Li ion pair.

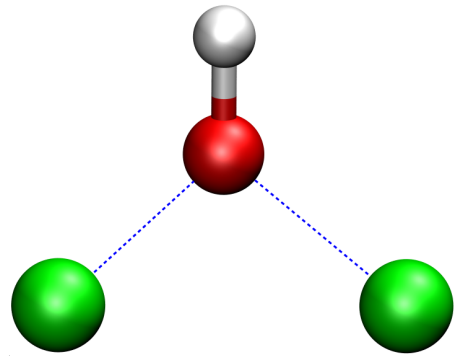

Figure 6.8: Snapshot of the hydroxide-bridged Li–Li ion pair.

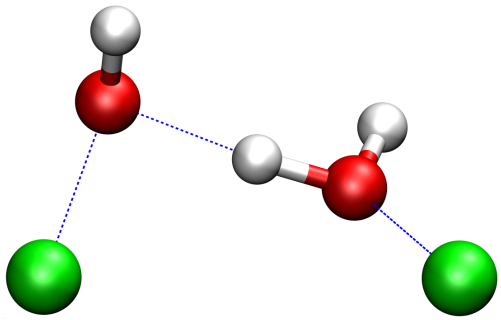

Figure 6.9: Representative snapshot of a lithium ion pair that is bridged by a water molecule and a hydroxide ion.

The first peak in the RDF is centred around 4.2 Å in the dilute solution. More water is available in this system to solvate the ions, so the lithium ions are not forced as close together as in the concentrated solution. In fact, the amount of single water-bridged lithium ion pairs is much smaller and if they occur, the Li–Li distance is larger than in the concentrated solution. The hydroxide-bridged lithium ion-pair is almost completely absent. Instead, we observe that the Li–Li distance of approximately 4.2 Å corresponds to a lithium ion pair that is separated by a hydroxide ion and a water molecule, as shown in figure 6.9. This structure is also observed in the concentrated solution, but, apparently it is relatively more stable in the dilute solution. In both RDFs a broad peak is present around approximately 5 Å. This Li–Li distance nicely corresponds to a lithium ion pair that is bridged by two water molecules, shown in figure 6.10. Actually, this conformation corresponds to two lithium ions that have been able to completely fill their solvation shell with water molecules. Due to the relatively high concentration of ions in both solutions, they cannot easily move further away from each other. The favourable hydrogen-bond interaction between water molecules from each solvation shell then makes this structure relatively stable. Although the

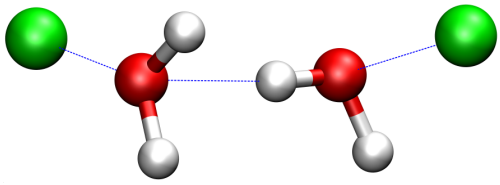

Figure 6.10: Structure of a double water-bridged lithium ion pair.

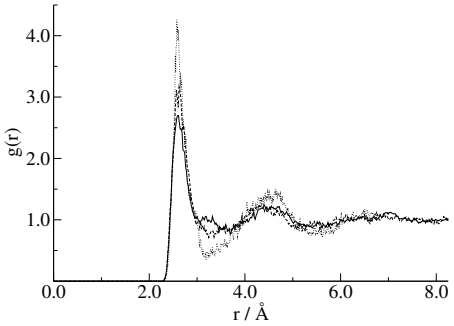

Figure 6.11: O-OH^- radial distribution functions for the dilute (dashed line) and concentrated (solid line) solution. The dotted line represents the O-OH^- RDF for the reference system of a single hydroxide ion in water.

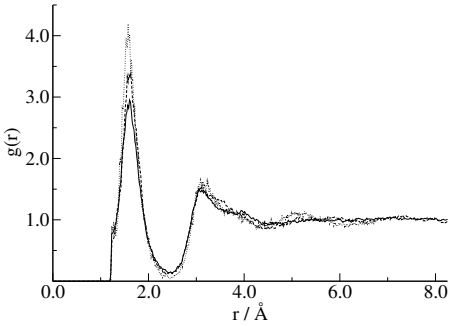

Figure 6.12: H-OH^- radial distribution functions for the dilute (dashed line) and concentrated (solid line) solution. The dotted line represents the H-OH^- RDF for the reference system of a single hydroxide ion in water.

interaction is rather flexible, which can be concluded from the relative broadness of the peak, a number of these structures have been observed during the entire length of the simulation, in both concentrations. Finally, the very last Li–Li RDF peak in the dilute concentration, around 8 Å, is more difficult to connect to a water-bridged lithium ion structure, due to limitations of the size of the simulation box. However, one can easily speculate that inserting an extra water molecule between two solvation shells around lithium would result in a Li–Li distance of ca. 8 Å. This would also explain the absence of a peak at this value in the concentrated solution, due to the lack of available water molecules to separate two solvation shells.

Figures 6.11 and 6.12 show the O–OH^- and H–OH^- RDFs, respectively. The coordination numbers, based on the integration of the first peaks, are shown in table 6.1, columns 5 and 6. The dilute and concentrated LiOH solutions are compared here to the reference solution of a single hydroxide ion in 64 water molecules. Water molecules surrounding the hydroxide ion point towards the ion with one of their hydrogen atoms, so the H–OH^- RDF is most important here. The structure of the RDF is identical for all concentrations, a sharp peak around 1.6 Å, followed by an minimum that almost reaches 0 at 2.5 Å. The concentration effect is clearly visible in the height of the first peak and, consequently, in the coordination numbers. The peak height decreases on increasing the concentration of LiOH in the solution. Chen *et al.* observed this effect in their studies of the solvation of KOH and NaOH.[144] We saw the same trend in the first peak of the Li–O RDF and the reasoning for the cause is the same here. A relatively smaller amount of water molecules is present to solvate

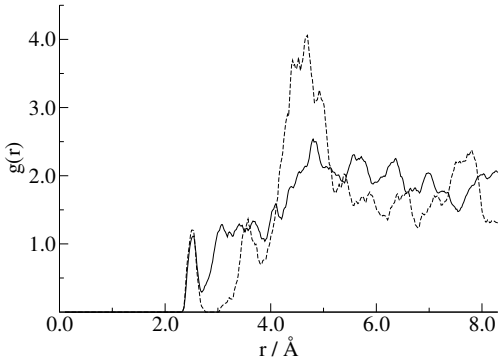

Figure 6.13: OH^-–OH^- radial distribution functions for the dilute (dashed line) and concentrated (solid line) solution.

the hydroxide ion completely. The coordination numbers quantitatively follow this trend, decreasing from 3.93, which corresponds very well to literature data, to 3.57 for the most concentrated LiOH solution. The O–OH^- RDFs qualitatively follow the same trend of a decreasing RDF peak height with increasing concentration. However, since the oxygen atom is not directly hydrogen bonded to the ion, and due to partly protruding water molecules from the second solvation shell, the first solvation shell is not so well-defined. The error margin on the coordination numbers is much larger and therefore they do not display this trend quantitatively.

The OH^-–OH^- RDFs are shown in figure 6.13. There are no noteworthy structures in the concentrated solution but in the dilute solution a very distinct peak around 4.5 Å is visible. Inspection of the simulation trajectories revealed that this maximum is due to the water-bridged structure of two hydroxide ions, shown in figure 6.14. This structure is also observed in the concentrated solution but, according to the clear peak in the RDF, it is stabilised more in the dilute solution.

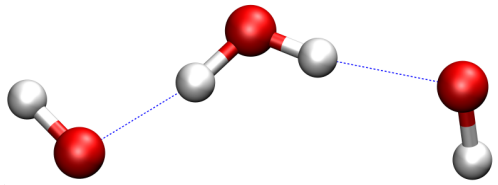

Figure 6.14: Structure of a water-bridged hydroxide ion pair.

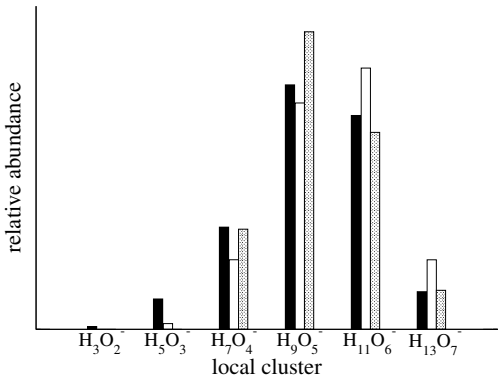

Figure 6.15: Histograms for the local hydroxide cluster for the dilute (empty bars) and concentrated (solid bars) solution. The dot-filled bars show the distribution of the local hydroxide cluster in the reference system of one hydroxide ion in water.

For insight in the local structure in which the hydroxide ion is present in the solution, we plotted the distribution of the size of these clusters in figure 6.15. A water molecule is counted as being part of the hydroxide cluster if the O–OH^- distance falls within the first peak of the O–OH^- RDF (figure 6.11). The reasoning behind this criterium is that these directly neighbouring water molecules can, in principle, participate in proton transfer without the need of large structural rearrangements. There is some arbitrariness in the choice of this criterium. A smaller criterium would shift the distribution left, towards smaller cluster sizes and a larger criterium would increase the average size of hydroxide clusters. Our choice to include the entire first solvation shell is mainly based on our observations, from visual inspection of the nuclear trajectories, that the proton hole is delocalised over the first solvation shell around a hydroxide ion. On a more phenomenological basis, this criterium yields a distribution that compares well with the recent studies[23,144] that are mentioned here.

Figure 6.15 shows that, using this criterium, the dominant species in the reference solution of one OH^- ion in water, is the $H_9O_5^-$ ion. This observation is consistent with the average coordination number of 4, as found in this work and literature. In their studies of the solvation of KOH and NaOH,[144] Chen *et al.* observed approximately the same distribution of dominant species, with $H_9O_5^-$ dominant, followed by $H_{11}O_6^-$ and $H_7O_4^-$. The dominance of this species is also in good agreement with the revised mechanism of proton transport in hydroxide solvations.[23] In the mechanism of hydroxide mobility, as proposed by Agmon,[22] the smaller $H_7O_4^-$ and $H_3O_2^-$ clusters are dominant. Our results therefore do not support this mechanism directly, although one

must keep the *caveat* of the choice of the criterium in mind.

The concentration effect is not as clear here as it is in the solvation of HCl. It is expected that an increase in the LiOH concentration would favour smaller hydroxide–water clusters instead of larger clusters, due to the relatively smaller amount of water that is available. The most concentrated solution shows an increase in the amount of smaller $H_5O_3^-$ clusters, at the cost of the $H_9O_5^-$ ion cluster, comparable with the results for the solvation of NaOH.[144] The dilute LiOH solution, however, shows some counterintuitive behaviour. Here, the amount of smaller clusters ($\leq H_9O_5^-$) is actually smaller than in the reference solution of a single OH^- ion. The proportion of large clusters ($> H_9O_5^-$) is bigger than in the reference solution. Although the deviations could be the result of statistical errors and fall within the margin of error, another, physical explanation could be related to the apparent stabilisation of the structure that is shown in figure 6.14. The OH^-–OH^- RDFs (figure 6.13) show that relatively large OH^-–H_2O–OH^- type structures are favoured in the dilute LiOH solution. This same effect can be the cause for the relatively larger amount of bigger hydroxide–water clusters.

Dynamics

Because of the relatively short duration of our simulations, we are limited in the analysis of the dynamical behaviour of the solvation of LiOH in water. The hydrogen bonds between the lithium ions and water molecules is so strong that we have observed only very occasional structural rearrangements in the first solvation shell around lithium. This is consistent with previous simulations that estimate the residence time of water molecules in the range 20-50 ps. Based on these limited water exchange processes we cannot address the residence time in a quantitative way. The dynamical properties of proton transfer, however, occur on a much smaller timescale than that of structural water rearrangements. We have analysed the hydroxide persistence correlation function that is a measure for the lifetime of a hydroxide ion, as introduced in chapter 5 (equation 5.1). This function, shown in figure 6.16, displays very fast decay. According to these plots, in all solutions the lifetime of a hydroxide ion is never longer than 7 fs. Compared to the hydronium ion, the hydroxide ion lives much shorter. This is most probably an indication of a strong delocalisation of the proton hole in a local OH^- cluster. As a consequence of the very short persistent lifetime of the hydroxide ion, our analysis of the dynamics of proton transfer is limited. Our definition of a proton transfer is a slightly modified version of the definition of a proton transfer in the HCl solvation. A proton transfer is characterised by one hydroxide ion that transforms into a water molecule within one MD timestep, while, during the same timestep, a water molecule in its first solvation shell transforms into a hydroxide ion. The number of observed proton hops as a function of the amount of time that the resulting hydroxide

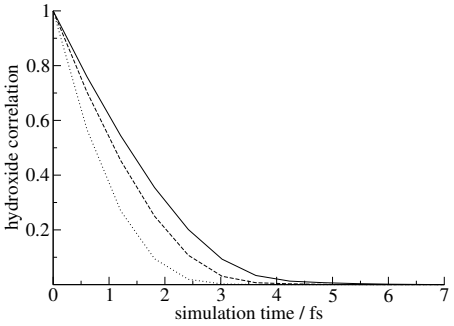

Figure 6.16: Hydroxide correlation functions for the concentrated solution (solid line), dilute solution (dashed line), and reference OH^- solution (dotted line).

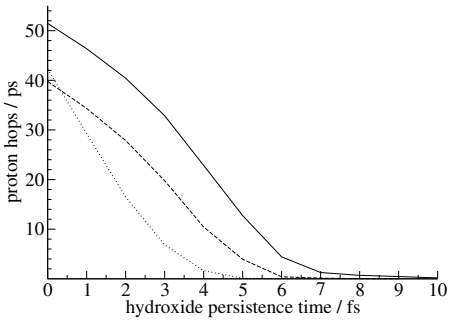

Figure 6.17: Number of observed proton hops per ps per proton hole as function of the persistent lifetime of the resulting hydroxide ion for the concentrated (solid line) and dilute (dashed line) LiOH solution. For comparison we also plotted the same quantity for the reference solution of one OH^- ion in water (dotted line).

ions is required to exist, is shown in figure 6.17. Because the hydroxide lifetime is so short, it is not possible to analyse the graph in as much detail as can be done for this quantity in the HCl solvation. We should conclude that our analysis methods of proton transfer has only limited applicability in the case of hydroxide dynamics. Our method is unable to handle the apparently very fast fluxional behaviour of hydroxide dynamics.

To extend our knowledge on the dynamical properties of the hydroxide and lithium dynamics, the obvious choice would be to increase the total simulation times. Longer simulations would enable us to estimate the residence time of water molecules in the solvation shell of lithium. Also, this would yield an increase in statistics concerning proton transfer. Longer timescale hydroxide position correlation functions, including intelligent averaging algorithms on the position of the hydroxide, would provide information on the transport of the hydroxide ion in a more macroscopic way. Due to the fast fluxional behaviour of hydroxide dynamics one could also decrease the timestep in the simulation as to increase the resolution of, for example, figure 6.17, and perhaps discover evidence of proton transfer mechanisms that occur on different timescales, comparable to our results for the solvation of HCl in the previous chapter. Furthermore, the dynamical behaviour of the electron density in hydroxide clusters and its correlation with nuclear motion would provide advanced insight in the dynamics of proton transfer. Finally, it has been shown that the quantum nature of the nuclei

is of great importance in the process of proton transfer,[21,23] and future studies would benefit from including these properly. All these options imply a large increase in the needed computational resources. However, due to the fundamental importance of a detailed and definitive understanding of the properties of basic solutions, these would surely be justified.

6.4 Conclusions

We have studied the aqueous solvation of lithium hydroxide using DFT-based molecular dynamics simulations at high and low concentrations. Large simulation box sizes allow us to identify larger-scale structures, such as water bridged lithium and hydroxide ions. The concentration has an effect on almost all structural properties. Upon increasing the concentration we observe a destructive effect on the natural hydrogen-bonded water structure. Furthermore, the coordination number of water molecules around the present ions, as well as the number of bridging water molecules between ions and the interionic distances, decrease on an increase of the LiOH concentration. In comparison with our previous study of the solvation of hydrochloric acid, we see many comparable features. However, due to the differences in the ion–water and ion–ion interactions, there are some notable qualitative and quantitative differences. The overall structural features, however, remain intact. The lithium ions form a semi-rigid water-bridged network while the solvated ions compete to complete their solvation shells. Due to our short simulation lengths, we are unable to quantitatively address the dynamical properties of the lithium–water interactions. Regarding the proton transport, we observe a very short lifetime of the hydroxide ion, indicating a very much delocalised negative charge in hydroxide–water clusters. The short lifetime of identifiable hydroxide species severely limits our analysis of the dynamical properties of proton transfer in solvated hydroxide solutions. However, our identification of the $H_7O_4^-$, $H_9O_5^-$ and $H_{11}O_6^-$ ions as the dominant species in the LiOH solution, agrees with the results from Chen *et al.*[144] in their studies of the solvation of NaOH and KOH. Consequently, our data support the view that the transport mechanism the hydroxide ions is different than that of protons,[23] although the somewhat arbitrary choice of our identification criterium does not make this study outright proof of this revised mechanism.

Bibliography

[1] S. A. Clough, Y. Beers, G. P. Klein, L. S. Rothman *J. Chem. Phys.* **1973**, *59*, 2254.

[2] P. L. Silvestrelli, M. Parrinello *Phys. Rev. Lett.* **1999**, *82*, 3308.

[3] G. E. Walrafen, M. R. Fisher, M. S. Hokmabadi, W.-H. Yang *J. Chem. Phys.* **1986**, *85*, 6970.

[4] J. D. Bernal, R. H. Fowler *J. Chem. Phys.* **1933**, *1*, 515.

[5] A. Grossfield *J. Chem. Phys.* **2005**, *122*, 024506.

[6] *Handbook of Chemistry and Physics*, 56 ed., edited by R. C. Weast CRC Press; U.S.A., 1975.

[7] P. Weis, P. R. Kemper, M. T. Bowers, S. S. Xantheas *J. Am. Chem. Soc.* **1999**, *121*, 3531.

[8] K. Hiraoka, S. Mizuse, S. Yamabe *J. Phys. Chem.* **1988**, *92*, 3943.

[9] A. W. Omta, M. F. Kropman, S. Woutersen, H. J. Bakker *Science* **2003**, *301*, 347.

[10] M. F. Kropman, H. J. Bakker *J. Chem. Phys.* **2001**, *115*, 8942.

[11] S. Raugei, M. L. Klein *J. Chem. Phys.* **2002**, *116*, 196.

[12] A. Brodsky *Chem. Phys. Lett.* **1996**, *261*, 563.

[13] W. L. Jorgensen, J. Chandrasekhar, J. D. Madura, R. W. Impey, M. L. Klein *J. Chem. Phys.* **1983**, *79*, 926.

[14] K. Laasonen, M. Sprik, M. Parrinello, R. Car *J. Chem. Phys.* **1993**, *99*, 9080.

[15] S. J. Stuart, B. J. Berne *J. Phys. Chem.* **1996**, *100*, 11934.

[16] C. J. D. von Grotthuss *Ann. Chim.* **1806**, *LVIII*, 54.

[17] O. F. Mohammed, D. Pines, J. Dreyer, E. Pines, E. T. J. Nibbering *Science* **2005**, *310*, 83.

[18] S. Izvekov, G. A. Voth *J. Chem. Phys.* **2005**, *123*, 044505.

[19] J. M. Headrick, E. G. Diken, R. S. Walters, N. I. Hammer, R. A. Christie, J. Cui, E. M. Myshakin, M. A. Duncan, M. A. Johnson, K. D. Jordan *Science* **2005**, *308*, 1765.

[20] N. Agmon *Chem. Phys. Lett.* **1995**, *244*, 456.

[21] D. Marx, M. E. Tuckerman, J. Hutter, M. Parrinello *Nature* **1999**, *397*, 601.

[22] N. Agmon *Chem. Phys. Lett.* **2000**, *319*, 247.

[23] M. E. Tuckerman, D. Marx, M. Parrinello *Nature* **2002**, *417*, 925.

[24] S. Imberti, A. Botti, F. Bruni, G. Cappa, M. A. Ricci, A. K. Soper *J. Phys. Chem.* **2005**, *122*, 194509.

[25] R. Car, M. Parrinello *Phys. Rev. Lett.* **1985**, *55*, 2471.

[26] W. Kohn, L. J. Sham *Phys. Rev.* **1965**, *140*, A1133.

[27] A. D. Becke *Phys. Rev. A* **1988**, *38*, 3098.

[28] C. Lee, W. Yang, R. G. Parr *Phys. Rev. B* **1988**, *37*, 785.

[29] P. L. Silvestrelli, M. Parrinello *J. Chem. Phys.* **1999**, *111*, 3572.

[30] D. Frenkel, B. Smit, *Understanding Molecular Simulations* Academic Press; London, 2002, Vol. 1.
[31] M.-P. Gaigeot, M. Sprik *J. Phys. Chem. B* **2003**, *107*, 10344.
[32] J. C. Grossman, E. Schwegler, E. W. Draeger, F. Gygi, G. Galli *J. Chem. Phys.* **2004**, *120*, 300.
[33] G. W. Neilson, J. E. Enderby *Adv. Inorg. Chem.* **1989**, *34*, 195.
[34] D. H. Powell, G. W. Neilson, J. E. Enderby *J. Phys.: Condens. Matter* **1993**, *5*, 5723.
[35] M. F. Kropman, H. J. Bakker *Science* **2001**, *291*, 2118.
[36] W. E. Price, R. Mills, L. A. Woolf *J. Phys. Chem.* **1996**, *100*, 1406.
[37] P.-Å. Bergström, J. Lindgren, O. Kristiansson *J. Phys. Chem.* **1991**, *95*, 8575.
[38] R. W. Impey, P. A. Madden, I. R. McDonald *J. Phys. Chem.* **1983**, *87*, 5071.
[39] X. G. Zhao, A. Gonzalez-Lafont, D. G. Truhlar, R. Steckler *J. Chem. Phys.* **1991**, *94*, 5544.
[40] L. X. Dang, B. C. Garrett *J. Chem. Phys.* **1993**, *99*, 2972.
[41] W. L. Jorgensen, D. L. Severance *J. Chem. Phys.* **1993**, *99*, 4233.
[42] T. Asada, K. Nishimoto, K. Kitaura *J. Phys. Chem.* **1993**, *97*, 7724.
[43] K. Laasonen, M. L. Klein *J. Am. Chem. Soc.* **1994**, *116*, 11620.
[44] D. E. Smith, L. X. Dang *J. Chem. Phys.* **1994**, *100*, 3757.
[45] S. H. Lee, J. C. Rasaiah *J. Phys. Chem.* **1996**, *100*, 1420.
[46] K. E. Laasonen, M. L. Klein *J. Phys. Chem. A* **1997**, *101*, 98.
[47] D. A. Yarne, M. E. Tuckerman, M. L. Klein *Chem. Phys.* **2000**, *258*, 163.
[48] A. P. Lyubartsev, K. Laasonen, A. Laaksonen *J. Chem. Phys.* **2001**, *114*, 3120.
[49] B. Ensing, E. J. Meijer, P. E. Blöchl, E. J. Baerends *J. Phys. Chem. A* **2001**, *105*, 3300.
[50] D. J. Tobias, P. Jungwirth, M. Parrinello *J. Chem. Phys.* **2001**, *114*, 7036.
[51] P. Jungwirth, D. J. Tobias *J. Phys. Chem. A* **2002**, *106*, 379.
[52] H. J. C. Berendsen, J. R. Grigera, T. P. Straatsma *J. Phys. Chem.* **1987**, *91*, 6269.
[53] L. X. Dang, J. E. Rice, J. Caldwell, P. A. Kollman *J. Am. Chem. Soc.* **1991**, *113*, 2481.
[54] L. X. Dang *J. Chem. Phys.* **1992**, *96*, 6970.
[55] P. Hohenberg, W. Kohn *Phys. Rev.* **1964**, *136*, B864.
[56] M. Sprik, J. Hutter, M. Parrinello *J. Chem. Phys.* **1996**, *105*, 1142.
[57] P. L. Silvestrelli, M. Bernasconi, M. Parrinello *Chem. Phys. Lett.* **1997**, *277*, 478.
[58] G. te Velde, F. M. Bickelhaupt, S. J. A. van Gisbergen, C. F. Guerra, E. J. Baerends, J. G. Snijders, T. Ziegler *J. Comput. Chem.* **2001**, *22*, 931.
[59] C. F. Guerra, J. G. Snijders, G. te Velde, E. J. Baerends *Theor. Chem. Acc.* **1998**, *99*, 391.
[60] R. N. Barnett, U. Landman *Phys. Rev. B* **1993**, *48*, 2081.
[61] W. G. Hoover *Phys. Rev. A* **1985**, *31*, 1695.
[62] A. Tongraar, B. M. Rode *Phys. Chem. Chem. Phys.* **2003**, *5*, 357.
[63] H. M. Lee, D. Kim, K. S. Kim *J. Chem. Phys.* **2002**, *116*, 5509.
[64] P. Ayotte, S. B. Nielsen, G. H. Weddle, M. A. Johnson, S. S. Xantheas *J. Phys. Chem. A* **1999**, *103*, 10665.
[65] A. Ignaczak, J. A. N. F. Gomes, M. N. D. S. Cordeiro *Electrochim. Acta* **1999**, *45*, 659.
[66] J. Baik, J. Kim, D. Majumdar, K. S. Kim *J. Chem. Phys.* **1999**, *110*, 9116.

[67] O. M. Cabarcos, C. J. Weinheimer, J. M. Lisy, S. S. Xantheas *J. Chem. Phys* **1999**, *110*, 5.
[68] R. A. Bryce, M. A. Vincent, N. O. J. Malcolm, I. H. Hillier, N. A. Burton *J. Chem. Phys.* **1998**, *109*, 3077.
[69] J. E. Combariza, N. R. Kestner *J. Phys. Chem.* **1994**, *98*, 3513.
[70] A. Öhrn, G. Karlström *J. Phys. Chem. B* **2004**, *108*, 8452.
[71] A. Botti, F. Bruni, S. Imberti, M. A. Ricci, A. K. Soper *J. Chem. Phys.* **2004**, *120*, 10154.
[72] J. M. Heuft, E. J. Meijer *J. Chem. Phys.* **2003**, *119*, 11788.
[73] A. Pasquarello, I. Petri, P. S. Salmon, O. Parisel, R. Car, E. Tóth, D. H. Powell, H. E. Fischer, L. Helm, A. E. Merbach *Science* **2001**, *291*, 856.
[74] A. Chandra *Phys. Rev. Lett.* **2000**, *85*, 768.
[75] J. D. C. Craig, M. H. Brooker *J. Sol. Chem.* **2000**, *29*, 879.
[76] S. S. Xantheas, L. X. Dang *J. Phys. Chem.* **1996**, *100*, 3989.
[77] H. Ohtaki, T. Radnai *Chem. Rev.* **1993**, *93*, 1157.
[78] K. A. Williams *Nature* **2000**, *403*, 112.
[79] J. Åqvist, V. Luzhkov *Nature* **2000**, *404*, 881.
[80] M. Kolbe, H. Besir, L.-O. Essen, D. Oesterhelt *Science* **2000**, *288*, 1390.
[81] D. S. Terekhova, A. I. Ryss, I. V. Radchenko *J. Struct. Chem.* **1969**, *10*, 807.
[82] S. Koneshan, J. C. Rasaiah, R. M. Lynden-Bell, S. H. Lee *J. Phys. Chem. B* **1998**, *102*, 4193.
[83] R. Ayala, J. M. Martínez, R. R. Pappalardo, E. S. Marcos *J. Chem. Phys.* **2003**, *119*, 9538.
[84] L. M. Ramaniah, M. Bernasconi, M. Parrinello *J. Chem. Phys.* **1998**, *109*, 6839.
[85] C. J. Mundy, J. Hutter, M. Parrinello *J. Am. Chem. Soc.* **2000**, *122*, 4837.
[86] I. Bakó, J. Hutter, G. Pálinkás *J. Chem. Phys.* **2002**, *117*, 9838.
[87] M. I. Lubin, E. J. Bylaska, J. H. Weare *Chem. Phys. Lett.* **2000**, *322*, 447.
[88] F. C. Lightsone, E. Schwegler, R. Q. Hood, F. Gygi, G. Galli *Chem. Phys. Lett* **2001**, *343*, 549.
[89] H. B. Schlegel, S. S. Iyengar, X. Li, J. M. Millam, G. A. Voth, G. E. Scuseria, M. J. Frisch *J. Chem. Phys.* **2002**, *117*, 8694.
[90] T. S. van Erp, E. J. Meijer *Chem. Phys. Lett.* **2001**, *333*, 290.
[91] N. Marzari, D. Vanderbilt *Phys. Rev. B* **1997**, *56*, 12847.
[92] P. L. Silvestrelli, N. Marzari, D. Vanderbilt, M. Parrinello *Sol. Stat. Comm.* **1998**, *107*, 7.
[93] D. Cauvi, C. Penel, M. C. Nlend, N. Venot, C. Allasia, O. Chabaud *Am. J. Physiol. Endocrinol. Metab.* **2000**, *279*, E546.
[94] A. de la Vieja, O. Dohan, O. Levy, N. Carrasco *Physiol. Rev.* **2000**, *80*, 1083.
[95] A. Yoshida, I. Hisatome, S. Taniguchi, N. Sasaki, Y. Yamamoto, J. Miake, H. Fukui, H. Shimizu, T. Okamura, T. Okura, O. Igawa, C. Shigemasa, E. D. Green, L. D. Kohn, K. Suzuki *Endocrinology* **2004**, *145*, 4301.
[96] K. Fukuyama, K. Sato, H. Itakura, S. Takahashi, T. Hosoya *J. Biol. Chem.* **1997**, *272*, 5752.

[97] R. M. Lawrence, R. F. Kruh *J. Chem. Phys.* **1967**, *47*, 4758.
[98] G. Markovich, R. Giniger, M. Levin, O. Cheshnovsky *J. Chem. Phys.* **1991**, *95*, 9416.
[99] J. E. Enderby, G. W. Neilson, *Water a Comprehensive Treatise* Plenum Press; New York, 1979, Vol. 1.
[100] H. Tanida, K. Kato, I. Watanabe *Bull. Chem. Soc. Jpn.* **2003**, *76*, 1735.
[101] W. H. Thompson, J. T. Hynes *J. Am. Chem. Soc.* **2000**, *122*, 6278.
[102] P. Ayotte, C. G. Bailey, G. H. Weddle, M. A. Johnson *J. Phys. Chem. A* **1998**, *102*, 3067.
[103] M. F. Kropman, H.-K. Nienhuys, H. J. Bakker *Phys. Rev. Lett.* **2002**, *88*, 077601.
[104] G. Markovich, S. Pollack, R. Giniger, O. Cheshnovsky *J. Chem. Phys.* **1994**, *101*, 9344.
[105] P. Ayotte, G. H. Weddle, J. Kim, J. Kelley, M. A. Johnson *J. Phys. Chem. A* **1999**, *103*, 443.
[106] D. M. Koch, G. H. Peslherbe *Chem. Phys. Lett.* **2002**, *359*, 381.
[107] J. V. Coe *J. Phys. Chem. A* **1997**, *101*, 2055.
[108] J. E. Combariza, N. R. Kestner, J. Jortner *Chem. Phys. Lett.* **1994**, *221*, 156.
[109] P. Jungwirth, D. J. Tobias *J. Phys. Chem. B* **2001**, *105*, 10468.
[110] P. B. Petersen, R. J. Saykally *J. Phys. Chem. B* **2005**, *109*, 7976.
[111] E. Brodskaya, A. P. Lyubartsev, A. Laaksonen *J. Chem. Phys.* **2002**, *116*, 7879.
[112] B. Hribar, N. T. Southall, V. Vlachy, K. A. Dill *J. Am. Chem. Soc.* **2002**, *124*, 12302.
[113] G. Tóth *J. Chem. Phys* **1996**, *105*, 5518.
[114] J. M. Heuft, E. J. Meijer *J. Chem. Phys.* **2005**, *122*, 094501.
[115] J. Kim, H. M. Lee, S. B. Suh, D. Majumdar, K. S. Kim *J. Chem. Phys.* **2000**, *113*, 5259.
[116] L. N. Trevani, E. Calvo, H. R. Corti *Electrochem. Commun.* **2000**, *2*, 312.
[117] R. Triolo, A. H. Narten *J. Chem. Phys.* **1975**, *63*, 3624.
[118] N. Agmon *J. Phys. Chem. A* **1998**, *102*, 192.
[119] P. Ayotte, G. H. Weddle, M. A. Johnson *J. Chem. Phys.* **1999**, *110*, 7129.
[120] A. Botti, F. Bruni, S. Imberti, M. A. Ricci, A. K. Soper *J. Chem. Phys.* **2004**, *121*, 7840.
[121] I. Harsányi, L. Pusztai *J. Phys.: Condens. Matter* **2005**, *17*, S59.
[122] M. F. Kropman, H. J. Bakker *J. Am. Chem. Soc.* **2004**, *126*, 9135.
[123] A. J. Sillanpää, K. Laasonen *Phys. Chem. Chem. Phys.* **2004**, *6*, 555.
[124] M. Masia, R. Rey *J. Chem. Phys.* **2005**, *122*, 094502.
[125] T. Dippel, K. D. Kreuer *Solid State Ionics* **1991**, *46*, 3.
[126] N. Agmon *J. Phys. Chem. A* **2005**, *109*, 13.
[127] J. Lobaugh, G. A. Voth *J. Chem. Phys.* **1995**, *104*, 2056.
[128] M. Tuckerman, K. Laasonen, M. Sprik, M. Parrinello *J. Phys. Chem.* **1995**, *5749*, 5749.
[129] R. Vuilleumier, D. Borgis *J. Chem. Phys.* **1999**, *111*, 4251.
[130] U. W. Schmitt, G. A. Voth *J. Chem. Phys.* **1999**, *111*, 9361.
[131] D. Marx, M. E. Tuckerman, M. Parrinello *J. Phys. Condens. Matt.* **2000**, *12*, A153.
[132] A. A. Kornyshev, A. M. Kuznetsov, E. Spohr, J. Ulstrup *J. Phys. Chem. B* **2003**, *107*, 3351.
[133] J.-C. Jiang, Y.-S. Wang, H.-C. Chang, S. H. Lin, Y. T. Lee, G. Niedner-Schatteburg, H.-C. Chang *J. Am. Chem. Soc.* **2000**, *122*, 1398.
[134] D. Asthagiri, L. R. Pratt, J. D. Kress *Proc. Natl. Acad. Sci.* **2005**, *102*, 6704.

[135] R. Vuilleumier, D. Borgis *J. Phys. Chem. B* **1998**, *102*, 4261.
[136] S. Walbran, A. A. Kornyshev *J. Chem. Phys.* **2001**, *114*, 10039.
[137] A. A. Chialvo, P. T. Cummings, J. M. Simonson *J. Chem. Phys.* **2000**, *113*, 8093.
[138] A. J. Sillanpää, C. Simon, M. L. Klein, K. Laasonen *J. Phys. Chem. B* **2002**, *106*, 11315.
[139] P. L. Geissler, C. Dellago, D. Chandler, J. Hutter, M. Parrinello *Chem. Phys. Lett* **2000**, *321*, 225.
[140] J. M. Heuft, E. J. Meijer *J. Chem. Phys.* **2005**, *123*, 094506.
[141] M. Tuckerman, K. Laasonen, M. Sprik, M. Parrinello *J. Chem. Phys.* **1995**, *103*, 150.
[142] R. Ludwig *Angew. Chem. Int. Ed.* **2003**, *42*, 258.
[143] B. Chen, J. M. Park, I. Ivanov, G. Tabacchi, M. L. Klein, M. Parrinello *J. Am. Chem. Soc.* **2002**, *124*, 8534.
[144] B. Chen, I. Ivanov, J. M. Park, M. Parrinello, M. L. Klein *J. Phys. Chem. B* **2002**, *106*, 12006.
[145] R. T. W. D. George E. Walrafen *J. Chem. Phys.* **2006**, *124*, 114504.
[146] F. Bruni, M. A. Ricci, A. K. Soper *J. Chem. Phys.* **2001**, *114*, 8056.
[147] A. Veerman, H. M. Lee, K. S. Kim *J. Chem. Phys* **2005**, *123*, 084321.
[148] T. Cartailler, W. Kunz, P. Turq, M.-C. Bellisent-Funel *J. Phys.: Condens. Matter* **1991**, *3*, 9511.
[149] J. R. Newsome, G. W. Neilson, J. E. Enderby *J. Phys. C* **1980**, *13*, L923.
[150] S. R. Dillon, R. C. Dougherty *J. Phys. Chem. A* **2003**, *107*, 10217.
[151] D. Spångberg, R. Rey, J. T. Hynes, K. Hermansson *J. Phys. Chem. B* **2003**, *107*, 4470.
[152] A. V. Egorov, A. V. Komolkin, V. I. Chizhik *J. Mol. Liq.* **2000**, *89*, 47.
[153] Z. Duan, Z. Zhang *Mol. Phys.* **2003**, *101*, 1501.
[154] H. H. Loeffler, B. M. Rode *J. Chem. Phys.* **2002**, *117*, 110.
[155] H. H. Loeffler, A. M. Mohammed, Y. Inada, S. Funahashi *Chem. Phys. Lett.* **2003**, *379*, 452.
[156] A. Tongraar, K. R. Liedl, B. M. Rode *Chem. Phys. Lett.* **1998**, *286*, 56.
[157] A. Yoshikawa, J. A. Morales *J. Mol. Str. Theochem.* **2004**, *681*, 27.

Summary

The subject of this thesis is the computational study of solutions of ions in water using molecular dynamics. The importance of water is so obvious that researching the properties of water does not need any justification. Water is a more complex fluid than its appearance would suggest. This complexity is clear when one studies water on the molecular level. The water molecule H_2O is strongly polarised; the hydrogen atoms have a relatively positive electrical charge, while the central oxygen atom is negatively charged. Water molecules can form hydrogen bonds, where the positive hydrogen atoms attract the negative oxygen atoms of other water molecules and vice versa. In pure water this leads to a structured network of water molecules where every water molecule tries to form an optimal amount of hydrogen bonds with its surrounding water molecules. A tetrahedral structure of water molecules that are connected by hydrogen bonds is formed. When ions are introduced in liquid water, they disrupt this natural network of hydrogen bonds. Ions themselves, however, can form hydrogen bonds with surrounding water molecules too, and thus induce a characteristic structure in their direct surroundings. Around the ion a solvation shell of water molecules is formed. The structural and dynamical properties of water molecules in this shell depend on the charge and size of the central ion. To study these properties using a theoretical model, an explicit description of the dynamical behaviour of the electron density is of great importance. The combination of density functional theory (DFT) and Car-Parrinello molecular dynamics (CPMD) offers this possibility precisely. The electron density, calculated with DFT, is propagated in time together with the movements of the nuclei by the Car-Parrinello equations of motion. This method is very efficient and yields excellent results for simulations of pure liquid water and solutions of ions in water.

In the first part of this thesis, chapter 2 to 4, the solvation of ions is systematically studied using a series of halogen ions, F^-, Cl^- and I^-. These halogen ions all have equal charge and outer electron configuration, only their size and mass vary. The effects on the dynamics and structure of the surrounding water molecules as a result of these properties of the ion can be compared consistently. Chapter 2 describes the dynamical and structural properties of water molecules in the direct surroundings of

the chloride ion. The shell around the chloride ion consists on average of almost six water molecules. The chloride–water interaction is relatively strong; a water molecule in the shell around chloride stays there for twelve picoseconds on average. The strong hydrogen bond with the chloride ion hinders a water molecule in its mobility. This mobility lies a factor two lower than that of water molecules in pure liquid water. Analysis of the structure of the solvation shell shows that the water molecules form a flexible octahedral structure around the chloride ion. The ion indeed induces a clear structure in its direct surroundings. This influence, however, is limited to the first shell of water molecules around the ion. Outside, the normal network of water molecules is almost directly completely restored. The internal geometry, bond lengths and angles, of water molecules that are bonded to the chloride ion are not distorted. Also the dipole moment of these water molecules is equal to that of water molecules in pure liquid water. The only discernible intramolecular effect is a decrease in the frequency of the O–H stretch vibration of these water molecules. This frequency decreases with ca. 100 cm^{-1} as a result of the strong hydrogen bond between the chloride ion and the water molecule.

The solvation of the fluoride ion is the subject of chapter 3. Fluoride is the smallest of all halogen ions. This results in a very strong interaction between the ion and surrounding water molecules, stronger than that of chloride. Water molecules in the solvation shell of fluoride stay there for sixteen picoseconds on average. The strong hydrogen bonds also lead to a well-defined geometry of the solvation shell. This consists mainly of five water molecules in a square pyramidal structure with the fluoride ion in the centre of the base of the pyramid. Exchange of water molecules from the shell and the rest of the solution proceeds by two different processes that are discussed in detail in chapter 3.

Regarding the influence on the surrounding water, chloride and fluoride largely show the same behaviour, albeit that the influence of fluoride is stronger and more pronounced. Iodide, the subject of chapter 4, clearly differs in its influence on the surrounding water structure. The iodide–water interaction is much weaker than that of fluoride and chloride, weaker even than the normal water–water interaction. Effectively iodide has a relatively water repelling character. This results in a weakly structured solvation shell around the ion. Water molecules in this shell move relatively fast and their persistence time in the direct vicinity of the ion is short (less than 10 picoseconds).

Chapter 5 and 6 present the research on solutions of hydrochloric acid and lithium hydroxide. In the previous chapters isolated ions were studied to examine their influence on the surrounding water in a well-defined way. Chapter 5 and 6, however, describe

much more complex systems in which the interaction between several and different ions is important. Both hydrochloric acid (HCl) and lithium hydroxide (LiOH) dissociate completely upon solvation in water. A large difference regarding chapters 2 to 4 is that, next to negative ions, positive ions are now present in the solution. Additionally, the concentration of HCl and LiOH is chosen to be higher, making the interaction between the ions very important. The nature of this interaction strongly depends on the concentration of the ions. To study the influence of the concentration, both solutions were simulated at two different concentrations.

Upon solvation in water, HCl dissociates into chloride ions and protons (H^+). Protons in water have been studied extensively in scientific literature. In solution, protons associate with surrounding water molecules to form Eigen ($H_9O_4^+$) and Zundel ($H_5O_2^+$) structures. The positively charged proton structures and negative chloride ions attract each other and hence both solvation shells are distorted. One of the consequences is a shortening of the persistence time of water molecules in the solvation shell of chloride when the concentration of protons increases. For protons, the effect of the solvation shell distortions is mainly visible in an effect on the speed of proton transfer. The above mentioned proton structures are not static, via hydrogen bonds the proton is transferred from one water molecule to the other with a certain frequency. In diluted solutions this process is very fast because the normal, highly structured network of hydrogen bonds is relatively undistorted. This network is distorted to a larger extent when the concentration of chloride ions increases. A direct effect is that the speed of proton transfer decreases with an increase of the concentration. The concentration also is of great importance for the structures on a larger scale that are present in the solutions. The protons and chloride ions form a network where water molecules connect the ions. When the concentration increases the amount of water that is available to make these connections, decreases. The influence on the formed structures are discussed in detail in chapter 5.

In the sixth and final chapter aqueous solutions of lithium hydroxide are studied. The procedure is largely identical to that of chapter 5 to facilitate a consistent comparison. The dynamics of the hydroxide ions (OH^-) that form as LiOH is dissolved in water, however, is much faster than that of protons. This makes studying these processes very difficult. One of the main conclusions is that the negative charge is very much delocalised over the water molecules that surround the ions. Comparable to the result in chapter 5, increasing the concentration of LiOH leads to a further disruption of the network of hydrogen bonds in the solution and the direct solvation shells of the ions.

Samenvatting

Dit proefschrift behandelt de computationele studie van oplossingen van ionen in water met behulp van moleculaire dynamica. Het belang van water is zo overduidelijk dat het doen van onderzoek naar de eigenschappen van water nauwelijks rechtvaardiging behoeft. Water is een complexere vloeistof dan het uiterlijk in eerste instantie doet vermoeden. Deze complexiteit wordt duidelijk wanneer je water op moleculair niveau bestudeert. Het water molecuul H_2O is sterk gepolariseerd; de waterstofatomen hebben een relatief positieve elektrische lading, terwijl het centrale zuurstofatoom negatief geladen is. Watermoleculen kunnen onderling waterstofbindingen of -bruggen vormen, waarbij de positieve waterstofatomen aangetrokken worden door de negatieve zuurstofatomen en vice versa. In zuiver water leidt dit tot een gestructureerd netwerk van watermoleculen waarbij elk watermolecuul probeert een optimaal aantal waterstofbindingen te vormen met zijn omringende watermoleculen. Hierbij onstaat een tetraëdrische structuur van watermoleculen die door waterstofbruggen verbonden zijn.

Wanneer nu ionen worden geïntroduceerd in vloeibaar water verstoren deze het natuurlijke netwerk van waterstofbindingen. Ionen kunnen echter zelf ook weer waterstofbindingen aangaan met omringende watermoleculen en induceren daardoor een karakteristieke structuur in hun direct omgeving. Rond het ion vormt zich een solvatatieschil van watermoleculen. De structurele en dynamische eigenschappen van watermoleculen in deze schil zijn afhankelijk van de lading en grootte van het centrale ion. Om deze eigenschappen te bestuderen met behulp van een theoretisch model is een expliciete beschrijving van het dynamische gedrag van de electronendichtheid van groot belang. De combinatie van dichtheids functionaal theorie (DFT) en Car-Parrinello moleculaire dynamica (CPMD) biedt precies deze mogelijkheid. De electronendichtheid, berekend met DFT, wordt tegelijk met de bewegingen van de atoomkernen gepropageerd in de tijd door de Car-Parrinello bewegingsvergelijkingen. Deze methode is zeer efficiënt en geeft uitstekende resultaten voor simulaties van puur vloeibaar water en oplossingen van ionen in water.

In de eerste helft van dit proefschrift, hoofdstukken 2 t/m 4, wordt de solvatatie van

ionen systematisch bestudeerd aan de hand van een reeks halogeen ionen, F^-, Cl^- en I^-. Deze halogeenionen hebben allen gelijke lading en buitenste electronenconfiguratie, alleen hun grootte en massa varieert onderling. De effecten op de dynamica en structuur van de omringende watermoleculen als gevolg van deze eigenschappen van het ion zijn dus op een consistente manier te vergelijken.

Hoofdstuk 2 beschrijft de dynamische en structurele eigenschappen van watermoleculen in de directe omgeving van het chloride ion. De schil rond het chloride ion bestaat gemiddeld uit bijna zes watermoleculen. De chloride–water interactie is relatief sterk; een watermolecuul in de schil rond chloride verblijft daar gemiddeld twaalf picoseconde. De sterke waterstofbinding met het chloride ion belemmert een water molecuul ook in zijn mobiliteit. Deze ligt een factor twee lager dan die van watermoleculen in puur vloeibaar water. Analyse van de structuur van de solvatatieschil laat zien dat de watermoleculen een flexibele octaëdrische omringing rond het chloride ion vormen. Het ion induceert dus inderdaad in zijn directe omgeving een duidelijke structuur, die echter beperkt blijft tot de eerste schil van watermoleculen rond het ion. Daarbuiten is het normale netwerk van watermoleculen vrijwel direct volledig hersteld. De interne geometrie, bindingslengten en -hoeken, van watermoleculen die gebonden zijn aan het chloride ion, wordt niet verstoord. Ook het dipoolmoment van deze watermoleculen is gelijk aan dat van watermoleculen in puur vloeibaar water. Het enige waarneembare intramoleculaire effect is een afname in de frequentie van de O–H strekvibratie van deze watermoleculen. Deze frequentie neemt af met ongeveer 100 cm^{-1} als gevolg van de sterke waterstofbinding tussen het chloride ion en het betreffende watermolecuul.

De solvatatie van het fluoride ion is het onderwerp van hoofdstuk 3. Fluoride is het kleinste van alle halogeenionen. Dit uit zich in een zeer sterke interactie tussen het ion en omringende watermoleculen, sterker dan die van chloride. Watermoleculen in de solvatatieschil van fluoride verblijven daar gemiddeld zestien picoseconde. De sterke waterstofbindingen leiden ook tot een goed gedefinieerde geometrie van de solvatatieschil. Deze bestaat overwegend uit vijf watermoleculen in een vlakvierkant pyramidale structuur met het fluoride ion in het midden van de vierkante basis van de pyramide. Uitwisseling van watermoleculen uit de schil en de rest van de oplossing vindt plaats door middel van twee verschillende processen, die uitgebreid staan beschreven in hoofdstuk 3.

Wat betreft de invloed op het omringende water vertonen chloride en fluoride in grote lijnen vergelijkbaar gedrag, zij het dat de invloed van fluoride sterker en duidelijker is. Iodide, beschreven in hoofdstuk 4, wijkt echter duidelijk af in zijn invloed op de omringende waterstructuur. De iodide–water interactie is veel zwakker dan die

van fluoride of chloride, en is zelfs zwakker dan de normale water–water interactie. Effectief heeft iodide dus een relatief waterafstotende eigenschap. Dit resulteert in een weinig gestructureerde solvatatieschil rond het ion. De watermoleculen in deze schil bewegen relatief snel en hun verblijftijd in de directe nabijheid van het ion is kort (minder dan 10 picoseconde).

De hoofdstukken 5 en 6 presenteren het onderzoek naar oplossingen van zoutzuur en lithiumhydroxide. In de voorgaande hoofdstukken zijn geïsoleerde ionen bestudeerd om de invloed van deze ionen op het omringende water eenduidig te onderzoeken. De hoofdstukken 5 en 6 echter, beschrijven veel complexere systemen waarbij juist ook de interactie tussen verscheidene en verschillende ionen van belang is. Zowel zoutzuur (HCl) als lithiumhydroxide (LiOH) splitsen bij oplossing in water volledig in ionen. Groot verschil met de hoofdstukken 2 t/m 4 is nu dus dat er, naast negatieve ionen, ook positieve ionen aanwezig zijn in de oplossing. Bovendien is de concentratie van HCl en LiOH veel hoger gekozen waardoor de aanwezige ionen in grote mate invloed van elkaar ondervinden. Deze invloed is in sterke mate afhankelijk van de concentratie van de ionen. Om de invloed van de concentratie te bestuderen zijn beide oplossingen bij twee verschillende concentraties gesimuleerd.

HCl splitst bij oplossing in water in chloride ionen en protonen (H^+). Protonen in water zijn al veelvuldig bestudeerd in de wetenschappelijke literatuur. In oplossing binden protonen met omringende watermoleculen om Eigen ($H_9O_4^+$) en Zundel ($H_5O_2^+$) structuren te vormen. De positieve protonstructuren en negative chloride ionen trekken elkaar aan en als gevolg hiervan worden beider solvatatieschillen verstoord. Voor de solvatatieschil van chloride is het gevolg dat de verblijftijd van watermoleculen in de schil korter wordt naarmate de protonconcentratie toeneemt. Bij de protonstructuren is de verstoring van de solvatatieschil vooral duidelijk in het effect op de snelheid van protonoverdracht. De genoemde protonstructuren zijn namelijk niet statisch; via waterstofbruggen wordt het proton met een bepaalde frequentie overgedragen van het ene watermolecuul naar het andere. In verdunde oplossingen verloopt dit proces zeer snel omdat het normale, gestructureerde netwerk van waterstofbruggen slechts weinig is verstoord. Dit netwerk wordt echter in toenemende mate verstoord als de concentratie van chloride ionen groter wordt. Het gevolg is derhalve dat de snelheid van protonoverdracht afneemt bij een toenemende concentratie. De concentratie is ook van groot belang voor de structuren op grotere schaal die herkenbaar zijn in de oplossingen. De protonen en chloride ionen vormen onderling een netwerk waarbij watermoleculen de ionen met elkaar verbinden. Als de concentratie toeneemt, neemt de hoeveelheid water die beschikbaar is om deze verbindingen te vormen, af. De consequenties voor de gevormde structuren worden in detail behandeld in hoofdstuk 5.

In het zesde en laatste hoofdstuk worden oplossingen van lithiumhydroxide bestudeerd. De aanpak is grotendeels identiek aan die van hoofdstuk 5 opdat de resulaten op een consistente wijze vergeleken kunnen worden. De dynamica van de hydroxide ionen (OH^-) die ontstaan bij het oplossen van LiOH in water, echter, verloopt op een veel kortere tijdschaal dan die van protonen. Hierdoor is het problematisch om deze processen in detail te bestuderen. Eén van de belangrijkste conclusies is wel dat de negatieve lading van OH^- zeer sterk gedelocaliseerd is over de watermoleculen die dit ion omringen. Analoog aan de bevindingen in hoofdstuk 5 leidt het verhogen van de concentratie van LiOH tot een verdere verstoring van het netwerk van de waterstofbruggen in de oplossing en de directe solvatatieschillen rond de ionen.

Publications

- ”Density functional theory based molecular-dynamics study of aqueous chloride solvation” - J. M. Heuft and E. J. Meijer, *J. Chem. Phys.*, 2003, **119**, 11788
- ”Density functional theory based molecular-dynamics study of aqueous fluoride solvation” - J. M. Heuft and E. J. Meijer, *J. Chem. Phys.*, 2005, **122**, 094501
- ”Density functional theory based molecular-dynamics study of aqueous iodide solvation” - J. M. Heuft and E. J. Meijer, *J. Chem. Phys.*, 2005, **123**, 094506
- ”A density functional theory based study of the microscopic structure and dynamics of aqueous HCl solutions” - J. M. Heuft and E. J. Meijer, *Phys. Chem. Chem. Phys.*, 2006, **8**, 3116
- ”NMR signatures of solvated ions from first principles calculations: case of HCl(aq)” - Tatiana Murakhtina, Jasper Heuft, Evert Jan Meijer and Daniel Sebastiani, *Chem. Phys. Chem.*, 2006, accepted for publication

Dankwoord

En af is het.

Niks geen tromgeroffel bij het tikken van de laatste ‘:wq’, triomftrompetten na de entertoets blijven stil. Maar dan is het toch echt af.
Gedurende mijn promotietijd hebben velen bijgedragen aan de totstandkoming van dit proefschrift, in directe of indirecte zin.

Als eerste wil ik Berend Smit bedanken voor de mogelijkheid om in zijn groep promotieonderzoek te doen. Voor de directe begeleiding van dit onderzoek ben ik Evert Jan Meijer veel dank verschuldigd. Ik dank Mike Klein voor de kans om gedurende twee maanden zijn groep in Philadelphia te bezoeken. Met name wil ik ook Bernd Ensing bedanken die mij daar opving. De discussies met hem over mijn onderzoek zijn erg nuttig geweest.

Verder was mijn promotietijd ook een ontzettend leuke periode. En dat is te danken aan mijn collega’s en vrienden. Het plezier om ’s ochtends naar de faculteit te komen kan tenslotte niet altijd een wetenschappelijke grondslag hebben. Allereerst natuurlijk Arjen, absoluut de nummer 0 in het lijstje van favoriete kamergenoten en verantwoordelijk voor ontelbare leuke momenten in C6.16’. Vervolgens Bart, mijn allereerste kamergenoot die mij al vroegtijdig leerde dat vier jaar toch heus niet zo’n oneindig lange periode is om honderd paginaatjes wetenschap vol te tikken. Saaie conferenties in Lunteren en Ascona fleurden zienderogen op door Elske, die in de laatste periode als één van de weinigen was overgebleven in ons CPMD subgroepje. De koffiepauzes, samen met Bas en Arjen in haar kamer waren een goed begin van de dag. De pauzes waren sowieso altijd een zeer welkome tijdelijke uitvlucht uit de -overigens natuurlijk mateloos intrigerende- wereld der ionen in water. Met Jochem en Abdon was er altijd wel iets te discussiëren, van het paarse kabinet tot de nieuwe XML-standaard. Na verloop van tijd kwam Evert de nerdgelederen versterken. En met verve, door 1337, w00t en lol als natuurlijk onderdeel van de dagelijkse vocabulaire te introduceren. Met vrijwel niemand was het wel en wee van het promoveren, en vaker nog alles daarbuiten, beter te bespreken dan met Tim, direct na de lunch. Gooitzen wil ik bedanken voor

zijn vertrouwen om mij leuk mee te laten sleutelen aan onze clusters, maar ook omdat hij altijd klaarstond voor een praatje over vanalles of niks.

Soms zou je vergeten dat er leven was buiten de faculteit of de Wildeman. Gelukkig waren daar dan de regelmatige filmdates met Floor of de wintersportvakanties. Ik vond het geweldig om me met ware doodsverachting van besneeuwde bergen af te storten in het gezelschap van m'n yo-yo-boarderhomies Erik en Lennart. Of om dat ietsje rustiger te doen samen met Thyra, Ellen, Rudmer en Jocelyne.

Zonder mijn ouders lag dit boekje hier niet. De liefde voor de chemie van mijn vader (en de chemicaliën die hij voor mij van het lab op zijn school mee naar huis nam) is een belangrijke motivatie geweest voor mijn keuze om te gaan promoveren. Ik weet dat hij trots op me zou zijn geweest. Het vertrouwen van mijn moeder is altijd een grote steun geweest, alsook haar interesse in alles wat mij maar bezig hield. Eveneens onmisbaar was de interesse van mijn zusjes, Annemieke en Linda, die zich veelvuldig herhaalde in de vorm van "Maar wat doe je nou eigenlijk precies?".
De felbegeerde laatste zin is, vanzelfsprekend, voor Jantien. Zij alleen maakte promoveren geheel en al de moeite waard.

" *That was wonderful!*
Bravo! I loved that!
Ah, that was great!
Well, it was pretty good...
It wasn't bad.
There were parts that weren't very good, though.
It could've been a lot better.
I didn't really like it.
It was pretty terrible.
It was bad!
It was awful!
Boo! Boo!! "
- **Statler & Waldorf, The Muppet Show**